Tsunami risk management for crustal earthquakes and non-seismic sources in Italy

J. Selva (1)*, A. Amato (1), A. Armigliato (2), R. Basili (1), F. Bernardi (1), B. Brizuela (1), M. Cerminara (1), M. de' Micheli Vitturi (1), D. Di Bucci (3), P. Di Manna (4), T. Esposti Ongaro (1), G. Lacanna (5), S. Lorito (1), Løvholt F. (6), D. Mangione (3), E. Panunzi (3), A. Piatanesi (1), A. Ricciardi (3), M. Ripepe (5), F. Romano (1), M. Santini (3), A. Scalzo (3), R. Tonini (1), M. Volpe (1), F. Zaniboni (2)

(1) Istituto Nazionale di Geofisica e Vulcanologia (INGV)
(2) Alma Mater Studiorum - Università di Bologna, Dipartimento di Fisica e Astronomia (DIFA) "Augusto Righi"
(3) Dipartimento della Protezione Civile (DPC)
(4) Istituto Superiore per la Protezione e la Ricerca Ambientale (ISPRA)
(5) Università degli studi di Firenze - Dipartimento di Scienze della Terra - Laboratorio di Geofisica Sperimentale (LGS)
(6) Norwegian Geotechnical Institute (NGI), Oslo, Norway

*** Correspondence:**
Jacopo Selva
jacopo.selva@ingv.it

Keywords: tsunami, hazard, warning, NEAM, Italian coasts

Abstract

Destructive tsunamis are most often generated by large earthquakes occurring at subduction interfaces, but also other "atypical" sources - defined as crustal earthquakes and non-seismic sources altogether - may cause significant tsunami threats. Tsunamis may indeed be generated by different sources, such as earthquakes, submarine or coastal landslides, volcano-related phenomena, and atmospheric perturbations. The consideration of atypical sources is important worldwide, but it is especially prominent in complex tectonic settings such as the Mediterranean, the Caribbean, or the Indonesian archipelago. The recent disasters in Indonesia in 2018, caused by the Palu-Sulawesi magnitude Mw 7.5 crustal earthquake and by the collapse of the Anak-Krakatau volcano, recall the importance of such sources. Dealing with atypical sources represents a scientific, technical, and computational challenge, which depends on the capability of quantifying and managing uncertainty efficiently and of reducing it with accurate physical modelling. Here, we first introduce the general framework in which tsunami threats are treated, and then we review the current status and the expected future development of tsunami hazard quantifications and of the tsunami warning systems in Italy, with a specific focus on the treatment of atypical sources. In Italy, where the memory of historical atypical events like the 1908 Messina earthquake or the relatively recent 2002 Stromboli tsunami is still vivid, specific attention has been indeed dedicated to the progressive development of innovative strategies to deal with such atypical sources. More specifically, we review the (national) hazard analyses and their application for coastal planning, as well as the two operating tsunami warning systems: the national warning system for seismically generated tsunamis (SiAM), whose upstream component - the CAT-INGV- is also a Tsunami Service Provider of the North-eastern Atlantic, the Mediterranean and connected seas Tsunami Warning System (NEAMTWS) coordinated by the Intergovernmental Coordination Group established by the Intergovernmental Oceanographic Commission (IOC) of UNESCO, and the local warning system for tsunamis generated by volcanic slides along the Sciara del Fuoco of Stromboli volcano. Finally, we review the state of knowledge about other potential tsunami sources that may generate significant tsunamis for the Italian coasts, but that are not presently considered in existing tsunami warning systems. This may be considered the first step towards their inclusion in the national tsunami hazard and warning programs.

1. Introduction

A tsunami is a series of gravity waves propagating in the water and generated by its sudden large-scale displacement due to one external source [1]. Tsunami waves are usually characterized by characteristic wavelengths longer than the sea depth. Most of the giant basin-wide tsunamis that are well known to the general public, such as the recent 2004 Indian ocean and the 2011 Tohoku tsunamis (e.g., [2]), are caused by very large megathrust earthquakes (M > 8.0), mostly occurring at subduction interfaces, which is where elastic energy is continuously stored and suddenly released by seismic events because of the friction between the incoming oceanic crust and the overlying continental crust, forced by the convergent motion between the two (e.g., [3]).

Some recent tsunamis, such as the Palu-Sulawesi and Sunda Strait events occurred in 2018, raised the attention toward tsunami sources different from the megathrust earthquakes occurring on the subduction interface. Indeed, the Palu-Sulawesi tsunami was generated by a magnitude Mw 7.5 crustal earthquake with a strike-slip source mechanism (that is, an earthquake occurring on a nearly vertical fault where two adjacent blocks move mostly horizontally with respect to each other) and with the possible contribution of landslides mobilized by the seismic shaking inside the Palu bay [4–6]; the Sunda Strait tsunami was instead generated by the collapse of the volcano edifice of Anak Krakatau, a volcanic island between Sumatra and Java islands [7–10]. Indeed, the initial water displacement developing in tsunami may be due to several causes, including the coseismic displacement caused by many kind of earthquakes and non-subduction-interface earthquakes occurring in subduction zones, as well as by other causes such as landslides, volcanic phenomena, meteorological perturbations, or even rarer events like the impact of asteroids [11]. As usually not covered by tsunami warning systems (TWSs), such sources were recently defined as “atypical” by the IOC/UNESCO TOWS-WG (Intergovernmental Oceanographic Commission of UNESCO - Working Group on Tsunamis and Other Hazards Related to Sea-Level Warning and Mitigation Systems; [12]).

Atypical sources, as said, include both seismic and non-seismic sources. Earthquakes are generated by the stress build-up determined by tectonic plate movements that induces sudden displacement on faults affecting the Earth’s brittle crust. Fault orientation in space and reciprocal movement of the two sides depends mainly on the orientation and sign of the stress field (compressional and dilatational), on the characteristics of the medium (e.g., elastic properties, rheology, friction), as well as on local geological features (e.g, pre-existing discontinuities) [1,13]. In subduction zones, large earthquakes tend to occur in the well-known interface that separates the two tectonic plates and that plunges with a relatively low angle into the Earth’s mantle, typically with thrust earthquakes (that is, with contractional movement on the fault rupture). Crustal seismicity occurs instead within the crust, at plate boundaries and even in plate interiors. Within the crust, different earthquake mechanisms may coexist even within small areas. Atypical sources include all these crustal earthquakes capable of generating tsunamis outside the subduction zones, which are not always equally well mapped [14]. Noteworthy, the definition of atypical sources also includes the subduction-zone earthquakes generated outside the subduction interface, such as splay and back-thrust faults branching from the interface in the upper plate and accretionary wedge, and outer-rise earthquakes, mostly occurring seaward from the trench on the oceanic crust as a result of stress redistribution following subduction earthquakes. Among all tsunamigenic earthquakes, the “tsunami earthquakes” deserve particular attention since they generate larger tsunamis than expected given their seismic moment magnitude, and both their mechanical process and frequency of occurrence are not completely understood [15]. Atypical sources also include all the other non-seismic tsunamigenic sources like sub-aerial near-coast and submarine landslides, a wide range of volcanic phenomena occurring both during eruptions or in non-eruptive periods (pyroclastic flows – fast currents of hot gas and volcanic materials, submarine explosions, caldera collapses, and flank instability are the most important ones), and meteotsunamis – tsunamis generated by atmospheric pressure disturbances (e.g., [16–22]).

In complex tectonic settings and small basins, such as, for example, the Mediterranean region, the Caribbean [23,24] , or around the Indonesian and Philippine archipelago north and east of the Sunda trench [19,25], atypical sources may even represent the majority of potential tsunamigenic sources. For example, in the Mediterranean Sea, numerous historical significant tsunamis were caused by non-subduction earthquakes or non-seismic sources [14,26–35], and such sources generated the majority of the events causing damaging tsunamis in the available historical record [36]. All the largest recent tsunamis in the Mediterranean were caused by crustal seismicity: the 2003 M6.8 Zemmouri-Boumerdes, the 2017 M6.8 Kos-Bodrum, and the recent 2020 M7.0 Samos-Izmir earthquakes, all generating tsunami whose maximum run-up was larger than 1 m [37–39]. Noteworthy, also non-seismic or mixed seismic/non-seismic sources generated in the recent past significant tsunamis, like the one generated at Stromboli in 2002 [40–43] as well as the most destructive tsunami in the record, related to the 1908 Mw 7.1 Messina Straits earthquake [44]. This non-subduction earthquake caused at least 80,000 deaths, and a few hundred were added by the tsunami [45], whose seismic generation was possibly enhanced by an earthquake-induced landslide [46–50]. More in general, hazard disaggregation results [31,51–53], which account for both source probability and tsunami potential and related uncertainty, show that the contribution to the total tsunami hazard of crustal sources is significant also along the coasts exposed to subduction tsunamis (e.g. eastern Sicily), and they may even represent the dominant contribution in many areas in the Mediterranean.

Tsunami forecast for Tsunami Warning Systems (TWSs) and Probabilistic Tsunami Hazard Analyses (PTHAs) are the main scientific inputs to the tsunami risk management [11,54,54–59]. For TWSs, it is required to timely produce a forecast of the tsunami intensity at different sites due to an event (for example, an earthquake) that has just occurred, or it is forecasted to occur in the relatively near future (for example, for a volcanic eruption or a subaerial landslide) based on the information registered by a monitoring system. The forecast is then generally used to define alert levels associated with specific short-term risk reduction measures, like population evacuation [55,60–63]. On the other hand, PTHA is a forecast of the potential future activity and it quantifies the probability of exceeding different tsunami intensities due to whatever possible tsunami in a target location within a relatively long time windows (e.g., 50 years). PTHA is based on the past behaviour of the system, and it is the main scientific input to long-term tsunami risk mitigation programs, like the definition of building codes or the design of evacuation areas themselves for TWSs [58,60–62].

In either case, TWS and PTHA, tsunami forecasts should be in principle based on the definition of a set of individual sources sampling the whole natural variability of relevant physical generation mechanisms, the quantification of the probability of occurrence of each source, and the evaluation of the potential consequent tsunamis. Tsunami forecast typically adopts the numerical simulation of the tsunami generation and propagation for each individual source, usually considering non-linear models in the shallow water approximation, to model the tsunami impact on the coast [11,54,64,65]. This procedure makes these assessments potentially very challenging from both the modelling and the computational points of view, especially if atypical sources have to be taken into account.

The computational challenge arises from the fact that typically large source variability has to be modelled, implying the requirement of running a very large number of individual simulations. Indeed, non-subduction seismicity takes place over large source areas, potentially covering the entire sea-floor and the near-coast areas and, as discussed above, includes a broad variety of source mechanisms, that is, a broad variety of fault orientations and fault movements. In comparison, large subduction zone earthquake behaviour is indeed more predictable, as it is largely dominated by thrust events on the plate interface. To model this variability a very large set of scenarios is needed (e.g., > 10^7, considering only seismic sources in a small

basin like the Mediterranean, see [31]) and thus their integration into tsunami hazard and warning depends on the development of specific methodological and computational strategies [31,54,66–70].

In addition, the identification and characterization of atypical sources is also difficult. Atypical earthquake faults and physics are usually less known than subduction sources, especially offshore, making it difficult to fully characterize their geometry and dynamics [14,31,71,72]. The characterization of the non-seismic sources is even more challenging due to their specific local geophysical (e.g. tectonic and geological) and geomechanical conditions (e.g. soil and rock properties), and the characterization and modelling of these sources and of the associated tsunamigenesis is still a matter of intense scientific research [16–18,20,73,74].

The modelling challenge consists of capturing the fundamentals of the dynamics or the kinematics of the source process (e.g., the generation and the propagation of a submarine landslide or the seafloor deformation induced by an earthquake) and of the solid-fluid coupling that determines the input to tsunami propagation model, as well as the fundamental physics that the propagation model should include.

The earthquake induced deformations are determined by the dynamic rupture, controlled in turn by the friction, the medium properties and the pre-existing stress field (e.g. [13]). The seismic rupture results in a time-dependent slip distribution on the fault, which produces in turn the deformation of the seafloor that, once transmitted to the ocean water column above it, induces a sea level perturbation then propagating under the action of gravity until the equilibrium is restored (e.g. [75,76]). The slower the rupture propagation and the local displacement on the fault, and the longer the earthquake duration, the larger are the departures from the widely used approximation of instantaneous sea floor displacement and hydrostatic transmission. The landslide rheology and related kinematics has direct consequence on the tsunami generation [77]. Advanced rheological and numerical models for the landslide dynamics normally distinguish between granular rheology (e.g. [78–81]) and viscoplastic rheology (e.g. [77,82]). Volcanic sources are especially difficult to model in this sense. Volcanic mass movements include subaerial pyroclastic currents, i.e., rapid granular flows at high (> 400 °C) temperature, characterized by broad and dominantly sub-millimetric grain-size spectrum, enhancing the transport of interstitial pressure and consequent friction drop. Their tsunamigenic capability is still a matter of fundamental research but claims for urgent assessment [19,20].

Constraining fluid resistance forces (pressure drag, skin friction, and added mass) may be as important as source properties (e.g. [83,84]). There are indeed still open questions also about the physics of the solid/fluid (earth, ocean, and atmosphere) coupling controlling the tsunami generation mechanisms. This includes, for instance, whether or not horizontal momentum transferred to the water body by sudden seafloor motion plays a substantial role ([85] and references therein), as well as the role played by water compressibility in generating hydro-acoustic precursors of gravity waves [86], or the generation mechanism of meteotsunamis [87,88]. Other important modelling challenges are related to tsunami shoaling inundation modelling, and thus in common to all tsunami sources. This includes, for example, phenomena that are sometimes observed, such as formation of near shore undular bores (e.g.[89]). More generally, conventional tsunami simulation typically simplifies the inundation modelling process through depth averaging the physics related to friction and boundary layer condition [64]. A recent investigation on this aspect was carried out by Qin et al. [90]. A deep understanding of these effects on tsunami hazards is still lacking.

To efficiently contribute to forecast procedures like TWS and PTHA, all the advancements in modelling techniques should also be accompanied by a synergic parallel effort dedicated to the management of existing uncertainty, both in forecasting the occurrence of the source process and in quantifying the

potential consequent tsunami, in order to increase precision without loosing in accuracy. This field is indeed a field of intense research activity [11,31,54,63,91–93], and it is particularly challenging when extending to the large variety of atypical tsunami sources (e.g. [11,17,32,54]).

As said, present TWSs primarily deal with large earthquakes occurring on subduction interfaces and were indeed created in response to tsunamis generated by this kind of seismic events [56]. This is often the case also for PTHA, because the subduction earthquakes may be thought to dominate the hazard either at the global (e.g., [94]) or at the local scale at specific places (e.g., [95]). Tsunamis generated by atypical sources are usually more local and probably less frequent than subduction zone events worldwide, and their effective hazard is more difficult to constrain, and thus it is often neglected [11,17]. Also, their forecasting in near-real-time for early warning purposes is rather challenging and not yet a well-established practice, particularly as far as non-seismic sources are concerned.

More specifically, TWSs and PTHA for seismically generated tsunamis are definitely the most advanced ones. Tsunami Service Providers (TSPs) of the IOC/UNESCO tsunami programme cover most of the seas worldwide. In the North-eastern Atlantic, the Mediterranean and connected seas Tsunami Early Warning and Mitigation System (NEAMTWS), to deal with crustal earthquakes and to deliver timely alerts also for local targets, all the TSPs operate based on decision matrices that define the alert levels solely based on the earthquake parameters (magnitude, location, and depth), the source-coast and the source-target distances. This simplifies extremely the forecasting procedure, as it ignores the specific characteristics of the source event and the asymmetric and complex tsunami propagation features while only considering attenuation with distance. For the future, more sophisticated forecasting strategies may be desired, which also explicitly deal with uncertainties (e.g., [96–98]).

PTHA for seismically induced tsunamis is, in most cases, limited to megathrust sources or based on the study of a few pre-selected scenarios ([11,54] and reference therein). In the NEAM region, a recent regional-wide hazard model (NEAMTHM18; [51–53]) has been developed, which includes crustal earthquakes making large use of High-Performance Computing (HPC) resources [31,53,66].

Tsunami early warning and hazard assessment from non-seismic sources such as landslides and volcano flank instabilities, which are closely related phenomena, are less developed than their seismic equivalents. Consequently, despite few prototypal examples of PTHA including non-seismic sources exist [11,17,32,99], a standardized approach to model the hazard and manage the warnings for tsunamis caused by such non-seismic sources does not exist (e.g. [11,17,54,65]). As discussed above, this is related both to the very large variability of potential sources, the difficulties in efficiently modelling them, and the difficulty in reasonably constraining recurrences. In addition, with reference to seismically generated tsunamis, the smaller scale of the sources and their complex dynamics require the adoption of more advanced tsunami modelling, including, for example, wave dispersion, increasing the difficulty in developing widely accepted methods. However, it is noted that important steps forward have been developed in very recent years [16–22,32,65].

For submarine landslides, which in principle could occur at any margin proximal to coastlines (as indirectly evident, for example, from the Mediterranean landslide database; [100]), there is no regional tsunami early warning system equivalent to those from earthquakes in place worldwide. We are not aware of local early warning systems either. A key challenge is the rapid quantification of a characteristic observable of the landslide, playing a role similar to magnitude in the case of earthquakes. Proposed methodologies are also scarce, although one proposed approach is the use of GPS monitoring, including measuring the flexural rebound of the lithosphere when a very large landslide is released [101]. Moreover, bottom pressure sensors should, in principle, be able to also detect the propagating wave, although not associated with similar source information as for earthquakes.

Similar issues remain for regional subaerial landslides. Yet, early warning systems are in place for site-specific local subaerial landslide tsunamis. Examples of such systems can be found in Norwegian fjords (e.g. [102]), and these are implemented in locations where there are significant slope instabilities and ongoing slope motion. These early warning systems in Norway differ significantly from conventional TWSs, as they are based on slope stability monitoring. Typically, this monitoring is extensive and consists of a range of different types of measurements, from remote characterization, microseismicity, to more local measurements using, for instance, strain and aperture motion. The early warning will be based on slope acceleration, and the alert system relies on warning the population days ahead of the expected incident. Part of the reason for this is the short travel times (can be less than 5 min) and the huge amplitudes of the tsunamis (can be even larger than 100 m run-up heights). Examples of instrumentation used for the early warning and slope characterization are reported in several publications (e.g. [103–105]). The localization of the unstable slopes makes use of extensive and continuous remote sensing techniques and is connected to a rudimentary (semi-quantitative) hazard analysis method based on the slope motion [106]. However, a firm link between tsunami hazard levels and evacuation zones are not yet in place (e.g. [17]).

Tsunami early warning in volcanic systems or for meteotsunamis face difficulties similar to the ones already discussed for landslides. Again, the main challenge is the early detection of the volcanic and atmospheric conditions that may favour the occurrence of tsunamigenic events (e.g. [10,74]). The focus on the triggering conditions is important to manage extended source areas, as for meteotsunamis, and to maximize the lead time to inundation, at the cost of increasing the uncertainty of the warning. Indeed, relying only on the tsunami signal drastically reduces the lead time for the warning, challenging the response to the warnings, at least in the near field. For example, in Norway, it has been decided that, because this lead time is too short, TWSs should not be based on the tsunami measurement but should rather be issued well in time of the slope failure. Obviously, this has implications for possible high numbers of false warnings and evacuations, as apparent from experience with the Mannen slope failure in Norway, where the local population has been evacuated many times before the slope failure actually happened. To monitor extended source areas, the alternative approach of direct detection of the tsunami waves is also challenging, since it might need very densely distributed measure points (DART - Deep-ocean Assessment and Reporting of Tsunamis, tide-gauges, elastic beacons, IDSL - Inexpensive Device for Sea Level Monitoring, etc.), with sufficiently high rates of sampling to measure the higher frequencies typically generated by non-seismic sources. Measure points must be densely distributed since an already propagating tsunami may reach inhabited areas in a few minutes; thus, very early detection is required. In this, it is interesting to note that a parallel can be drawn with near field first alert from seismic TWSs, which is only based on earthquake detection, and for which both near-field monitoring and automatizations are very important [107–109]. For tsunamis, however, even with high quality and spatially dense data, the characterization of such sources from these signals could be excessively expensive and technically challenging too. At local level and for well-defined tsunamigenic sources, a combined approach based on both tsunami detection and source monitoring may instead be adopted, as in the case of the Stromboli TWS, which will be discussed in detail below.

The central position of Italy in the Mediterranean and the evident importance of atypical sources for Italian coasts stimulated the scientific community and decision-makers to develop innovative procedures that progressively extended tsunami hazard analyses and warning systems to such atypical sources. The Italian national warning system for seismically generated tsunamis (Sistema di Allertamento nazionale per i Maremoti - SiAM, which includes the Italian National Civil Protection (DPC), the Istituto Superiore per la Protezione e la Ricerca Ambientale (ISPRA), and the Istituto Nazionale di Geofisica e Vulcanologia (INGV) [110] deals with all potential seismic sources in the Mediterranean basin, including both subduction and crustal seismicity. The upstream component of the SiAM, the CAT-INGV (Centro Allerta Tsunami of INGV;

http://www.ingv.it/cat/it/, [111,112]) is also a TSP (Tsunami Service Provider) of the North-eastern Atlantic, the Mediterranean and connected seas Tsunami Warning System (NEAMTWS), coordinated by the Intergovernmental Coordination Group established by the Intergovernmental Oceanographic Commission of UNESCO. Also, coastal planning for SiAM is defined considering non-subduction zone earthquakes, being based on a regional PTHA including them [31,51–53,62,63]. Another local warning system is dedicated to tsunamis generated by collapses occurring within the volcanic system of Stromboli. This system represents, to our knowledge, the only fully operational tsunami warning system for volcano sources. It has been operational since 2003, and it combines activations related to the early detection of the volcanic conditions that may lead to a tsunami with activations triggered by the early detection of the tsunami wave signal in the very near-field. Two recent small tsunamis, generated in 2019, challenged the system, providing the first indications for its further developments.

Here, we first introduce the general framework in which tsunami threats are treated by briefly reviewing the tsunami forecasting methods and the tsunami generation and propagation modelling techniques. Then we present the tectonic settings for the Mediterranean region in some details (Section 2). Next, we discuss the state of the art and the planned developments of tsunami monitoring and tsunami warning systems in Italy (Sections 3 and 4), with specific reference to the treatment of atypical sources and related uncertainty. Starting from the existing records of historical tsunamis, we also offer a brief overview of the present state of knowledge about the most important sources for tsunamis that are not yet considered in present-day tsunami warning systems in Italy (Section 5). Finally, we outline the potential scientific paths toward the improvement of the efficiency and the source coverage of the tsunami warning service (Section 6).

2. Tsunami hazard modelling

2.1 Probabilistic Tsunami Hazard Analysis and Tsunami forecast for warning

Tsunami forecasting for TWSs and PTHAs are both forecasting techniques, where PTHA is focused on quantifying the long-term probability of exceedance of different tsunami intensities in the next years (usually tens of years) due to whatever tsunami that may occur, while tsunami forecasting for TWSs is instead oriented to forecasting the impact of an ongoing event.

Historically, tsunami forecasting procedures were based on numerical modelling of the tsunami generation and propagation process of one or a few scenarios. In the 1980s, some pioneering studies started better considering the source variability (e.g. [113–115]), as well as their probability of occurrence in the future. The occurrence of the 2004 Indian ocean tsunami, as well as the 2011 Tohoku tsunami, gave momentum to the development of more robust tsunami forecasting procedures, both for the management of the tsunami warnings and the development of appropriate planning strategies based on tsunami hazard, leading to the full establishment of probabilistic forecast approaches, progressively better and better incorporating uncertainty (e.g., [31,52,53,94,95,116–130]).

Taking as a reference the equivalent development in the seismological field (e.g., from [131]; a recent review can be found in [132]), the attention was initially focused on the long-term forecasting procedure, namely on the Probabilistic Tsunami Hazard Analysis (PTHA; a recent review can be found in [11]). These studies mainly concentrated on seismically generated tsunamis (often named SPTHA) since they represent the most common source for tsunamis (> 75%, [36,133]) and also because SPTHA could be rooted in techniques already developed for seismic hazard (e.g., [116,130]). Progressively, SPTHA specialized in treating the peculiarity of tsunami sources and managing its inherent uncertainty, like techniques to account for the sensitivity of tsunamis to source magnitude, depth, and geometry or procedures to reduce the computational effort of inundation modelling (e.g., [31,94,95,134,135]).

The long-term forecast of PTHA consists of quantifying at each point *x* of the target domain the hazard curves, reporting the probability of exceeding different levels of tsunami intensity (using specific intensity measures like, for instance, wave height, momentum flux) at least once in a time window ΔT, called exposure time. The hazard curves are usually evaluated in two steps. First, the mean annual rate of exceedance is evaluated by combining a "source factor" with a "propagation factor", that is:

$$\lambda(z > Z; x) = \int_{\Sigma} P(z > Z; x|\sigma)\, \lambda(\sigma) d\sigma \approx \sum_i P(z > Z; x|\sigma_i)\, \lambda(\sigma_i) \quad (1)$$

where the source factor $\lambda(\sigma)$ represents the mean annual rate of the source scenario σ, the propagation factor $P(z > Z; x|\sigma_i)$ represents the exceedance probability at the target position *x* of the intensity *Z*, conditional upon the scenario σ, and the integration is made over the space Σ containing all possible scenarios. The computation is usually performed over a discrete set of scenarios, as illustrated with the approximation by a discrete series in the right-hand side of eq. 1.

This type of approach, which combines source observations with numerical tsunami simulations, is most often preferred for direct quantification of tsunami hazard based tsunami observations, as they are typically few and sparse and hardly can represent the full variability of potential sources [11,54,65,116,136]. The evaluation of the source factor is based on seismic historical catalogues, geological constraints, and existing statistical laws (e.g., the Gutenberg-Richter distribution controlling the relative abundance of small vs. large earthquakes; [137,138]). This term is in many ways similar to the equivalent term in seismic hazard, with the difference that more parameters should be considered to describe tsunami generation (e.g., fault geometry and mechanism). The propagation factor is instead mainly based on the numerical modelling of tsunami generation, propagation, and inundation (see next section). This is very different from the seismic hazard, where this task is usually performed adopting empirical laws, the Ground Motion Prediction Equations (e.g., [139]). This is required to account for the tsunami impact patterns that are largely path-dependent. Yet, for the inundation phase, a stochastic approach to coastal evolution is sometimes introduced, based on tsunami observations and on numerical simulations (e.g. [94,140]), as discussed in Section 3.1.

The probability of exceedance in ΔT is then quantified assuming that exceedance events are independent and occur randomly in time with a constant annual rate (stationary Poisson process) so that the probability of having one or more exceedances in ΔT can be evaluated as:

$$P(z > Z; x, \Delta T) = 1 - e^{-\lambda(z>Z;x)\Delta T} \quad (2)$$

that is, it is evaluated as one minus the probability of no exceedances in ΔT. As we will discuss in the next sections, intensity values to design long-term risk reduction measures (e.g., building codes, evacuation zones, etc.; [58,60–62]) are defined either in terms of probability of exceedance in ΔT or equivalently in terms of the mean return periods (often called average return periods - ARPs, reciprocal of $\lambda(z > Z; x)$ of eq. 1). For example, seismic hazard design intensity usually corresponds to an exceedance probability of 2% or 5% in 50 years, corresponding to average return periods of 2475 and 475 years, respectively [132]. As discussed in Section 3.3, a common choice for the definition of evacuation areas for TWS is an average return period of 2500 years [60–62].

Given that hazard quantifications may be related to significant regulatory concerns, usually also the uncertainty on the hazard model is explicitly quantified [141]. This uncertainty is evaluated producing a number of alternative but "scientifically acceptable" models, that is a number of alternative estimations of

$\lambda(z > Z; x)$. Such alternatives are usually not considered completely equivalent; rather, their different "credibility" is expressed by assigning weights to them in some specific framework. Different approaches have been developed to deal with this problem, ranging from logic trees to Bayesian and ensemble approaches [141–145]. This uncertainty is usually called *epistemic uncertainty,* as it arises from incomplete knowledge, giving rise to alternative models of nature, in contraposition to the so-called *aleatory uncertainty* arising from the natural variability of the phenomena [146]. Typically, epistemic uncertainty emerges from alternative models for the tsunami generation and propagation, alternative input and boundary conditions for source and propagation models, as well as alternative statistical distributions to describe the natural variability, for example, of the source (e.g. [11,53,54,116]). In principle, the epistemic uncertainty is reducible as new data and more accurate models become available, while aleatory uncertainty is not reducible, being related to the natural unpredictability. For this reason, epistemic uncertainty is usually kept separated, and represented as families of hazard curves and related statistics (mean hazard, percentiles, etc.; [11,132,143,146]).

Tsunami warning systems base their operational procedures on quasi-real-time tsunami forecasting of a possibly already ongoing tsunami. Nowadays, tsunami warning systems targeted to trans-oceanic seismic tsunamis (with travel times on the order of hours) are mostly based on the evaluation of the potential impact of one or few scenarios, selected inverting seismic and/or off-shore tsunami measures (e.g., [56]). When treated, near-source tsunami warnings are usually issued either based solely on source parameters or on near-source tsunami detection [59,147–151]. Source parameters are often used as input to decision matrices that link magnitude, epicentre, and depth to tsunami intensity and alert levels. Such alert levels are usually also linked to specific actions in response to the tsunami (see, for example, Sections 3.3 and 4.3). Quantitative and explicit management of the uncertainty affecting the short-term tsunami forecasting is still lacking, even if its importance has been already clearly acknowledged for a long time [96,97]. To this end, two main directions are being explored. On the one side, technologically-driven improvements of the monitoring network may and likely will substantially improve the time and accuracy of source parameter determination and tsunami detection [152,153]. On the other hand, formal procedures to quantitatively manage forecast uncertainty have been developed (e.g., [67–69,154–156]) to be appropriately shaped for real-time use and accurately and systematically tested against real-data [68,69,157]. These probabilistic methods, similarly to long-term hazard, may be transparently connected to decision making for tsunami early warning, allowing for the separation between the scientific forecast regarding the hazard intensity and the political choices regarding safety levels and management of existing uncertainty [68,69,158,159].

2.2 Tsunami generation and propagation models

Numerical hydrodynamic modelling of tsunami evolution is an essential step of tsunami forecast procedures. Tsunami modelling consists of three fundamental steps: i) the tsunami generation process, ii) the propagation of the gravity waves generated by the source in the open sea/ocean, and iii) the land inundation. A general review of modelling approaches and present-day challenges in the context of hazard and risk analysis can be found in [11,54] and in the references reported therein.

2.2.1 Tsunami generation models

The first step in tsunami modelling is the definition of the source and generation mechanism. The most common sources for tsunamis are earthquakes, landslides, volcanic eruptions, and meteorological perturbations of the sea surface [11].

Earthquake sources generate tsunamis mainly by sudden deformations of the seafloor, inducing a disturbance of the overlying water body, which can be approximated as a sudden change of its potential energy. Tsunamigenic strength is primarily controlled by the fault dislocation (slip) and rupture areal extent

(proportional to the seismic moment and hence linked to the magnitude), the geometry and the dynamics of the fault displacement, as well as the depth of the fault and the distance from the coast. Also, more complex features of the seismic source may have primary effects, like, for example, the spatial variability of dislocations (causing local slip concentrations) as well as spatiotemporal evolution of the seismic rupture, especially for large earthquakes featuring slow ruptures [160]. Seafloor deformation is modelled based on principles of continuum mechanics. Analytical expressions to calculate crustal deformation due to buried planar faults with instantaneous uniform slip in an elastic half-space exist [161,162], still representing a standard in many applications as they can also be extended to incorporate heterogeneous time-dependent slip in a simplified way. More advanced modelling approaches account for the details of Earth rheology, for example, considering layered elastic properties or even 3D variations through finite element models or models defining heterogeneous slip ruptures over non planar faults [93,163–169]. While until recently tsunami forecasts were mainly based on the most simplistic approaches (uniform slip over planar faults), the recent scientific and technological advances allowed for the gradual inclusion of more complex modelling strategies [66,67,164,168,170], which made it imperative to cover complex slip distribution that can have first-order effects on the hazard. Even with these recent developments, many issues about seismic source modelling remain open [54], mainly related to the scarce knowledge about faulting, especially offshore, and to the variety and complexity of fault mechanics, with difficult-to-constrain features like slip distributions, potential surficial amplifications, slow events generating unusually large tsunamis (so-called, tsunami-earthquakes, [15]), characterized by relatively slow dislocations.

Landslide sources vary from large submarine slides to more localized submarine landslides and subaerial landslides that enter the sea. As for the seismic case, the tsunami is primarily generated by the volumetric water displacement. Contrary to seismic sources, the time-dependent motion of the landslide plays a fundamental role in tsunami generation. Consequently, advanced models of tsunami generation from landslides should consider the landslide dynamics [16,18]. The main governing factors of landslide sources are acceleration, speed, volume, water depth, and geometrical configuration [16,171,172]. However, the generation mechanisms for submarine and subaerial landslides are distinctly different (e.g., the discussion in [17]. Submarine landslides are particularly sensitive to water depth and acceleration, hence not only the landslide dynamics is important, but also the slope failure rate and the mass mobilization rate, including remolding (e.g. [82,171–174]). Subaerial landslides may impact the water at high speed, causing a different tsunami generation mechanism compared to submarine slides. The generation mechanisms scale non-linearly to the frontal area, Froude number, slope angle, and material density (e.g. [175–178]). Advanced tsunami generation models include the modelling of the landslide internal dynamics, with terms describing landslide rheology and density of different kinds, from viscoplastic models to frictional collisional models of different complexity and spatial averaging (e.g. [77–80,82,179]).

Volcanic sources are diverse and include source mechanisms occurring on all volcanic phases, that is, in quiet periods, unrest episodes, as well as during eruptions. Tsunamigenic phenomena include slope failures and landslides, volcanic earthquakes, lahars - mudflow or debris flow composed of pyroclastic material - entering the water, as well as underwater explosions, pyroclastic flows, shock waves, or caldera subsidence [11,20,180–183]. Notably, different potentially tsunamigenic processes can even concur in the tsunami generating phase, especially during large caldera-forming eruptions [20]. Similar to landslides, most of these source types require the joint modelling of source events and tsunami generation. However, some empirical models for some of these sources (e.g., explosions for which the water cavity scales with the energy forming the volcanic craters; e.g. [32,184–187]), provide reasonable approximations also in the near field. Notably, some of these source processes overlap with seismic and landslide sources, like volcanic earthquakes, or flank collapses, slope failures and even pyroclastic flows [16,20], even though the peculiar material properties of volcanic systems and their potential transformations during the flow may force toward the development of ad hoc modelling strategies.

Strong, high-energy atmospheric phenomena may produce significant sea-level responses over a broad frequency band, which may generate significant oscillation due to resonance in the range between few minutes to hours [21,87,188,189] with dynamics significantly similar to tsunamis and different from wind-related long periodic storm surges. A very useful review of the processes underlying the generation of meteotsunamis can be found, for instance, in [88,190]. A moving atmospheric pressure disturbance and the related inverse barometer effect are the main driving source mechanisms. For a meteotsunami to be generated, the moving atmospheric pressure disturbance must attain suitable values in terms of magnitude, velocity (and hence of Froude number), duration and wavelength of the disturbance itself to be able trigger resonance phenomena, the most important of which is the Proudman resonance. Other, additional amplification mechanisms can occur when the pressure disturbance acts in the alongshore direction amplifying specific edge wave modes (Greenspan resonance) or due to topographic effects. In turn, the parent moving atmospheric pressure disturbance can be associated with very different atmospheric processes, such as squalls, thunderstorms, tropical and extratropical storms, atmospheric gravity waves. As each of these phenomena are often more frequent in specific geographical areas than in others, the processes that lead to the generation of a meteotsunami tend to be unique to a particular region, making them more frequent in favourable areas like Adriatic and the Baltic Seas, or the East Coast of the United States [22,191,192]. The tsunami generation may be modelled with coupled atmosphere-ocean models or coupling numerical wave propagation models with some source and parameter combination (e.g., [193,194]).

Other less frequent tsunami generating events exist. Among them, it is worth noting tsunamis generated by asteroid impacts, for which the source process scale from large impacts causing dry seabed to smaller events causing a surface cavity due to the direct impact of the asteroid or to its explosion near to the sea surface [11,195–200]. Notably, especially for large-scale events, specific modelling approaches, including multi-phase (air, water, and solid) dynamics, are required to handle the thermodynamics and turbulence of the tsunami generation.

An important aspect of the deep-water tsunami generation process is that the water column here effectively works as a low-pass filter, suppressing short wavelengths (shorter than several times the water depth; [201]). For large earthquakes, this is only a relative problem, being dominated by long wavelengths, except perhaps for slip reaching at the trench in subduction zones (see anyway [202] and references therein for analytical treatment of the generation of tsunamis by underwater earthquakes). On the contrary, smaller earthquakes, but particularly in deep-water landslide sources, needs the introduction of low pass filters, with an efficiency that increases with depth and wave-number [41,76,201,203], to be applied at each step of the source evolution to avoid the introduction of short wavelengths determined by rapid accelerations in source dynamics. Recently, some authors performed 2D fully coupled earthquake and tsunami simulations of the subduction zones, documenting the smoothing effects induced by the nonhydrostatic response of the ocean at short wavelengths [204]. For landslides, unless a fully coupled multiphase Navier-Stokes model is used, filtering sources needs to be applied sequentially, which adds an additional computational burden (e.g. [16,171]).

2.2.2 Tsunami propagation and inundation models

The first numerical tsunami modelling procedures were developed in the early 80'ies [205,206], with the development of the first models based on a time-stepping scheme to solve the shallow water equations. To date, a large number of models have been developed, along with benchmarking and validation procedures against exact solutions for simplified problems, laboratory experiments, and/or past tsunami events (e.g., [207,208]).

The full three-dimensional Navier-Stokes equations are only rarely used for tsunami simulations: typically, they are needed only when non-hydrostatic and non-linear effects may be relevant [209]. The effect of the curvature of the earth and of the Coriolis acceleration have only a minor impact on tsunami propagation [210] and they are usually neglected, but in very large domains to model trans-oceanic propagation where they play a more significant role. More commonly, different approximations are adopted based on the physics of the problem, with the purpose of making it computationally more accessible to enable a faster exploration of source variability. For most tsunamis, the vertical structure can be neglected, and two-dimensional depth-averaged systems of equations can generally be used, such as dispersive Boussinesq type or non-dispersive shallow-water approximation. In the deep sea, such equations may be linearized, being wave amplitude much smaller than sea depth, while the nonlinear shallow water equations should be solved approaching the shore (at depth < smaller than few tens of meters). This approximation is appropriate for sources dominated by long wavelength (e.g., large earthquakes), while strategies to include the vertical structure and to keep additional non-linear terms in asymptotic expansions are required for smaller and non-instantaneous sources like landslides and volcanic sources, as well as when nearshore coastal interaction and wave-induced currents in restricted environments (such as harbours or fjords) are significant. Many different sets of depth-averaged dispersive equations and layered non-hydrostatic models have been proposed through time to address these sources, often adopting dispersive Boussinesq solvers with more sophisticated numerical solution techniques (e.g., [211–220]).

Shoaling and inundation models are based on high-resolution bathymetric and topographic data, either including features such as buildings or vegetation or using Manning's roughness coefficients for accounting for their presence and, more in general, for the bottom friction. At the same time, inundation details may be sensitive to characteristics of the source, especially but not only in the near-field (e.g. [168,221]), thus, an appropriate level of details in the source process should be adopted depending on the distance of the source and characteristics of the target (see also [65]). Given the impossibility of extending high-resolution modelling techniques to entire basins, telescopic grids and different levels of approximations are usually adopted in the different phases of the propagation process. Non-linear shallow water models are most frequently used for this purpose (e.g., the review [64]); Boussinesq model applications are used as well, despite that they are more prone to instabilities (see discussion in [222]). Despite the relatively high accuracy of these modelling techniques, large uncertainty still exists (e.g., [54,63,70,93,128,223]), and the potential impact of uncertainty in initial/boundary conditions or of different modelling techniques still have to be fully understood.

Source characteristics are the primary driver for the selection of the appropriate modelling strategy. Tsunamis generated by large earthquakes are dominated by long wavelengths. These waves propagate more efficiently, reaching transoceanic distances, and are, in first approximation, non dispersive. On the contrary, landslide and volcanic sources, even if they encompass a broad range of source size, mostly generate localized tsunamis dominated by short-period waves with greater dispersion and limited far-field effects compared to earthquake-generated tsunamis (e.g., [19,92,185,224–234]). Large volcanic explosions (e.g., caldera forming eruptions) and oceanic impacts of large asteroids may produce huge waves for which non-linearity may play a significant role for hundreds or even thousands of kilometres [199], with significant dispersive behaviours [198].

Boundary conditions also play a role. A typical computational domain used in tsunami simulations involves both offshore and coastal boundaries. In principle, tsunami waves should be fully transmitted through an offshore (open sea) boundary. In practice, the numerical implementation of these boundary conditions can lead to undesired effects, such as spurious reflections. To overcome this problem, several techniques have been proposed, including radiation conditions and absorbing layers (such as sponge layers and the

"perfectly matched layer" method; see for instance [235,236] for a detailed discussion). The applicability and effectiveness of either methods is often dictated by the equations to be solved (shallow water, Boussinesq), by the specific numerical method adopted to solve the equations and by the geographical extension of the computational domain. The coastal boundary is treated in different ways depending on whether shoaling and inundation must be accounted for or not. In the first case, the complexity of the problem can vary significantly depending on whether the inundation process is simulated over a simplified topography or more realistic effects such as turbulence and the interaction with built environment must be taken into account: for the scope of this paper, it will be sufficient to address the interested reader to the review by Qin et al. [90]. To avoid unnecessary modelling of shoaling and inundation, reflecting boundaries are often used at shore-lines, with nearshore bathymetry corrections to manage, for example, minimum water depths. Since these conditions may introduce spurious reflections, a number of different approaches have been developed to manage such boundary conditions (e.g. [237]).

In regional studies, where inundation modelling is generally avoided, propagation modelling is stopped at the limit of linear shallow water approximations, that is several tens of meters depth (usually between 10 and 100 m, [11]). Then, amplifications models are applied to estimate the potential tsunami intensity (e.g., run-up) inland, ranging from a Green's law accounting for shoaling up to a bathymetric reference level, models amplifying solitary waves (e.g. [238,239]) or N-waves (e.g. [240–242]), or more advanced amplification models that account for the local bathymetric profiles and main characteristics (e.g. dominant period and polarity) of the incoming tsunami waves [140,243].

The availability of topographic and bathymetric data with suitable resolution and the capability of implementing them on properly built computational grids is a key yet often neglected aspect of any propagation and inundation modelling strategy. While this appears to be obvious when dealing with inland inundation, it is important to stress the importance of this aspect also for the propagation phase, where typical wave-related phenomena, like refraction and diffraction induced by the sea-bottom morphology, can be properly captured only by proper-resolution bathymetric data and computational grids.

2.3 Tectonic setting of the Mediterranean region

The Mediterranean region is characterized by basins and orogens resulting from a complex tectonic history started with the opening of oceans during the breakup of Pangea in the Triassic (~ 250 million years ago), then followed by subduction and collision accommodating the convergence between the African (or Nubian) and Eurasian plates since the Jurassic (~ 200 million years ago) [244]. Subduction also generated back-arc basins in the upper plate, leading to the formation of extended continental crust or even new oceans, such as the Gulf of Lion Basin, the Algerian Basin, and the Tyrrhenian Basin in the western Mediterranean [244]. As of today, the tectonic activity within the Mediterranean region is mainly driven by the still active convergence between Africa and Europe, in which the deformation pattern is further complicated by the presence of smaller plates (like the Aegean and Anatolian plates) or promontories (like the Adriatic block). A sketch map of the Mediterranean seismotectonic settings is reported in Figure 1.

The boundary between the African and Eurasian plates takes a different character from place to place. From west to east, in southern Spain and northern Morocco across the Gibraltar Straits, one finds the Betic-Rif orogen surrounding the Alboran Basin. Then the Maghrebides orogen characterizes the western part of northern Africa from Morocco to Sicily and the Messina Straits. Next to the Messina Straits, southern Italy, the Calabrian Arc subduction accommodates the NW-directed subduction of the Ionian Basin lithosphere. Then the plate boundary bends sharply by wrapping around the Adria microplate, a promontory of the African plate and common foreland of the collisional belts of the East-directed Apennines, characterized by an extensional and contractional pair, the Alps, and the West-directed Dinarides, Albanides, and Hellenides.

Here the plate boundary changes again its character into subduction with the Hellenic and the Cyprus Arcs, where the African plate is overridden by the Aegean and Anatolian plates (comprising Greece, Cyprus, and Turkey). The rates of convergence across the three subduction zones of the Mediterranean (Calabrian, Hellenic, and Cyprus Arcs) are in the order of few millimetres per year in the Calabrian Arc and in the eastern part of the Cyprus Arc [245–248], and of few tens of millimetres per year in the Hellenic Arc and in the western part of the Cyprus Arc [247,249–251]. All other orogenic belts, in general, accommodate only a few millimetres per year of contraction. Extension in the order of a few millimetres per year characterizes the axis of peninsular Italy (inner Apennines chain) and the Aegean region, with faster extension rates in the Gulf of Corinth.

This complex geological setting is associated with frequent and intense seismicity throughout the Mediterranean basin. Offshore earthquakes in the region include different types of events: from subduction-related earthquakes, in the Calabrian, Hellenic, and Cyprus arcs, to crustal events, on thrust faults belonging to the Maghrebides, Apennines, Dinarides, Albanides, and Hellenides fronts, on normal faults in the Messina Straits, the Aegean Sea, and Corinth Gulf, and on strike-slip faults such as the Kefalonia-Lefkada (Ionian Sea), Paphos (Cyprus), and North Anatolia fault (Aegean and Marmara Seas). In association with this complex tectonic setting of oceanic and continental subduction/collision, several volcanoes have developed throughout the Mediterranean region, including syn- and post-orogenic volcanoes, many of which lie near the coasts or directly on the seafloor. Most of the active volcanoes are located in the back-arc of the Calabrian and Hellenic Arcs, in the Tyrrhenian and in the Aegenan seas, along with few other important volcanoes such as Mt. Etna, which is one of the most active volcanoes in the World, Mt. Vesuvius, Campi Flegrei, and Ischia in the Tyrrhenian coasts of southern Italy, as well as several volcanic edifices in the Sicily channel.

For the subduction-related events, either on slab interface or splay faults, magnitudes as high as 8+ have been hypothesized based on inferences from historical and geological data [252,253]. For crustal events occurring outside subduction zones, the maximum recorded magnitudes are slightly below magnitude 8, but with high tsunamigenic potential due to shallow faulting and dip-slip motion (when faulting mainly induces vertical displacement), as for the 1908 Messina-Reggio Calabria M7.1 or the 1956 Amorgos M7.8 earthquakes. Indeed, for both events, a tsunami run-up of up to 13 m and 25 m was reported, respectively [254–257]. It is possible that some of these events have triggered landslides, as hypothesized for the 1908 case [50,255,258] and for the 1956 case [257,259], that could have increased the tsunami impact. More information about the past seismicity and the tsunami records in the Mediterranean area have been systematically collected in several historical and instrumental catalogues [36,45,260–263].

3. Tsunami warning for earthquake-generated tsunamis

In the following sections, we briefly discuss hazard quantification, coastal planning, and tsunami warning in Italy for what it concerns seismic sources. Particular attention is given to the specific management of crustal sources, which constitute the large majority of potential tsunami sources in the Mediterranean.

3.1 Hazard quantification

The NEAM region (Northeastern Atlantic, the Mediterranean and connected seas) has its own recent S-PTHA model, called NEAMTHM18 (NEAM Tsunami Hazard Model 2018; [51–53]), produced by the TSUMAPS-NEAM project (http://www.tsumaps-neam.eu/). NEAMTHM18 is a hazard model obtained through the collaboration of a large scientific community, with the goal of building the input for a common and homogeneous strategy for tsunami risk management in the region. The methodology employed and the results are documented by Basili et al. [52,53].

672
673 NEAMTHM18 considers subduction zones and both inter-plate crustal seismicity (including oceanic ridges)
674 and intra-plate diffuse seismicity. Subduction zone seismicity in the accretionary wedge, the continental
675 crust, including splay faults, and outer-rise earthquakes in the oceanic crust are also included. As a general
676 rule, NEAMTHM18 assumes that crustal earthquakes can take place everywhere. Only in few areas, when
677 the regions are very stable and hence the seismicity rates are very low, the intraplate seismicity is
678 disregarded, as in the oceanic crust in the Atlantic Ocean far from the ridges and other principal faults. No
679 such areas are present in the Mediterranean.
680
681 The knowledge of the potential earthquake sources is somehow limited in many areas, and certain faults
682 are known better than others [14]. To optimally deal with this heterogeneous degree of knowledge while
683 maximizing the use of all the available information, the seismicity is subdivided into two categories,
684 background seismicity, used for treating crustal earthquakes, and predominant seismicity, used for dealing
685 mainly with subductions. Either type of seismicity adopts a different modelling approach for one or more
686 parameters. Some values of the earthquake parameters can even be set constant when their variability is
687 considered negligible with respect to other parameters. One example is fault geometry on subduction
688 interfaces, which can be considered relatively well constrained with respect to other source parameters.
689 This approach to seismicity types in probabilistic calculations was introduced into SPTHA by [31], in line
690 with other approaches introducing faults into Probabilistic Seismic Hazard Analyses [264–266].
691
692 The sources considered, when focussing on the coasts of Italy, may be restricted to those located within the
693 Mediterranean basin. Three subduction zones are taken into account (the Hellenic Arc, the Calabrian Arc,
694 and the Cyprus Arc, the latter probably representing a relatively minor threat for Italian coasts). The
695 subduction zone characterization and modelling in NEAMTHM18 are detailed in several papers
696 [52,53,164,267,268]. We only note that a magnitude range from 6.0 to 9.1 over the 3D subduction
697 geometries is used, and different alternatives are sampled for building slip distributions, including depth-
698 dependent rigidity hence potentially enhanced shallow slip. The background crustal seismicity is instead
699 modelled everywhere on a regular grid covering the entire Mediterranean, considering a magnitude range
700 from 6 to 8.1, a depth range from the surface to the Moho, and 144 potential focal mechanisms exploring
701 the variability of the strike, dip, and rake, for a total of more than 10^3 scenarios in each grid point. At each
702 node of the grid, the distribution of faulting mechanisms is constrained by moment tensor catalogues and
703 mapped faults [31]. Collectively, the number of subduction and background scenarios explored is very large
704 ($> 10^7$), the majority of which are background seismicity. Hazard disaggregation results show that for the
705 largest part of the Italian coasts, the background seismicity dominates over subduction seismicity,
706 especially at the largest tsunami intensities [31,52,53], demonstrating the importance of including atypical
707 sources in areas like the Mediterranean.
708
709 Tsunami propagation from each individual source is modelled up to a set of Points Of Interest (POIs).
710 Considering the challenging number of individual scenarios, an ad hoc computational strategy has been
711 adopted [66], mainly based on the tsunami wave reconstruction in the deep sea with linear combinations
712 of elementary Gaussian sources or in some cases rectangular subfaults, modelled with the Tsunami-HySEA
713 code (a finite volume solver for the non-linear shallow water equations developed for multi - Graphics
714 Processing Unit- architectures; [269]) into a High-Performance Computing (HPC) environment. The POIs
715 have been selected offshore approximately on the 50 m bathymetric line at a distance of approximately 20
716 km from each other. POI locations can be considered representative of a roughly 20 km long stretch of the
717 coast behind them. Tsunami inundation is evaluated by adopting an amplification model that considers the
718 tsunami characteristics (polarity, dominant period, and wave height) at the POI and the local bathymetric
719 profile. The significant uncertainty introduced by this simplified model for inundation is propagated into the
720 PTHA results.

The tsunami intensity is measured in terms of the Maximum Inundation Height (MIH; [94,140]). MIH is the maximum height reached by the water with respect to the sea level at rest (water + topography) on profiles orthogonal to the coast, and thus it can be higher than the run-up (maximum topographic altitude reached by the flood). MIH then represents the maximum inundation height averaged along the ~20km long stretch of coast represented by each POI. It follows that the locally maximum MIH and run-up values can be (up to 3-4 times) larger than those indicated by the hazard model, for example, due to tsunami energy focusing by topographic features [53,62,140].

In agreement with the PTHA approach, NEAMTHM18 evaluates results in terms of a suite of hazard curves, reporting the probability of exceeding different MIH values in 50 years in each POI (**Figure 2**). More specifically, NEAMTHM18 provides mean hazard curves, and the model uncertainty is reported through different curves at different percentiles (**Figure 2b**).

Being the most recent available hazard model, including all Italian coasts, NEAMTHM18 was adopted as a starting point for the Italian national coastal planning for seismically-generated tsunamis [62], while working on a national hazard model (see Sections 3.3 and 3.4). NEAMTHM18 is indeed the only one today that uses a homogeneous approach over the entire Italian coast, and which deals with all types of seismic sources. Cautious usage of the model is suggested when used for local planning due to the relatively coarse spatial scale of tsunami probability output and the relatively coarse sampling of the source parameter variability. Both scales of discretization are suitable for a large (NEAM region) scale model but certainly less well-calibrated for local (national) scale hazard analysis. For this reason, the practical use of NEAMTHM18 in coastal planning has been integrated with a specific strategy to account for its spatial resolution (Section 3.3).

3.2 Italian Tsunami Warning System for seismically-induced tsunamis

After the 2004 Indian Ocean tsunami, the UNESCO IOC (Intergovernmental Oceanographic Commission) has coordinated the birth and growth through the establishment of four ICGs (Intergovernmental Coordination Groups) to steer the TWS, covering all the oceans and seas worldwide. The NEAMTWS deals with tsunamis in the North-East Atlantic, the Mediterranean and connected seas (http://www.ioc-tsunami.org/). In the NEAMTWS, five national tsunami warning centres operate as Tsunami Service Providers (TSP) in different and partially overlapped subregions, providing tsunami alert messages to member States. All TWSs of NEAMTWS TSPs and of the other ICGs activate only for seismically induced tsunamis. The 5 NEAMTWS TSPs are KOERI (Kandilli Observatory and Earthquake Research Institute, http://www.koeri.boun.edu.tr/new/en), NOA (National Observatory of Athens, http://www.gein.noa.gr/en/), CENALT (CENtre d'Alerte aux Tsunamis, http://www.info-tsunami.fr/), IPMA (Instituto Português do Mar e da Atmosfera, https://www.ipma.pt/en/), and CAT-INGV (Centro Allerta Tsunami of INGV, http://www.ingv.it/cat/en/).

CAT-INGV operates as NTWC (National Tsunami Warning Centre) for the whole Mediterranean region (**Figure 3a**), from Gibraltar to Eastern Mediterranean, and serves as NTWC and as TSP for the DPC and for several member States of UNESCO and European Institutions. CAT-INGV started monitoring the Mediterranean Sea in autumn 2014 as a candidate TSP. Monitoring at a global scale is also performed as a permanent training activity. Dedicated personnel are present on a 24/7 basis at the Seismic Surveillance Room of the INGV in Rome, assisted by a supervisor officer on call H24.

After some years of pre-operational mode, CAT-INGV has been accredited as TSP by IOC/UNESCO in 2016, including the entire Mediterranean Sea in its monitoring area for tsunami sources. Since then, it has

delivered 9 Information messages and six tsunami alerts, including 2 Advisory messages and four local Watch messages for earthquakes with a magnitude between 5.7 and 7.0 that occurred in the Mediterranean region [111,112]. As all the five accredited Tsunami Service Providers (TSPs) of the NEAMTWS, CAT-INGV is in charge of providing tsunami forecasting when earthquakes of magnitude greater or equal to 5.5 occur in their monitoring area. TSPs use combinations of global, regional, and national seismic and tide-gauge networks.

In Italy, the national seismic tsunami warning system for the Italian coasts (SiAM - Sistema di Allertamento da Maremoti) operates since January 2017 [110] (http://www.protezionecivile.gov.it/en/risk-activities/tsunami-risk/activities). Seismic monitoring, first alerting, and tide-gauge analysis are carried out by CAT-INGV, based on predefined and agreed rules. As in all NEAMTWS TSPs, CAT-INGV's tsunami forecasting relies on a decision matrix that converts the main earthquake parameters (hypocentral location and magnitude) into alert levels at predefined forecast points along the potentially threatened coastal locations. Forecast points generally correspond to the locations of sea-level gauges and/or to highly exposed/vulnerable locations. The national mareographic network (Rete Mareografica Nazionale, RMN, https://www.mareografico.it/) is managed by ISPRA. CAT-INGV communicates alerts to DPC, which is in charge of the dissemination to the operational structures and components of the National Civil Protection Service, aiming at reaching, in the shortest possible time, the population who would be potentially affected.

In NEAMTWS and in SiAM, two alert levels are foreseen:

- Advisory/Orange: the detected seismic event could produce a tsunami wave height <= 0.5 m in front of the coast and run-up <= 1 m above the sea level; this may represent a marine and near-coast tsunami threat;
- Watch/Red: the tsunami wave height is expected to be > 0.5 m in front of the coast and the run-up > 1 m above the sea level; hence, it may cause a significant inundation.

Moreover, information messages are sent when significant earthquakes (M >= 5.5) occur in the competence area, but it is unlikely that a tsunami will impact the coast because, according to the decision matrix, the seismic event is evaluated as not able to produce a tsunami wave that represents a relevant threat for the exposed coasts.

There are two different decision matrices, for the Mediterranean and for the North-East Atlantic. Moreover, slightly different decision matrices, especially for the chosen earthquake magnitude thresholds, are used by the different TSPs. Each TSP has presented its own decision matrix during the accreditation procedure. The one currently used in Italy at CAT-INGV is presented in Table 1.

Since these decision matrices are based on the analysis of historical events, tsunami modelling and expert judgement, one can argue that they implicitly account for all types of seismic sources (including crustal non-subduction earthquakes); however, despite some degree of intended conservatism, as discussed below, decision matrices were certainly not conceived for including secondary events (e.g., seismically induced landslides), as present in the historical record (see **Section 4**). Those secondary events could have been initially accommodated in this scheme by operating on the thresholds for distance and magnitude.

More specifically, the decision matrices in the NEAMTWS are distance-based, so that the potential threat decreases with the distance from the earthquake source. Tsunami ranges (local, regional, basin-wide) are referred to as the distances between the earthquake epicentre and the forecast points. Each range is associated with a circle of fixed radius, as reported in Table 1. They do not take into account the source orientation (described by strike and dip angles) and mechanism (described by the rake angle) of the earthquake. Also, for this reason, while considering only tsunamis generated directly by seismic sources,

decision matices are often quite conservative on average, in the sense that they are “worst-case” oriented. **Figure 3b,c** reports the alert levels obtained by applying the decision matrix of Table 1 for two events in the western and eastern Mediterranean, respectively: M6.8 2003 Zemmouri-Boumerdes and M6.8 2017 Kos-Bodrum earthquakes and tsunamis.

Based on the real-time analysis of seismic data, TSPs strive to issue initial alert messages within a few minutes (< 10’) from any strong earthquake occurring at sea or near the coasts. At CAT-INGV, seismic parameters are obtained through the software Early-est [270–274], which elaborates in real-time data from hundreds of seismic stations worldwide and calculates a series of progressive localisations, with magnitude and hypocentre determination. While the first estimate is produced about 2 minutes after the earthquake, a good compromise between speed of calculation and accuracy was found with the Early-est 5th solution, generated about 7-8 minutes after the earthquake occurred. If no specific issues occur, this solution is used as input to the decision matrix and the consequent alert level is delivered within 10 minutes from origin time (in SiAM *Informazione* or *Allerta Iniziale*; in NEAMTWS Information or Advisory/Watch). In recent events, however, initial alert messages have been issued based on the Early-est 2nd solution, thus gaining 1-3 minutes; indeed, for both May 2020 (Crete) and October 2020 (Samos) events, initial messages were issued 8 minutes after the earthquakes’ origin times. If seismic parameters significantly change afterward, an updating message (in SiAM *Aggiornamento*/Update; in NEAMTWS Ongoing) is delivered.

After the first alert is issued, eventual sea level anomalies around the earthquake epicentre are observed through the RMN (https://www.mareografico.it/) as well as the other national mareographic networks whose data are collected and distributed by IOC/UNESCO tide-gauges (http://www.ioc-sealevelmonitoring.org), by the JRC (Joint Research Centre of the European Union; [275], or exchanged as a result of bilateral agreements.

The RMN and the other national mareographic networks operating in the Mediterranean consist of telemetered tide gauges only. The Italian network is composed of 36 tide gauges located in the harbours and/or close to the coast and equipped with a radar sensor coupled with a second floating back-up sensor based on a "shaft-encoder" technology. UMTS public channels are used for data transmission, furthermore signal redundancy is ensured through the IRIDIUM network. In the period 2014-2016, JRC started an installation campaign of a total of 20 IDSL (Inexpensive Device for Sea Level Measurements) devices in the NEAMS area integrating the national monitoring networks [275]. A floating GPS buoy suitable for the offshore installation has been tested in 2018 by JRC and ISPRA in the La Spezia Gulf. The testing returned good results but the device is not yet in production. In addition, recently a thematic board between ISPRA, INGV and MISE (Ministry of Economic Development) started analysing the possibility to put instruments in the dismissed submarine cables present in the Mediterranean Sea floor with bottom pressure sensors.

Despite all these valid initiatives, unfortunately, to date, bottom pressure sensors like DART buoys or other sea-bottom real-time instruments (e.g. [152,153]) are not operational in the Mediterranean. In case of significant sea-level anomalies in one (or more) of the tide gauges located near the epicentre, a confirmation message (in SiAM *Conferma*; in NEAMTWS Ongoing) is delivered, reporting also sea level observations, and an ending message (in Siam *Fine Evento*; in NEAMTWS Ending) is sent when all sea-level measures go back to background values. A cancellation message (in SiAM *Revoca*; in NEAMTWS Cancellation) is instead delivered when no sea level anomalies are detected.

All the messages produced by CAT-INGV are delivered in Italian to DPC and in English to all other countries/organizations which have subscribed to its service, based on predefined formats. DPC automatically disseminates these messages to all the interested emergency management system operators, including those at the local level. At present, the national tsunami warning system, SiAM, does not directly reach the population with its alerts.

3.3 Evacuation zones and civil protection coastal planning

As PTHA (and especially the Seismic-PTHA, SPTHA) is emerging as a standard method for tsunami hazard quantification [11,65], coastal planning is currently based on the most recent available SPTHA model that homogeneously covers all Italian coasts. As discussed in Section 3.1, this is NEAMTHM18.

In SiAM, both Advisory/Orange and Watch/Red levels are connected to evacuation, corresponding to warning zones of type 1 and 2, respectively. Warning zones of type 1 are the inundation zones corresponding to a maximum run-up of 1 m (or a wave height at the coast of 0.5 m). These thresholds directly derive from the definition of the alert level (Section 3.2). To define the tsunami inundation zones of type 2 to be used for evacuation in case of a Watch message, it is necessary to define an upper-bound since the Watch message corresponds to a possible run-up greater than 1 m. For this reason, the DPC chose as a reference the MIH value corresponding to the 2500 years average return period on the 84th percentile curve of the epistemic uncertainty in the reference hazard model NEAMTHM18 (**Figure 2b**). This choice is consistent with what is suggested for evacuation mapping in New Zealand and for tsunami building codes in the US [58,60,61]. It is worth noting that the type 2 inundation zone is also used for coastal planning, which is discussed later in this Section.

The full procedure describing the conversion between MIH to maximum run-up and inundation areas is described in detail in [62,63]. Nevertheless, we provide here a short description of this procedure for the sake of completeness.

Through the inclusion of several safety factors, this procedure is meant to account for the limitations in the spatial resolution of the input hazard model (Section 3.1) and the limited resolution of digital elevation models available for all the Italian coasts. In short, to take into account the MIH fluctuations over the stretch of the coast behind the POI, a multiplicative safety factor of 3 is applied to translate MIH into maximum run-up along the coast. This factor corresponds to a very high percentile (> 95th) of the distribution of the ratio between the maximum run-up and the average MIH on stretches of coast, as modelled through nonlinear shallow water inundation for numerous tsunamis with different polarities and periods at different locations [52,53,63,140].

The limited spatial resolution and the relatively coarse sampling of the source parameter space (for example, the fault centres are discretized with a step of about 25 km, and their strike angles - indication fault orientation - with a 45° step) of NEAMTHM18 may hide un-modelled inter-POI finer scale run-up fluctuations. To account for this, the design run-up values were chosen by taking the maximum between several adjacent maximum run-up values within a search radius of 40 km. A specific procedure was reserved for some areas that had peculiar geographical and morpho-bathymetric features: the Northern Adriatic Sea, the southern Tyrrhenian Calabria, and several smaller islands.

To evaluate the inundation zones from maximum run-up values in a large coastal region, the so-called “bathtub” approach is the easiest and fast method. This hydrostatic approach, in which any coastal location with an altitude lower than the design run-up would be flooded, does not consider the dissipation of waves for the inland propagation and may provide overestimations, especially for the coastal areas with a flat morphology. To account for dissipation, a simple GIS-based approach was used, introducing an empirical dissipation factor in a rule linking the maximum run-up values with the maximum distance of inundation,

and considering nominal Digital Elevation Model (DEM) uncertainty. The maximum inundation distance is calculated in 200 m per meter of the design run-up value. This rule is applied if the design run-up is not already reached on the local topographic model (**Figure 4**). The dissipation is halved (hence the maximum allowed inundation distance is doubled, 400 m per run-up meter) in the presence of rivers. These empirical relationships are very similar to those proposed for New Zealand and estimated on the basis of the numerous observations conducted following recent and historical tsunami events, which mainly occurred in the Pacific area [55,60,61,276]. This approach should, in principle, produce more realistic results than the simple hydrostatic model, even if it certainly does not take into account the actual physical behaviour in a complex coastline. More complex effects like interferences, interactions with territory and infrastructures, and between waves are to some extent incorporated when applying the safety factor and the adoption of the maxima within search radii.

The procedure described above is applied to a predefined set of reference maximum run-up values (2, 5, 10, 15, and 20 m) for all the Italian coasts. In each area, to the design run-up value obtained from the hazard analysis, it is summed 1 m to account for the uncertainty in the Digital Terrain Model, and the reference maximum run-up value just larger than the obtained value is selected to define the evacuation areas. The obtained evacuation areas, available through the Tsunami Map Viewer (http://sgi2.isprambiente.it/tsunamimap), finally were tested against a few data available in the Mediterranean, for example, by comparing the obtained inundation zones to the inundation values observed for the historical Messina 1908 tsunami. More specific testing is discussed in [63].

In 2018, Operational Guidelines were issued by the Head of DPC to support civil protection planning for tsunami risk [62]. These Guidelines, issued as an implementing act of the Directive that established the national warning system for seismically generated tsunamis (SiAM), refer to civil protection planning for the management of the risk arising from possible tsunami waves generated by earthquakes. The document provides indications to all levels of the public administrations and operational bodies of the National Service of Civil Protection for the protection of the coastal population from tsunami events.

It is useful to clarify the meaning of “civil protection planning” in the Italian system. Planning does not only mean organizing the actions of civil protection operators to intervene when an emergency occurs. A plan is also intended as a tool to increase risk awareness in “ordinary times” and encompasses pooling of resources, capacity-building activities among professionals, guaranteeing the link between different administrations and authorities. Civil protection planning is a consequent system-wide activity, to be carried out jointly by all local authorities and bodies involved in emergency preparedness and management, whether public or private. They provide a consistent and unique set of reference procedures and terminology. The plans must be constantly updated to accommodate changes in land use planning and flexible enough to be used in all emergencies, including unexpected ones.
In the Guidelines to support civil protection planning for tsunami risk in Italy, alert levels and corresponding expected tsunami inundation areas are defined for each part of the Italian coastline. In particular, national guidelines include:

- a detailed explanation of the tsunami early warning system at the national level;
- the tsunami inundation areas for each part of the Italian coastline for the two considered alert levels, “advisory” and “warning”, corresponding to warning zones 1 and 2, respectively;

- indications on the required contents of the civil protection plans, with specific sections dedicated to the municipal, provincial, regional level and one section dedicated to civil protection plans of operational bodies and lifeline providers;
- reference material for the tsunami signs, which are recommended to be installed, and best practices on tsunami public alert communication measures.

The Guidelines foresee that plans at the territorial level must be defined according to the different SiAM alert messages produced by DPC on the basis of CAT/INGV messages: *Informazione* (information), *Allerta* (alert), *Aggiornamento* (update), *Conferma* (confirmation), *Revoca* (cancellation) and *Fine Evento* (end of the event). The various institutional levels have to translate the information received with the alert message in procedures to address the specific needs of the territory under their jurisdiction. According to the current legal framework, the public warning is the responsibility of Mayors; therefore, the population must be alerted through the procedures defined in the municipal management plans, with the support of public administrations at territorial levels (regions and prefectures).

The general strategy adopted is the preventive evacuation of the population present in pre-defined coastal zones at risk (zones 1 and 2). This evacuation can be either vertical, moving upward to the highest floors of buildings suitable to withstand the tsunami impact or to higher topographical heights, or horizontal, moving inland. The operational procedures should be inspired by those foreseen for the seismic risk, with the necessary adaptations, starting -for example- with verifying the location of the headquarters of the operational coordination centres with respect to the expected inundation areas and corresponding warning zones.

The plans at regional and provincial levels (Regions, Prefectures, and Maritime Authority) must both ensure the necessary support to the activities of coastal municipalities during an emergency, and promote the organization of exercises and local hazard and vulnerability studies, to provide a higher level of detail for the tsunami risk management initiatives in their territory. The largest part of the Guidelines is the one addressed to Municipalities, which should prepare the municipal plans in four main sections: local hazard and corresponding warning zones; public warning procedures; operational response model and connected activities (e.g., installation of emergency signs for tsunami risk); communication plan and related activities (e.g., to increase community awareness and preparedness).

In the case of tsunamigenic earthquakes very close to the Italian coast, messages will most probably not reach near-field areas in time to activate preventive measures. In those cases, it is up to the citizens' ability to autonomously recognize potential precursor phenomena and immediately implement self-protection behaviours.

In this respect, periodic risk information campaigns and exercises become a crucial activity to engage, inform and develop a self-protection culture among the coastal population, such as the yearly nation-wide public information campaign "I don't take risks" (http://iononrischio.protezionecivile.it/en/homepage/), "I don't take risks - Tsunami", in particular, started in 2013 within the international exercise Twist - Tidal Wave In Southern Tyrrhenian Sea, funded by the European Commission.

In terms of exercises, SiAM (or its components) has participated in all the regional NEAMWave exercises organized by the Intergovernmental Coordination Group (ICG) of the NEAMTWS (NEAMWave12,

NEAMWave14, NEAMWave17) and is going to participate in NEAMWave2021 with an Ionian Sea earthquake-tsunami scenario.

Starting from 2020, Italy has started to pursue the Tsunami Ready initiative, following the examples of the US National Weather Service (NWS) of the National Ocean and Atmospheric Administration (NOAA) that first launched this program in 2001, then followed by all TWS worldwide, including NEAMTWS in the last year. The goal of Tsunami Ready is to assist coastal communities to be better prepared to save lives through better planning, education, and awareness, involving all community levels.

3.4 Ongoing developments

Two main developments are being carried out to improve the forecasting procedures: the revision of the tsunami hazard model at the national scale and the development of a new real-time probabilistic tsunami forecasting. In addition, several activities are ongoing to improve coastal planning.

3.4.1 Toward a national S-PTHA

NEAMTHM18 is designed to produce a homogeneous assessment over the entire target area, extended to all the NEAM region (**Figure 2a**). Limiting the target area to the Italian coasts would allow refinement of the hazard model; in fact, a specific S-PTHA model for the Italian coasts is under development. This model is largely based on NEAMTHM18, but the following updates are being evaluated:

- The use of updated local databases, like for example, the ones in development within the new European PSHA model [277] and the consequent re-evaluation of catalogue completeness (defining the minimum magnitude above which all the events are present in the catalogue in a given temporal window);
- A revision of the regionalization (the process of defining homogeneous areas within the source domain) and all statistical models;
- The improvement of the sampling of aleatory uncertainty, updating the sampling procedure for the sources most relevant for the Italian coasts;
- The use of nonlinear shallow water simulations to update the tsunami intensity estimations of the scenarios relevant for Italian coasts.
- The use of a set of target POIs more densely distributed along Italian coasts (from ~ 20 km to ~ 5 km of average distance among POIs), also considering propagation in water shallower than 50 m (e.g., up to 10 m);
- The update and refinement of the amplification model for the Italian coasts (similarly to [140]).

Once the national S-PTHA model is finalized, it may also be required to review the inundation zones, using a more accurate DEM, if available. Moreover, specific approaches could be adopted in the presence of, for example, high population density or critical infrastructures, and the GIS-based approach might be integrated with high-resolution numerical modelling [63].

3.4.2 Toward a tsunami warning based on real-time probabilistic tsunami forecast

Considering that the alert levels are connected to the expected local tsunami intensity at the forecast points, decision matrices provide a basic tsunami forecasting procedure. As already discussed earlier, the main advantage of using decision matrices is the fact that forecasts and alert levels may be timely produced as soon as basic information about the source earthquake is available. Location, depth, and magnitude are typically available and sufficiently stable just a few minutes after the origin time [274]. More sophisticated source parameters (such as source geometry), which usually are produced later in time with respect to localization and magnitude, are not required for decision matrices.

There are several known drawbacks when decision matrices are adopted as the basis for tsunami forecasting. Some examples are shown in **Figure 5**, where we report the results of the application of the DM to the Norcia 2016 (M6.7) event, occurred at the core of the Apennines chain, and to the Peloponnese scenario (M8.5), adopted in the NEAMWave17 exercise [278].

In the case of the Norcia earthquake, both the Adriatic and Tyrrhenian Seas were within the areas with higher alert levels (advisory or watch), even if the likelihood of tsunamis from an earthquake located in that area (usually faulting oriented NW-SE along the mountain chain) is clearly quite low. In the NEAMWave17 scenario, instead, the whole basin would be in a "Watch" status, while simulations show that many areas of the Mediterranean would be only slightly affected by a similar scenario. These issues are due to the fact that the decision matrix, as discussed in the previous section, does not consider the following: 1) any preferential earthquake fault orientation and mechanism, which in turn determines the extent of induced seafloor displacement and the directivity of the tsunami energy; 2) the tsunami propagation, not even at the first order. For example, in the specific case of the NEAMWave17 Peloponnese scenario, tsunami propagation would be limited through the Messina Straits and, to some extent, the Sicily channel, as well as within the Aegean Sea because of the chain of islands, and surely through the Dardanelles towards the Marmara Sea.

However, this cautionary approach not only leads to a large number of false alarms (when the tsunami is smaller than expected), but it may also be misleading, since it does not necessarily completely avoid the occurrence of missed alarms (when a tsunami larger than expected occurs) at specific locations, where energy focus may occur. Complex and asymmetrical propagation patterns of tsunamis, like the directivity of tsunami energy flux and the azimuthal anisotropy of the tsunami propagation on a complex bathymetry, may lead to important tsunami amplifications also far from the seismic source. Hence, depending on the relative source-forecast point positions, despite decision matrices are in average conservative, under- and over-estimation of the alert level may be expected (e.g. [68,69,279]). For example, for the 2003 Zemmouri-Boumerdes M6.8 tsunami (**Figure 4**), according to the decision matrix, the Balearic islands are inside the advisory alert level (forecasting a tsunami with a run-up < 1 m or wave height < 0.5 m), but local amplifications lead to a tsunami intensity larger than expected [37,280].

To account for propagation is, however, a complex scientific challenge, considering the very vast variability of the potential sources and the need to provide robust estimations within the short times required in relatively small basins like the Mediterranean. To this end, a new probabilistic method coined "Probabilistic Tsunami Forecasting (PTF)" is being developed [68,69]. The PTF is based on the propagation of the uncertainty from the source parameters, as estimated in near real-time from the monitoring room, to the potential impact zone, through pre-calculated tsunami simulations and relative uncertainty. The method allows updating the input data through time, as new information about the seismic source and/or the propagating tsunami is available. The PTF provides as output the probability distribution of the tsunami inundation height at predefined target points.

To overcome computational issues and assure timely estimations, the PTF evaluation is based on a pre-computed database derived from the regional hazard model NEAMTHM18, therefore it includes, as discussed above, both subduction and crustal seismicity [51–53].

Given the requirement of very rapid assessment of the PTF within a relatively small area like the Mediterranean, the reference implementation of the method to deal with near-field tsunamis (with warnings delivered within 10'/15' from the earthquake occurrence; see [68,69,111,112]) is based on the evaluation of the uncertainty on magnitude and epicentre from the seismic monitoring room. On the contrary, uncertainty on the focal mechanism (defining geometry and relative movements on the fault through three angles, strike, dip, rake) from the monitoring room is typically delivered too late to be included. To compensate for this lack of information, estimations derived from long-term hazard quantifications can be used. For example, Selva et al. [68,69] adopt the results of NEAMTHM18, which extend to all the source area the method developed in [31], in which the long-term probability distribution of potential source mechanisms is set based on local geological (e.g., mapped faults) and historical (e.g., earthquake focal mechanisms) information. New rapid source inversion techniques are rapidly progressing [270,281–287] and will probably reduce this uncertainty in the future. In any case, in the Mediterranean region, the possibility to quantify this uncertainty is particularly important since it allows dealing with crustal seismicity, which is generally less constrained than subduction seismicity, for which it is customary in several TWS worldwide to assume a pure thrust faulting occurring at a depth of the subduction interface corresponding to the epicentral location.

In **Figure 6a**, we report an example of the results for the M6.8 2003 Zemmouri-Boumerdes earthquake and tsunami. The figure shows a map of the probability of exceeding 0.1 m (map in the background) and, in 4 specific target points, the complete probability distribution for the tsunami intensity. It can be noted that the results follow the expected tsunami focusing patterns in the area (e.g., toward SW Sardinia) and that the uncertainty stemming from limited source parameter knowledge just after the earthquake occurrence (strike, dip, rake, slip distribution) is propagated to the forecast points and expressed with probability distributions (instead of single intensity values). Similar results can be obtained for any earthquake of any magnitude occurring in the Mediterranean Sea.

The PTF results can be automatically connected to alert levels (**Figure 6b**). For example, if we define a reference interval of tsunami intensities for each alert level, the level of each target point can be assigned by verifying in which interval fall some PTF statistics, like, for example, the mean or a pre-defined percentile [68,69].

Considering the three NEAMTWS alert levels (information, advisory, and watch) and assigning them as reference interval wave heights < 0.1 m, between 0.1 m and 0.5 m, and > 0.5 m respectively, [69] tested the performance of alert levels adopting different PTF statistics (mean, median, different percentiles) for several recent significant earthquakes and tsunami in the Mediterranean. The results show that different rates of missed- and false-alarms are reached by selecting different statistics. Being connected to risk reduction actions, the definition of the translation rule is not a task connected to tsunami forecasting, but it is connected to specific choices of decision-makers (e.g., [288]), following a hazard-risk separation principle [158]. Before a PTF-based warning system can become operational, the Italian DPC, supported by the expert advice of its scientific community, would be called upon to define standardized rules to translate PTF's probability distributions into alert levels. Specific rules have not been defined so far.

PTF results seem promising. They have been quantitatively tested only against the records of recent (occurred after 2015) small tsunamis in the Mediterranean, with the addition of a few other significant scenarios [69]. However, before becoming operational, we think that an innovative method like PTF needs to pass through a thorough scientific revision and statistical validation both in hindcasting (retrospective)

and forecasting modes, for example, including larger magnitude earthquakes and larger tsunamis, as well as more accurate tsunami records like the ones available from DART data [157]. To this end, to deal with the computational difficulties of extending PTF estimation worldwide, a specific workflow for High-Performance Computing (HPC) machines is under development, to extensively test PTF performances worldwide through HPC urgent computing [67].

3.4.3 Improving civil protection Coastal Planning

Planned steps for the future include the development of proactive initiatives in coastal areas, following a bottom-up approach to encourage Regions and Municipalities to apply the national Guidelines, drafting/updating their respective emergency plans for tsunami events. This process could take advantage of the promotion, at the national level, of the "International Tsunami Ready Guidelines". These guidelines, whose drafting is being coordinated by IOC/UNESCO in collaboration with experts from the Intergovernmental Coordination Groups of all tsunami warning systems at the global level, foresee a recognition process of the local community who manages to fulfil the 12 key indicators addressed to strengthen local capacities in case of a tsunami.

Given the importance of reaching the population in the shortest possible time, DPC is also working on the implementation of a multi-channel emergency messaging system, which will send messages via cell-broadcast technology, mobile apps, and web services. The system, called It-Alert, will be able to send also SiAM alert messages directly to the population. This channel will be implemented in parallel to the one already operating, which is targeted to all emergency management operators.

4. Tsunami warning at Stromboli volcano

Stromboli Island is an active volcano located in the southern Tyrrhenian Sea and characterized by persistent Strombolian activity (**Figure 7a**). Flank eruptions or paroxysmal explosions often contribute to generating large mass failures along the Sciara del Fuoco (SdF), which is the most unstable sector of the volcanic edifice. Massive landslides (e.g., in the order 10^6 - 10^7 m^3) at Stromboli can potentially trigger tsunamis, possibly impacting not only Stromboli but also the other Aeolian islands (in particular the closest, Panarea, 20 km SSW of Stromboli) and even mainland Italy [34,35,40]. Since the early 20th century, six tsunamis generated by landslides within the SdF have been documented [36], and the latest relevant one occurred on 30 December 2002 as a consequence of the collapse of a large portion of the SdF, during the 2002–2003 eruption [41,289,290]. The waves, up to an altitude of about 10 m above sea level, caused significant damage to the buildings located near the beaches of Stromboli, and also reached the near Panarea island and the Southern Tyrrhenian Sea coasts [40,41,43]. Fortunately, no fatalities occurred, mainly due to the fact that most of the affected houses were empty in winter-time and the few locals were alerted by the noise produced by the arriving tsunamis [42].

Landslides, and therefore tsunamis, triggered by paroxysms, usually occur a few minutes after the explosion. These explosions typically do not show any kind of precursors in the short-term (hours or days), in terms of changes in the parameters recorded by the monitoring networks, but in the very short-term (minutes) they show changes in deformation of the edifice [291–294]. Slope failures induced by magma intrusions are part of a slow and progressive dynamics, which could be detected several days before it occurs [292].

4.1 Hazard quantification

Proper probabilistic hazard quantification for the tsunami generated at the SdF of Stromboli is nowadays impossible, since i) the tsunami source conditions are difficult to predict, observe, and model; ii) the source is close to the shoreline; iii) the bathymetry is very steep and irregular [290,295,296]. Therefore, in the past years, research has aimed to identify the most effective modelling approach (in terms of accuracy and computational efficiency) to inform the early warning system and to build a solid basis for future tsunami hazard assessments.

To this aim, several benchmarked models, at different levels of approximation and accuracy, have been used: the NHWAVE three-dimensional non-hydrostatic model in sigma-coordinates [217] and the HySEA family of geophysical codes [297] based on either single layer, two-layer [298] stratified systems or multilayer non-hydrostatic formulations [299] of the wave model.

Models results have been compared for the maximum run-up, inundation maps at the Stromboli village, and the waveform sampled at four proximal sites (two of them corresponding to the locations of the monitoring gauges offshore the SdF). Both rigid and deformable submarine landslide models (with granular flow rheology described by the Savage and Hutter model [300] and the Pouliquen and Forterre friction law [301]), with volumes ranging from 6 to 20 millions cubic meters, have been used to trigger the water waves.

The comparisons between hydrostatic and non-hydrostatic models show that the simulated inundation maps at the Stromboli village are relatively similar, despite differences likely associated with differences in wave-breaking effects. On the other hand, as expected (i.e., due to frequency dispersion and other model differences), preliminary results indicate strong differences between the proximal waveforms produced by the considered models. Such an aspect is particularly critical in the perspective of using proximal sea-level gauges installed at Stromboli to characterize the tsunami source in an early-warning system (discussed in Section 4.2). In addition, we stress that subaerial landslides almost invariably generate dispersive waves (e.g. [16]).

This suggests that the use of non-hydrostatic models allows a better description of the proximal waveforms, but the source description remains the most sensitive (and uncertain) aspect of the modelling. On the other hand, hydrostatic models are computationally less expensive when it comes to modelling larger domains and hence the propagation of the waves far from the source [216]. However, the use of High-Performance Computing (HPC) techniques, and in particular of Graphics Processing Unit (GPU) accelerators for the numerical solution [302], has now allowed much faster simulations even with complex non-hydrostatic models, which have opened a new avenue for probabilistic tsunami hazard assessment and tsunami early warning [67].

Based on benchmark study results, waveforms obtained with a non-hydrostatic model (**Figure 7b,c**) have been selected to preliminary calibrate the tsunami alert system on the Stromboli island, as discussed below. In addition, a set of synthetic scenarios has been created to investigate the potential impact of a landslide-induced tsunami along the shoreline of Stromboli Island, with varying landslide volume, the initial height of the centre of mass, and the landslide-water density ratio.

4.2 Tsunami early-warning system at Stromboli

The tsunami early-warning system at Stromboli is based on three main components (outlined in separate subsections below) [151]:

1. The multi-parametric monitoring network, designed to identify any anomalies which may lead to the transition from explosive (equilibrium) to effusive phase (disequilibrium);
2. Two elastic beacons located in front of the SdF (Punta Labronzo and Punta dei Corvi, see **Figure 8**), which are able to identify tsunami waves in real-time, and the data transmission infrastructure to the civil protection's Advanced Operational Centre (COA);
3. An acoustic warning system made of eight sirens distributed in Stromboli, Ginostra (village of Stromboli), Panarea Islands and one beeper inside the Coast Guard premises in Milazzo (Sicily island), interconnected by a dedicated VHF radio network [303].

The system has been operative since 2003, but several significant changes have been implemented through time, as discussed in detail below.

4.2.1 The multi-parametric monitoring network and tsunami warning

Although the mechanism of triggering tsunami waves at Stromboli is not well known, the literature shows that these phenomena occurred more frequently during periods of intense volcanic activity characterized by effusive phases, as well as a few minutes after the occurrence of paroxysmal explosions.

The higher supply of magma to the shallow reservoir is recorded by the multi-parametric monitoring network (Seismo-acoustic stations, thermal cameras, tiltmeters) months before the effusive onset and is responsible for the progressive transition towards a higher explosive regime with respect to the usual Strombolian activity [293,304,305].

When the dike reaches the surface, a new effusive vent opens, and lava is drained out of the shallow conduit system. During this stage, there is the highest probability of having a flank instability and potential generation of tsunamis (e.g., 2002). Ground deformation based on tiltmeter [291,293] and SAR interferometry (GB-InSAR) [292] of the SdF flank dynamics are therefore crucial to identify early stages of magma intrusions and assess instability scenarios.

According to the civil protection procedures implemented on the island and the overall hazard assessment, these slow and progressive dynamics could allow the civil protection authorities to issue a pre-warning, which could include preparation for the evacuation of people living in the tsunami inundation zone (e.g., 2007 eruptive crisis described in [304,306]). Furthermore, the activation of the acoustic warning system is automatic and triggered by the elastic beacons after the detection of the tsunami.

The direct consequence of the transition to the effusive regime is the progressive collapse of the crater terrace, revealing the gravitational instability induced by a large amount of drained magma from the shallow portion of the conduit system [304,305]. In this phase, the main hazard is thus no longer the flank instability and potential generation of tsunamis [293].

The increasing hazard posed by volcanic activity (transition from explosive to effusive phase) is assessed through the adoption of a Volcanic Alert Level system based on four-color codes (from green to red). Depending on the alert level and on the overall risk assessment, local and national civil protection authorities implement appropriate actions to ensure public and private safety.

4.2.2 The elastic beacons (MEDA)

The University of Firenze – Laboratorio di Geofisica Sperimentale deployed two elastic beacons (MEDA) used to detect the tsunami proximal to the SdF. The first one (PDC) was installed in 2008, 260 m off the

coast of Punta dei Corvi, while the second one (PLB) was set in 2017, at a distance of 350 m from Punta Labronzo (**Figure 8a**).

The MEDA is a semi-rigid structure made of a 35 m long metallic pole, anchored to the shoal with a 20 Tons deadweight. The deadweight connects to the upper structure through an anti-torsion steel cable (**Figure 8b**). The MEDA reaches 8 m of height above the sea surface and is equipped with sensors, power supply equipment, and a radio transmission system [151]. Sensors include hydrostatic pressure (125 Hz), temperature (1 Hz), Hydroacoustic (40 Hz), GPS, and two Tiltmeters (4 Hz), combining measures of interest for the tsunami detection and measures to verify the station performance. The MEDAs are installed 260 m off Punta dei Corvi and 350 m off Punta Labronzo (Figure 8), have a length of 30 m, a height above sea level of 8 m, and a deadweight of 20 Tons.

Three different networks send data to the COA, as shown in **Figure 8c-d-e**, in order to guarantee data transmission and redundancy.

4.2.3 Tsunami detection

Tsunami automatic detection algorithm [151,307] has been tested adopting two main criteria: 1) surface waves dispersion and 2) STA/LTA (Short Time Average over Long Time Average) ratio analysis.

For the surface wave dispersion, underwater hydrostatic pressure sensors (one at a depth of 50 m and the second on the seafloor) are used to make the sea-noise effect negligible and to increase tsunami wave detection capabilities. For the STA/LTA method, which is largely used in seismology for the automatic detection of earthquakes, we calculate the average absolute value of the signal's amplitude based on two-time windows.

Sensitivity analysis of the algorithm and of the threshold efficiency has been performed for at least five years of recorded data from PDC MEDA, using the database of simulations performed for the hazard quantification (Section 4.1) and the real-time measures (for non-tsunami signals). As a result, the algorithm is theoretically able to automatically detect tsunami waves in any sea condition since tsunami signals produce STA/LTA values well above the identified threshold [307]. The first real-time testing occurred during the small tsunamis that occurred in July and August 2019, as discussed below.

4.2.4 The acoustic warning system

The acoustic warning system is made of 8 sirens and one beeper (**Figure 9**), interconnected by a dedicated radio network (VHF band), and three main base stations (radio links) located in Antennamare (in the province of Messina), Stromboli, and Panarea, that allow the simultaneous activation of the above-mentioned sirens [303].

Management software that runs on a workstation located inside the COA gives the opportunity to select three possible combinations:

- Single: activation of one siren (out of the nine available);
- Group: activation of a pre-selected group of sirens (i.e., only Stromboli group or Panarea group);
- Global: activation of all the sirens.

4.3 Evacuation zones and civil protection coastal planning

The national civil protection emergency plan for volcanic events in the Island of Stromboli was first issued in 2003, after the 30 December 2002 tsunami caused by the sudden failure of the SdF. The plan was drawn up with the contribution of the Regional Civil Protection, the Prefecture - UTG of Messina and the Municipality

of Lipari. In August 2015, a new updated version was released (http://www.protezionecivile.gov.it/attivita-rischi/rischio-vulcanico/vulcani-italia/stromboli/pianificazione, [303]), taking into account new scenarios and the introduction of the national volcanic alert level system.

The plan is based on a tsunami inundation zone drawn upon the in-situ observation and measurements of the 30 December 2002 waves [40–42]. This choice is determined by the fact that this event is, to date, the best documented in terms of impact on the island. In terms of emergency management, this densely inhabited zone represents the exposed area which will be evacuated in case of i) evidence of intrusion and deformations in the SdF, which can lead to a possible collapse and subsequent tsunami (e.g., 2007 eruptive crisis described in [306]); ii) automatic activation of the acoustic warning system (sirens) after the detection of a tsunami. Noteworthy, it is in place also an automatic early warning system for paroxysmal explosions [308]. This system triggers sirens locally at the villages of the island of Stromboli (Stromboli and Ginostra) [303]. The tsunami early warning system is instead automatically triggered only when a tsunami is detected by the MEDAs and activates the entire network of sirens. The sirens have two different acoustic signals assigned to each phenomenon: i) bi-tonal for paroxysmal explosions and ii) mono-tonal for tsunamis.

Evacuation routes have been identified to guide people to the safe areas and reach the gathering points. Each evacuation route has its own emergency signals explaining the correct path to follow. More details can be found in [303].

4.4 Further developments following the July and August 2019 paroxysms

4.4.1 Modelling of the 2019 events

On July the 3rd 2019, a paroxysmal eruption at Stromboli produced a sequence of high-energy pyroclastic flows, which generated several tsunami wave trains detected by the sea gauges (see Section 2.3). In response to the event, a preliminary assessment of the physical parameters characterizing the tsunami source was done by first comparing the recorded waveforms with the pre-computed synthetic waveforms and then running additional simulations with the multilayer-HySEA non-hydrostatic model.

Either one or two simultaneous pyroclastic flows were modelled starting from four different initial positions and using three different volumes. Simulated flows average speeds were compatible with that observed by webcams. Two possible scenarios were therefore taken into consideration: in one scenario, a single pyroclastic flow dominated the wave generation; in the other one, two pyroclastic flows contributed in a comparable way to wave generation.

The preliminary results of the numerical modelling allowed us to estimate, based on the wave heights observed at the wave gauges (see Section 2.2.2), the rock avalanche volumes and generation height. The simulated waveforms and arrival times appear to have characteristics very similar to those measured in the event.

The study of this event allowed comparing, for the first time in Stromboli, the wave generation and propagation model with the signals measured in the presence of a tsunamigenic event. The model has proven to be capable of reproducing the main characteristics of the waves in the two gauges, with satisfactory accuracy, at least in the first minutes of evolution.

4.4.2 Warning system

The acoustic warning system for tsunamis has been working in manual mode since its installation in 2003, following the 30 December 2002 landslide and tsunami. It was first activated on 27 February 2007 during the phases that preceded the lateral vent opening on the SdF, fearing a new flank collapse and subsequent

tsunami [306]. Fortunately, the vent opened, and just a minor landslide occurred with no tsunami observed.

After the deployment of the two MEDAs, the DPC and the University of Firenze - Laboratorio of Geofisica Sperimentale started working on an automated procedure to activate the sirens through a radio-modem (working on the same frequency of the acoustic sirens) connected to the server running the detection algorithm [151].

On 3 April 2019, the first successful test was performed, and one single siren was remotely activated. The testing phase was still on-going when on 3 July 2019, a paroxysmal explosion occurred, and the two elastic beacons recorded a small tsunami (1 m wave peak-to-through, **Figure 10a**) generated by pyroclastic flows, and this tsunami had no significant impact on the coast. The event was sudden, and the monitoring equipment located on the volcano was not able to detect any precursors, so there was no chance of activating the sirens manually.

On 28 August 2019, a new paroxysmal explosion was recorded, but this time local civil protection personnel deployed on the island were able to activate the sirens in manual mode as soon as the pyroclastic density currents reached the sea. In this case, a minor tsunami was recorded (60 cm peak-to-through, **Figure 10b**, but with negligible impact on the coasts. In this event, the pyroclastic flow entered the sea approximately 35" after the volcanic eruption. The tsunami was generated a few seconds later, approximately 60" after the occurrence of the volcanic explosion (after 60").

In **Figure 10c** we report, as an example, the automatic tsunami detection for this event, based on the STA/LTA ratio [307]. The automatic trigger overcame the predefined threshold approximately 15" second after the generation of the tsunami, that is, 1' and 15" after the volcanic explosion. As far as we know, this is the first time a warning is delivered before the tsunami wave is fully developed.

The testing phase of the automated procedure ended on 9 September 2019 when the Mayor of Lipari, Regional and National civil protection authorities tested the entire chain of the procedure, simulating a trigger signal from the MEDAs.

Therefore, at this stage, if the MEDAs record a tsunami, the acoustic warning system is automatically activated (global mode) by the server that runs the tsunami detection algorithm (**Figure 9b**) [151]. Should the automated system be down for any reason, there is the chance to manually activate the sirens from the workstation inside the COA or from three portable radios, which have been given to the Municipality of Lipari.

5. Other non-seismic tsunami sources in Italy

In this section, non-seismic tsunami sources are considered as a whole set of known and potential tsunamigenic sources, including landslides (in its widest meaning), volcanic activity, and atmospheric pressure disturbances. The portion of the Euro-Mediterranean Tsunami Catalogue (EMTC; [36]) describing the sources of the historical tsunamis hitting the Italian coastlines (**Figure 11**) indicates that, although tectonic sources are the primary triggering mechanism (**Figure 11a**, 49 entries), non-seismic sources are a non-negligible part of the reported events (**Figure 11b**, 23 entries)

Looking at **Figure 11b**, it is easily recognizable that historical tsunamis generated by sources other than earthquakes concentrate in volcanic areas (Gulf of Naples, Aeolian Archipelago, offshore Mount Etna) and along steep coastal slopes where pure gravitational instability of seismic shaking can trigger mass transport

phenomena. We stress again that these can both take place as submarine (fully submerged) landslides or subaerial landslides plunging into the sea (e.g., the 1783 Scilla landslide; [309,310]). No mention is made in the EMTC to meteotsunami events, although some of these may fall under the events reported with "unknown" cause.

Regarding earthquake sources, the EMTC is considered complete starting approximately from the seventeenth century. However, it is very reasonable to argue that the EMTC is significantly incomplete as regards non-seismic sources due to their relatively more local impact and the fact that such sources were previously not equally well understood as potential triggers. Some of the most destructive historical tsunamis hitting the Italian coasts, such as the 11th January 1693 and the 28 December 1908 events, are traditionally associated with the large magnitude earthquakes occurred a few minutes before the tsunami, but studies published in the last decade have introduced and critically discussed the possibility that submarine landslides have contributed in a very significant way to the generation of the tsunami waves.

In the perspective of tsunami hazard assessment and warning related to non-seismic generation mechanisms, improved and deeper knowledge of historical events must be accompanied by systematic and detailed characterization of all potential sources. Significant progress in this sense was achieved by the MAGIC project, financed by DPC in the period 2007-2012 (http://www.protezionecivile.gov.it/media-communication/dossier/detail/-/asset_publisher/default/content/progetto-magic). Many of the results matured in the framework of MAGIC were published in the scientific literature, allowing to get a significantly improved picture of the coastal areas where careful investigation on slope instability and possible future tsunamigenesis must be carried out.

In **Figures 12** and **13**, with no claims to be exhaustive, we summarize the main geographical areas of Italy where tsunami generation by non-seismic sources occurred in the past, likely representing a threat also in the future. The main identified potential sources are discussed below.

5.1 Ligurian Sea

Only two historical tsunamis are present in EMTC for the Ligurian Sea (LS) with a non-seismic source generation. They occurred respectively on July 2nd, 1703, and on July 3rd, 1809, and both were moderate-intensity event (intensity 2 in the Sieberg-Ambraseys scale). Both events are labelled with an "unknown" source, which is an indicator of the lack of a thorough analysis of the tsunami hazard from non-seismic sources in this area.

Studies on offshore slope instability and on mass transport evidence along the Ligurian margin indeed exist (e.g., [311–313]), but a systematic approach to tsunami hazard and warning related to this domain appears to be still lacking, especially as regards the Italian coasts. It is important to recall that landslide-generated tsunamis can pose a serious threat for the coasts facing the Ligurian Sea, as demonstrated by the 1979 event in Nice (e.g., [314,315]).

5.2 Tyrrhenian Sea

5.2.1 Ischia and the Gulf of Naples (IGN)

The Ischia island is characterized by an intense volcanic activity whose main expression is the resurgence of Mt. Epomeo, causing instability phenomena along the slopes of the main relief due to both seismic shaking and increased slope gradients [234,316,317]. Several bathymetric campaigns highlighted the existence of slide deposits offshore the northern and western coasts of Ischia (e.g., [318]). Moreover, a debris avalanche

offshore the southern coast of the island was mapped at about 1000 m depth, with a volume of 1.5 - 3.0 km^3, composed of blocks (hummocks) and mixed and finer facies, up to 45-km distance from the coast [28,319]. An extreme scenario of tsunami generation by a single collapse involving the island top (about 800 m a.s.l.) down to 700 m depth b.s.l., with a total volume of more than 3 km^3, was simulated by Tinti et al. [27]. The resulting simulated tsunami is catastrophic along the coasts of Ischia and Capri, with waves as high as 40 m; several meter-high waves are also expected inside the Gulf of Naples and in several locations to the north (Latium) and to the south (southern Campania and northern Calabria).

Another potential source of catastrophic collapse and consequent tsunami generation at Ischia is represented by the Monte Nuovo, which is a deep-seated block found at 400 m a.s.l. on the north-western flank of Mt. Epomeo (e.g., [234,320]). Zaniboni et al. [29] investigated the potential tsunami generation by a 160 million m^3 rock collapse and its propagation in the Gulf of Naples area. Paparo and Tinti [321] performed a stability analysis for Monte Nuovo and found that it could be mobilized if an earthquake with magnitude comparable to the 1883 Casamicciola earthquake occurred on a nearby fault: the consequence of the destabilization would be a catastrophic mass failure with the potential to generate a disastrous tsunami. However, this possibility is still debated in the literature [234].

The activity of Mt. Vesuvius is responsible for the largest part of the historical tsunamis reported in EMTC: the two most famous and catastrophic eruptions occurred on 24 August 79 AD and on 17 December 1631, and they are both reported to have been accompanied by significant sea movements. A short review of the numerical simulations of pyroclastic flow impact and consequent tsunami generation in the Gulf of Naples can be found in [46,99,322].

Recently, the potential for generating tsunamis due to underwater explosions at the Campi Flegrei caldera has also been explored by Paris et al. [32]. Even in the absence of a past record of tsunamis generated by this mechanism, underwater vent opening cannot be excluded (e.g., [323,324]), and they have the potential for large tsunamis impacting mainly within the Gulf of Naples. Submarine explosions appear to be the main potential generating mechanisms at Campi Flegrei because pyroclastic flows are highly dilute and, consequently, they have a low potential for generating tsunamis [20,325].

5.2.2 Southern Tyrrhenian Sea Mounts (STSM)

The complex tectonic setting related to the Tyrrhenian Sea evolution (Ionian slab moving towards NW and subducting underneath the Tyrrhenian crust) finds expression in a series of volcanic features that characterize its morphology. While the Aeolian Archipelago represents a typical volcanic-arc configuration, the back-arc expansion zone shows submarine volcanic structures, which were generated in different periods but that exhibit, in some cases, similar peculiarities.

The western one, named Vavilov seamount, is the oldest and presents an asymmetric morphology [326], suggesting the possible collapse of its western flank. The eastern slope average dip is about 15°, while the western one is higher (25°) and with a typical amphitheatre-like shape, supporting the hypothesis of a singular ancient catastrophic event [327], with volume ranging 40 km^3. A first attempt to assess the consequences of such an event in terms of tsunami generation has been conducted by Arcangeli [328], with the use of numerical codes. The supposedly generated wave would impact the whole Tyrrhenian coasts with relevant waves.

The eastern seamount characterizing the area, named Marsili, is the highest volcanic edifice in the whole Mediterranean Sea, with dimensions 70 km x 20 km and height from the sea bottom exceeding 3000 m [329]. Even though no significant pieces of evidence of instability exist [330], there are some elements that justify the study concerning the potential collapse of portions of the Marsili volcanic edifice:

- the presence of tectonic structures along its slopes, possibly contributing to volcano flank instability;
- similarity, both in genesis and morphology, with the Vavilov seamount, that already was affected by a gigantic lateral collapse;
- the presence, on the abyssal plain at the basis of the volcano, of deposits associated with mass-wasting processes originating from the volcano flanks.

The generation of tsunamis from mass collapses has been scarcely investigated yet. One first attempt to quantify the waves induced by landslide scenarios of different dimensions and depths has been conducted by Gallotti et al. [331] .

Moving further to the east, close to the Campanian coast, recent studies have described the Palinuro volcanic chain, which displays a W-E trend [332] and is characterized by several volcanic cones and intense activity that can induce flank instability. The involved volumes range from 0.5 to a few km^3 [333]. This fact, combined with the relatively shallow water of the area and the steep slope of the southern margin, contributes to enhancing considerably the potential hazard associated with this area.

The other existing emerged (Ustica) or submerged (Enarete, Eolo, Alcione, Lamentini, Glabro, Enotrio, Ovidio) volcanic edifices in the southern sector of the Tyrrhenian Sea, in spite of some record of submarine gravitational fluxes, do not seem to present the conditions for a significant tsunami threat [334].

5.2.3 Aeolian Archipelago (AA)

Apart from the activity on the SdF, thoroughly discussed in Section 4, other tsunamigenic sources at Stromboli cannot be excluded, like sector collapses in the south-eastern zone (Sciara Vecchia, Schicciole, Rina Grande) or submarine eruptions, especially in the area between Punta Lena and Strombolicchio [334]. Also, other volcanic phenomena generated above the sea level and propagating into the sea in sectors different from the SdF cannot be excluded. However, the potential tsunami hazard due to these phenomena has never been quantitatively assessed.

The island of Volcano is another island of the Aeolian Archipelago where historical tsunamis occurred and where a potential for future events exists [26,233]. On April 20th, 1988, a $2x10^5$ m^3 body [26,335,336] detached from the La Fossa crater and collapsed into the sea, generating a small local tsunami hitting Porto di Levante with a 1 m amplitude wave. The landslide dynamics and the ensuing tsunami have been simulated numerically by Tinti et al. [26]. It is important to stress here that the La Fossa crater is characterized by frequent sliding phenomena (e.g. [337,338]), and hence it represents a potential repeating tsunamigenic source. Apart from gravitational sources, even though no records of eruption-generated tsunamis are available (either submarine eruptions or volcanic phenomena entering the sea), this cause cannot be ruled out [233].

In addition to Stromboli and Vulcano, other gravitational instabilities potentially generating significant tsunamis have been tracked in Lipari, especially in its eastern sector and both in the emerged and the submerged parts of the volcanic edifice, and, with relatively smaller tsunamigenic potential, in Panarea [334].

5.2.4 Western Calabria Margin (WCM)

Tyrrhenian Calabria has been affected by several large historical earthquakes, often accompanied by moderate to destructive tsunamis [309]. Examples are the events that occurred in 1184 (M_w=6.8), 1638 (M_w=7.1), 1783 (a long sequence with three M_w>6.7 earthquakes in two months, M_w=7.1 being the largest), 1905 (M_w=7.0), and 1908 (M_w=7.1). For some of them (mainly 1783, but also 1908), a significant

contribution may be ascribed to seismically induced landslides (for the 1783 event see [339–342]; for the 1905 event see [343]).

Moderate-to-large landslides have also been mapped by offshore surveys (e.g., the late-Quaternary landslide mapped offshore Cape Licosa and in the Paola basin) and represent potential tsunamigenic sources (e.g. [344]); moreover, the Scilla landslide, triggered by the 6th February 1783 earthquake, is a historical example of a landslide-generated tsunami hitting the Tyrrhenian coasts of Calabria violently. On that date, a rockslide detached from Mt. Campallà, entering the sea and generating a tsunami which impacted the nearby village of Scilla with waves up to 9 m high, killing around 1500 people. The simulation of the rockslide dynamics and of the ensuing tsunami has been addressed by several authors [339–342].

The Gioia Tauro basin is another sector that deserves special attention. It is characterized by a canyon [345] where past mass transport phenomena have been mapped and described. On 12 July 1977, a tsunami was observed with an initial withdrawal of 2-3 m, subsequently attacking the western dock of the Gioia Tauro harbour with 5 m maximum amplitude. The tsunami was likely generated by a submarine landslide channelling along the Gioia canyon: two different landslide scenarios, together with the ensuing tsunamis, were proposed and modelled by [346].

5.3 Ionian Sea

5.3.1 Eastern Calabria Margin (ECM)

The Assi landslide has been studied and characterized in the frame of the MAGIC project [347]. The main mass transport evidence is found offshore the Monasterace town and has been dated at about 2850 years ago, possibly resulting from two distinct events. The first of them involves a 1.85 km^3 volume, with an average thickness of 27 m. The landslide supposedly detached from a depth of 750 m b.s.l. and the deposit is found at 1400-1600 m depth, resulting in a run-out of the order of 20 km. The landslide has been simulated numerically [348]: the main result is that a landslide of this type could be responsible for waves with maximum amplitudes in the order of 1 m along a limited stretch of coast between Monasterace and Roccella Jonica. Although not catastrophic, such a tsunami might cause significant damage to small harbours along the coast and could also result in a threat to the local population, especially during the seasons with more intense touristic flows. In addition, this type of landslide poses a significant challenge from the warning point of view, as the first wave is likely to impact the closest coastlines nearly 7 minutes after the slide onset.

A second, highly debated area is offshore the Crotone peninsula and is the so-called Crotone Swell (e.g. [349]), which is a morphological high approximately 16 km long and 30 km wide, exhibiting a very complicated structure. Zecchin et al. [349] interpret the Crotone Swell as a mega-landslide, up to 1.6 km thick, which started moving between Late Zanclean (5.3 – 3.6 Myr ago) and Early Piacenzian (3.6 – 2.6 Myr ago). According to the same authors, the seaward migration of such a mega-landslide significantly slowed down in the last 0.5 Ma and currently its behaviour is not expected to pose any significant threat as a whole. Nonetheless, the complex and the not fully-understood structure of the landslide deserves a careful evaluation of the possibility that some portions, particularly the shallower parts of the Crotone Swell, might be set in motion by the seismic activity of the area, which is characterized by historical earthquakes with magnitude larger than 6.5 (08/06/1638 with equivalent magnitude 6.8 and 08/03/1832 with equivalent magnitude 6.6). For example, a seismic profile analysed in the framework of the recent (2017-2018) SPOT Project [350], financed by the Italian Ministry of Economic Development with the technical support of the Italian DPC, has highlighted the possible presence of a huge submarine landslide in the southern portion of the swell (offshore Capo Rizzuto). A possible reconstruction involves a 25 km^3 slump, covering an area of 85 km^2 with an average thickness of 300 m. Even with a limited run-out to its mainly rotational movement, it is

reasonable to expect that this source could have been responsible for a very significant tsunami hitting the entire Ionian coasts of Calabria.

We have commented on only two main areas that have been extensively described in the literature. Other areas along the eastern Calabria margin deserve further investigation and careful assessment of the tsunami hazard related to coastal and offshore slope instabilities.

5.3.2 Eastern Sicily (ES): Messina Straits

The Messina Straits is an extremely complex area with very peculiar morphological features. As described recently by Ridente et al. [351], the main morpho-structural feature is represented by the Messina Canyon, striking mainly NNE-SSW and intercepting many tributary slope canyons that incise the steep Calabrian and Sicilian continental slopes. The landslides triggered by a cloudburst on 1 October 2009 in the area of Giampilieri and Roccalumera (Sicilian side of the Straits), resulting in 28 ascertained victims, and the intense debate on the source of the 1908 tsunami following the already mentioned devastating M 7.1 earthquake are the demonstration of the importance of a proper assessment of the susceptibility of the area to coastal and submarine mass movements. Regarding the debate on the 1908 tsunami, we will recall here that in the lack of any recognized primary faulting evidence ([352], with references), many hypotheses on possible underwater slide positions and mechanisms have been proposed, starting from [47], with further contributions including the studies by Favalli et al. [50] and Schambach et al. [258]. In particular, in this very recent study, a key role in the generation of the 1908 tsunami is assigned to a $\sim$2 km^3 submarine mass failure mapped at the foot of the Fiumefreddo Valley, NE of Mount Etna. For the scope of the present discussion, we stress in particular what was proposed by Ridente et al. [351]: based on the results of high-resolution swath bathymetry, they pointed out that several relatively small-scale landslides are observed on both the Calabrian and Sicilian margins of the Straits, possibly related to the shaking associated with past earthquakes such as the relatively recent 1908 event. From the tsunami hazard assessment point of view, this must be carefully kept in mind as even small-scale landslides might determine local amplification of tsunami inundation effects along the coasts of the Straits.

5.3.3 Eastern Sicily (ES): Mount Etna

The area offshore Mount Etna has been intensively investigated by marine geology campaigns in the past, and several descriptions and interpretations about mass transport deposits can be found in the literature. A full review of the available studies is beyond the scope of this paper, but it is important to recall that Mount Etna is affected by sliding of its eastern flank, whose nature is the subject of intense debate (e.g. [353]). The recognized instability of this flank ([353–357], among many others) and its ongoing deformation represent a critical subject in the frame of tsunami hazard and warning, at least for the eastern Sicily coastlines.

No unique view on the history of mass transport phenomena exists: the spectrum of hypotheses ranges from the small-scale deposits described in [355], reasonably triggered by volcano induced seismicity and flank deformation connected to the eruptive activity, to the catastrophic debris-avalanche deposit discussed in [358], related to the Valle del Bove scar and characterized by a 16-21 km^3 volume and up to 20 km offshore run-outs. A careful revision and a deeper understanding of the ongoing processes that might lead to future offshore mass movements are needed for a credible tsunami hazard assessment in this area.

5.3.4 Eastern Sicily (ES): Hyblean-Malta Escarpment

The Hyblean-Malta Escarpment (HME) is a geomorphological structure characterized by large bathymetric gradients. In principle, this is an important prerequisite to consider the HME as a place where mass collapses may occur, due either to pure gravitational instability or to earthquake shaking. Nonetheless, very

few examples exist in the literature of documented slide deposits, or of scarps suggesting the occurrence of past slides, or of potentially unstable mass bodies.

The only clear evidence is reported in [359], where a 5 km^3 deposit mapped at 2000 m depth, offshore just north of the bay of Augusta, is described. It is argued that the main movement of the mapped mass was rotational, hence describing a slump, with an inferred 200 m dislocation over a 40 km^2 area, involving an average thickness of 100 m. Tonini et al. [360] and Argnani et al. [359] discussed the possible triggering of the slump by the 11th January 1693 earthquake, which was followed by a violent tsunami whose most dramatic effects were experienced by the town of Augusta, with observed wave amplitudes of more than 8 m [36,361]. Based on the results of numerical tsunami simulations, Tonini et al. [360] and Argnani et al. [359] agree that that a slump could not be the main responsible for the observed tsunami, hence leaving open the problem of the source of the 1693 tsunami.

More recently, Paparo et al. [362] studied the slope stability of the HME under seismic loading on a number of transects, trying to identify those sectors that may move under the effect of realistic earthquakes. One of the outputs of the study was the estimation of landslide volumes that might be set in motion by seismic shaking, representing a fundamental step toward quantitative tsunami hazard assessment for the nearby coastal areas.

5.3.5 Gela Margin (GM) and Sicily Channel (SC)

The Gela Basin Margin (GBM) is located in the Sicily Channel, south of central Sicily. This structure connects the shallow water characterizing the Malta Plateau (around 200 m) to the east, with a depression in deeper water (800 m depth b.s.l.). The whole area was the object of geophysical surveys, describing many features possibly related to mass-wasting processes: scars and canyons along the slope, huge amounts of sediments at its toe [363].

The most noticeable feature, in terms of involved volume, is the Gela slide [364], related to a prehistoric event (~600 kyr BP) with a volume estimated at 630 km^3. Such submarine collapse has been adopted as one of the scenarios for the study of the tsunami hazard involving the Malta archipelago [365] and has been found to be the major source of potentially catastrophic waves impacting the coasts.

More recent surveys have characterized further episodes along the escarpment. This is the case of the so-called Twin Slides, related to a double event placed in the northern portion of the GBM. Two evident scars develop just from the continental platform at 200 m depth b.s.l., 30 km offshore the city of Gela, with the corresponding deposit laying at their toes [366]. These two failures are the final phase of a complex series of collapses, tentatively reconstructed by Kuhlmann et al. [367], that repeatedly occurred in the last 10 thousands years. The Twin Slides volumes are estimated at about 0.5 km^3 each; the Northernmost one has been selected for scenario reconstruction and tsunami simulation [368]. The generated tsunami affects 60 km of southern Sicily coast with waves of at least 1 m maximum, with peaks of 3 to 4 m.

A larger scar, with the correspondent deposit at its toe, has been discovered on the southern part of GBM, 40 km offshore the Maltan island of Gozo. This landslide, whose volume has been estimated more than 3 km^3, has been simulated numerically and further been coupled to a tsunami model obtaining large tsunami intensities (maximum wave height reaching 6 m [368].

No historical tsunami generated by non-seismic sources is present in the Sicily Channel, according to EMTC. Despite this fact, a careful approach to tsunami hazard in the area must take into serious consideration at least the submarine volcanoes mapped in the NW sector of the Channel.

For the Graham, Terrible, and Nerita banks (e.g. [369,370]), an important historical record of submarine eruption exists (e.g., the formation of the Ferdinandea island in 1831). While the potential for tsunamigenic gravitational instability seems rather low, eruptive activity potentially generating tsunamis cannot be excluded [334].

Other volcanic edifices are the Pelagie islands [371,372]. While tsunamigenic activity for these volcanoes has never been quantitatively studied, in Pantelleria and Linosa, the generation of tsunamigenic gravitational collapses and of potentially tsunamigenic submarine eruptions cannot be ruled out [334].

5.5 Adriatic Sea

The main potential tsunami source in the Adriatic Sea is the South Adriatic Margin (SAM). The SAM is a peculiar structure, interrupting the gentle slopes and shallow water characterizing the remaining part of the Adriatic Sea and presenting many features that can be linked to mass mobilization and rapid failures. In particular, the western flank, offshore Apulia, is characterized by extensive evidence of slope instability for at least 150 km, especially on the shelf edge and upper slope [373,374].

The main features of the Western SAM are:

- the Bari Canyon System, characterized by intense bottom currents causing intense sediment deposition and erosion [375];
- the Vieste slide, on the north, involving low-gradient areas [376];
- the Gondola slide, which is the main body characterizing the margin, probably related to an event occurring simultaneously to that of the Vieste slide, due to the shaking provoked by a big earthquake during the Last Glacial Maximum (approximately 62 kyrs BP; [377]). Its failure mechanism is quite complex, mainly divided into three phases, and involves around 4.5 km^3 of material, with a run-out of more than 50 km for the looser portion. A pronounced scar (10 km wide, 250 m deep) cuts the platform at about 150 m depth, clearly marking the landslide detachment zone.

An attempt to assess the tsunami generation of the Gondola slide through numerical codes has been done by Tinti et al. (2008): in the simulation, the sea level has been lowered by more than 100 m, accounting for the likely coeval water depth. The ensuing waves reached 10 to 20 m on the Apulian coasts.

A historical tsunami in this area is also documented in association with the Mw 6.7 1627 Capitanata earthquake (CFTI5Med; [45]). The epicentre and the causative fault of this earthquake are located onshore [44,378]; therefore, the source of the related tsunami is still unknown.

5.6 Meteotsunamis

Several cases of meteotsunamis are documented throughout the Mediterranean, as in the cases described in **Figure 13a**, which is taken from [379]. By investigating the resonance conditions in terms of Froude number (Fr), the authors showed that the most favourable conditions for meteotsunami generation ($0.9 < Fr < 1.1$) exist along most of the Italian coasts, especially in the Adriatic Sea and in the Strait of Sicily (**Figure 13a**).

For example, a recent publication by Šepić et al. [380] describes the occurrence of a meteotsunami in the city of Mazara del Vallo in 2014, producing inundation of about 1 m, channelling upstream along the local river and some damages on boats.

Another recent example of meteotsunami along the Italian coasts is reported in Figure 13b, showing the record of a meteo-tsunami in the Adriatic Sea occurred on 1 August 2019. The inundation in some places may be quite sudden, as in the case of Ancona, where a sea-level rise of almost 1 m has been recorded by the tide gauge located in the harbour.

Attempts to quantify the probability of meteotsunami occurrence exist, based on probabilistic synoptic meteotsunami index [74] that can be potentially extended to integrate nonstationarities and time-dependencies induced by climatic factors (http://www.savemedcoasts.eu/). These forecasts require the monitoring of synoptic conditions (highlighting the favourable condition for their generation), as well as the need to track small-scale air pressure disturbances (meteotsunami source) and atmosphere-sea interaction (meteotsunami generation and propagation). As pointed out above for seismic sources, these probabilistic methods may represent the future for science-informed tsunami warnings, but currently extensive testing against data is still needed.

6. Outlook

The critical challenge in common to all atypical (seismic and non-seismic) sources is the need to deal with significant uncertainty due to a large number of different and difficult-to-model potential sources and source mechanisms. The quantification of this uncertainty, which is even larger when there is a need to act fast to increase the lead time for local evacuation for tsunami warning, is fundamental for tsunami risk management. This is a challenge from the scientific, computational, and decision-making points of view. Significant scientific research is still required to characterize many of the atypical sources in a simple and unified way, provided it is possible, and in many case it is still needed to develop ad hoc modelling procedures, as well as monitoring (e.g., of the triggering conditions) and warning strategies. Moving away from deterministic previsions to probabilistic forecasts that manage source uncertainty (e.g. [97]), while reducing the uncertainty through the improvement of the source and tsunami monitoring systems and processing algorithms (e.g. [152]), are tasks that should be pursued synergically. Indeed, only within a coherent uncertainty treatment framework, the technologically- and modelling-driven uncertainty-reduction strategies can be exploited without creating dangerous biases due to overconfidence. In fact, uncertainty will never be eliminated, and a certain degree of unpredictability will always need to be managed.

The increasing number and quality of probabilistic hazard and risk analyses show that there are a growing capability and intent to study and characterize complex sources such as the atypical ones, especially the seismic ones. Recent hazard studies on seismically generated tsunamis have already started including non-megathrust events [11,31,52,53], and many efforts are also ongoing to improve the computational efficiency [66,67,70] and to extend toward non-seismic sources [11,17,32,99,193]. These hazard studies may provide important information also for tsunami warning, such as i) the description of the full variability of the source mechanisms (e.g., [31]); ii) the prioritization of sources based on the capability of generating tsunamis and the long-term frequency of tsunamigenic events (e.g., based on hazard disaggregation; [31,381]); iii) the development of databases of pre-defined sources and related tsunami propagation scenarios that may be used in real-time tsunami warning (e.g. [52,53,66,68,69]). Important contributions may also arise from the development of optimized workflows making use of high-performance computing, like the ones in development within the ChEESE Centre of Excellence project (https://cheese-coe.eu/), providing the opportunity to refine the uncertainty quantification, as well as to improve the management

of disasters caused by tsunamis through the post-event characterization evaluated by means of urgent computing [67].

Hazard quantifications for non-seismic sources are still very limited [11,54]. While a few prototypal probabilistic hazard analyses have been discussed in the literature (e.g., [17,30,32,65,99]), most present-day analyses are limited to the identification of reference past scenarios and the search of appropriate modelling tools to define datasets of possible scenarios, like in the discussed case of Stromboli. The lack of recognized modelling procedures and of probabilistic source models prevented until now the development of proper hazard characterization, and a strong research effort in this direction is still needed.

The main pathway for implementing tsunami warnings for atypical sources is the development of suitable source and tsunami monitoring systems, possibly keeping in mind some lessons from the present-day systems for seismic tsunamis. For the volcanic sources, the situation is complicated by the large variety of possible tsunami-generating events. In the case of Stromboli, the frequency of occurrence of tsunami generating events from one specific source area (the SdF slope) pushed toward the development of a specialized system completely devoted to this single source. Specialized systems focusing on only one or a few potential source areas may not be appropriate for many volcanoes. Even assuming that all the relevant source areas can be identified, due to their number, their direct monitoring may be practically impossible. In either case, the only viable solution is the implementation of prioritization efforts, based on a profound uncertainty analysis to allow the decision-makers to define which volcanoes and/or areas of gravitational instability are the most important ones to concentrate the efforts, based on both hazard frequency and intensity, as well as the potential impact due to high vulnerability and exposure. Ideally, it should be first clarified what is the level of residual risk is being accepted in order to establish to which extent different source mechanisms should be considered, even if risk is very difficult to be achieved at present given the large uncertainty associated with these phenomena.

The development of new tsunami monitoring technologies will bring new opportunities for tsunami warning [152,382], reinforcing the source monitoring that is foreseen to be subject as well to dramatic progress, including specific progress related to specific atypical sources such as for example tsunami earthquakes (e.g. [286,383]). The Stromboli warning system shows that source and tsunami monitoring should co-exist, as indeed is also the case for the existing warning systems for tsunamigenic landslides in Norway. The current system at Stromboli Island is based on the direct detection of the tsunami that has been optimized by focusing on an exact location as the most probable source (SdF). Nevertheless, it is evident that a more constrained forecasting of the conditions for the tsunami generation can significantly increase the lead time and allow for a more effective evacuation.

The need for joint improvements in the forecasting/monitoring procedures for the triggering event is indeed a general remark valid for all sources, in which any tsunami detection should be at least accompanied by a specific monitoring system focused on the early detection of the triggering phenomena that may facilitate the tsunami generation [10,17,73,151,271,281]. This principle can also be extended to secondary sources like induced landslides, for which statistical methods are able to forecast the events based on the observation of triggering events, like rain or earthquakes. In the future, such forecasts may be coupled with local susceptibility analyses to develop probabilistic forecasts of the tsunami impact. While perhaps they will never reach high probability values in their forecasts, such methods may be used to provide significant probability gains that may help decision-making (e.g., [384]).

Probabilistic forecasting methods for tsunami warning may provide the background to merge the different strategies discussed above [68,96,97,154,155,385]. Indeed, they are based on the explicit consideration of ensembles of sources that virtually cover the whole natural variability, as well as of the uncertainty of tsunami generation and propagation. The definition and the weights of the ensembles can be based on direct monitoring of the tsunami-generating event, as well as by the monitoring of potential triggering

1798 events and/or by direct tsunami measures (e.g., through data assimilation techniques; [386–388]). The
1799 recent developments on the management of uncertainty in the short-term forecast of tsunamis caused by
1800 crustal sources show that the shift from empirical decision matrix or deterministic scenarios to
1801 computationally based probabilistic tsunami forecast is possible in the near future. The development of
1802 similar methods is ongoing also for meteotsunamis (e.g., [74,379]), based on the monitoring of the
1803 atmospheric conditions leading to these phenomena. In either case, thorough testing of existing
1804 procedures against future data will be required before this kind of system may become operational.

1805

1806

References

1. Lay T, Wallace TC (1995) Modern global seismology, San Diego, Academic Press.
2. Lorito S, Romano F, Lay T (2016) Tsunamigenic Major and Great Earthquakes (2004–2013): Source Processes Inverted from Seismic, Geodetic, and Sea-Level Data, In: Meyers RA (Ed.), *Encyclopedia of Complexity and Systems Science*, Berlin, Heidelberg, Springer, 1–52.
3. Hayes GP, Moore GL, Portner DE, et al. (2018) Slab2, a comprehensive subduction zone geometry model. *Science* 362: 58–61.
4. Ulrich T, Vater S, Madden EH, et al. (2019) Coupled, Physics-Based Modeling Reveals Earthquake Displacements are Critical to the 2018 Palu, Sulawesi Tsunami. *Pure Appl Geophys* 176: 4069–4109.
5. Carvajal M, Araya-Cornejo C, Sepúlveda I, et al. (2019) Nearly Instantaneous Tsunamis Following the Mw 7.5 2018 Palu Earthquake. *Geophysical Research Letters* 46: 5117–5126.
6. Schamback L, Grilli S, Tappin D (2020) New high-resolution modeling of the 2018 Palu tsunami, based on supershear earthquake mechanisms and mapped coastal landslides, supports a dual source. *Front Earth Sci*.
7. Omira R, Dogan GG, Hidayat R, et al. (2019) The September 28th, 2018, Tsunami In Palu-Sulawesi, Indonesia: A Post-Event Field Survey. *Pure Appl Geophys* 176: 1379–1395.
8. Widiyanto W, Santoso PB, Hsiao S-C, et al. (2019) Post-event Field Survey of 28 September 2018 Sulawesi Earthquake and Tsunami, Sea, Ocean and Coastal Hazards.
9. Zengaffinen T, Løvholt F, Pedersen GK, et al. (2020) Modelling 2018 Anak Krakatoa Flank Collapse and Tsunami: Effect of Landslide Failure Mechanism and Dynamics on Tsunami Generation. *Pure Appl Geophys* 177: 2493–2516.
10. Walter TR, Haghshenas Haghighi M, Schneider FM, et al. (2019) Complex hazard cascade culminating in the Anak Krakatau sector collapse. *Nature Communications* 10: 4339.
11. Grezio A, Babeyko A, Baptista MA, et al. (2017) Probabilistic Tsunami Hazard Analysis: Multiple Sources and Global Applications. *Reviews of Geophysics* 55: 1158–1198.
12. IOC/UNESCO (2020) [Intergovernmental Oceanographic Commission / UNESCO] TOWS-WG Inter-ICG Task Team on Tsunami Watch Operations Meeting, 2020. Available from: http://www.ioc-unesco.org/index.php?option=com_oe&task=viewEventRecord&eventID=2597.
13. Bizzarri A (2011) ON THE DETERMINISTIC DESCRIPTION OF EARTHQUAKES. *Rev Geophys* 49: RG3002.
14. Basili R, Tiberti MM, Kastelic V, et al. (2013) Integrating geologic fault data into tsunami hazard studies. *Natural Hazards and Earth System Sciences* 13: 1025–1050.
15. Polet J, Kanamori H (2016) Tsunami Earthquakes, In: Meyers RA (Ed.), *Encyclopedia of Complexity and Systems Science*, Berlin, Heidelberg, Springer, 1–22.
16. Løvholt F, Pedersen G, Harbitz CB, et al. (2015) On the characteristics of landslide tsunamis. *Phil Trans R Soc A* 373: 20140376.
17. Løvholt F, Glimsdal S, Harbitz CB (2020) On the landslide tsunami uncertainty and hazard. *Landslides*.
18. Yavari-Ramshe S, Ataie-Ashtiani B (2016) Numerical modeling of subaerial and submarine landslide-generated tsunami waves—recent advances and future challenges. *Landslides* 13: 1325–1368.
19. Paris R, Switzer AD, Belousova M, et al. (2014) Volcanic tsunami: a review of source mechanisms, past events and hazards in Southeast Asia (Indonesia, Philippines, Papua New Guinea). *Nat Hazards* 70: 447–470.
20. Paris R (2015) Source mechanisms of volcanic tsunamis. *Philosophical Transactions of the Royal Society A: Mathematical, Physical and Engineering Sciences* 373: 20140380.
21. Rabinovich AB, Monserrat S (1998) Generation of Meteorological Tsunamis (Large Amplitude Seiches) Near the Balearic and Kuril Islands. *Natural Hazards* 18: 27–55.
22. Vilibić I, Šepić J (2009) Destructive meteotsunamis along the eastern Adriatic coast: Overview. *Physics and Chemistry of the Earth, Parts A/B/C* 34: 904–917.
23. Harbitz CB, Glimsdal S, Bazin S, et al. (2012) Tsunami hazard in the Caribbean: Regional exposure derived from credible worst case scenarios. *Continental Shelf Research* 38: 1–23.
24. Parsons T, Geist EL (2008) Tsunami Probability in the Caribbean Region, In: Cummins PR, Satake K, Kong LSL (Eds.), *Tsunami Science Four Years after the 2004 Indian Ocean Tsunami*, Basel, Birkhäuser Basel, 2089–2116.

25. Løvholt F, Kühn D, Bungum H, et al. (2012) Historical tsunamis and present tsunami hazard in eastern Indonesia and the southern Philippines: TSUNAMI HAZARD IN EASTERN INDONESIA. *J Geophys Res* 117.
26. Tinti S, Bortolucci E, Armigliato A (1999) Numerical simulation of the landslide-induced tsunami of 1988 on Vulcano Island, Italy. *Bull Volcanol* 61: 121–137.
27. Tinti S, Chiocci FL, Zaniboni F, et al. (2011) Numerical simulation of the tsunami generated by a past catastrophic landslide on the volcanic island of Ischia, Italy. *Mar Geophys Res* 32: 287–297.
28. Chiocci FL, Alteriis GD (2006) The Ischia debris avalanche: first clear submarine evidence in the Mediterranean of a volcanic island prehistorical collapse. *Terra Nova* 18: 202–209.
29. Zaniboni F, Pagnoni G, Tinti S, et al. (2013) The potential failure of Monte Nuovo at Ischia Island (Southern Italy): numerical assessment of a likely induced tsunami and its effects on a densely inhabited area. *Bull Volcanol* 75: 763.
30. Grezio A, Tonini R, Sandri L, et al. (2015) A Methodology for a Comprehensive Probabilistic Tsunami Hazard Assessment: Multiple Sources and Short-Term Interactions. *Journal of Marine Science and Engineering* 3: 23–51.
31. Selva J, Tonini R, Molinari I, et al. (2016) Quantification of source uncertainties in Seismic Probabilistic Tsunami Hazard Analysis (SPTHA). *Geophys J Int* 205: 1780–1803.
32. Paris R, Ulvrova M, Selva J, et al. (2019) Probabilistic hazard analysis for tsunamis generated by subaqueous volcanic explosions in the Campi Flegrei caldera, Italy. *Journal of Volcanology and Geothermal Research* 379: 106–116.
33. Volpe M, Lorito S, Selva J, et al. (2019) From regional to local SPTHA: efficient computation of probabilistic tsunami inundation maps addressing near-field sources. *Nat Hazards Earth Syst Sci* 19: 455–469.
34. Pistolesi M, Bertagnini A, Roberto AD, et al. (2020) Tsunami and tephra deposits record interactions between past eruptive activity and landslides at Stromboli volcano, Italy. *Geology* 48: 436–440.
35. Rosi M, Levi ST, Pistolesi M, et al. (2019) Geoarchaeological Evidence of Middle-Age Tsunamis at Stromboli and Consequences for the Tsunami Hazard in the Southern Tyrrhenian Sea. *Scientific Reports* 9: 677.
36. Maramai A, Brizuela B, Graziani L (2014) The Euro-Mediterranean Tsunami Catalogue. *Annals of Geophysics* 57: 0435.
37. Heidarzadeh M, Satake K (2013) The 21 May 2003 Tsunami in the Western Mediterranean Sea: Statistical and Wavelet Analyses. *Pure Appl Geophys* 170: 1449–1462.
38. Dogan GG, Annunziato A, Papadopoulos GA, et al. (2019) The 20th July 2017 Bodrum–Kos Tsunami Field Survey. *Pure Appl Geophys* 176: 2925–2949.
39. Yalciner AC, Dogan GG, Ulutas E, et al. (2020) The 30 October 2020 (11:51 UTC) Izmir-Samos earthquake and tsunami; Post-tsunami field survey preliminary results.
40. Maramai A, Graziani L, Alessio G, et al. (2005) Near- and far-field survey report of the 30 December 2002 Stromboli (Southern Italy) tsunami. *Marine Geology* 215: 93–106.
41. Tinti S, Pagnoni G, Zaniboni F (2006) The landslides and tsunamis of the 30th of December 2002 in Stromboli analysed through numerical simulations. *Bull Volcanol* 68: 462–479.
42. Tinti S, Maramai A, Armigliato A, et al. (2006) Observations of physical effects from tsunamis of December 30, 2002 at Stromboli volcano, southern Italy. *Bull Volcanol* 68: 450–461.
43. Tinti S, Manucci A, Pagnoni G, et al. (2005) The 30 December 2002 landslide-induced tsunamis in Stromboli: sequence of the events reconstructed from the eyewitness accounts. *Nat Hazards Earth Syst Sci* 5: 763–775.
44. Rovida A, Locati M, Camassi R, et al. (2020) The Italian earthquake catalogue CPTI15. *Bull Earthquake Eng* 18: 2953–2984.
45. Guidoboni E, Ferrari G, Tarabusi G, et al. (2019) CFTI5Med, the new release of the catalogue of strong earthquakes in Italy and in the Mediterranean area. *Sci Data* 6: 80.
46. Tinti S, Armigliato A (2003) The use of scenarios to evaluate the tsunami impact in southern Italy. *Marine Geology* 199: 221–243.

47. Billi A, Funiciello R, Minelli L, et al. (2008) On the cause of the 1908 Messina tsunami, southern Italy. *Geophysical Research Letters* 35.
48. Argnani A, Brancolini G, Bonazzi C, et al. (2009) The results of the Taormina 2006 seismic survey: Possible implications for active tectonics in the Messina Straits. *Tectonophysics* 476: 159–169.
49. Argnani A, Chiocci FL, Tinti S, et al. (2009) Comment on "On the cause of the 1908 Messina tsunami, southern Italy" by Andrea Billi et al. *Geophysical Research Letters* 36.
50. Favalli M, Boschi E, Mazzarini F, et al. (2009) Seismic and landslide source of the 1908 Straits of Messina tsunami (Sicily, Italy). *Geophysical Research Letters* 36.
51. Basili R, Brizuela B, Herrero A, et al. (2018) NEAM Tsunami Hazard Model 2018 (NEAMTHM18): online data of the Probabilistic Tsunami Hazard Model for the NEAM Region from the TSUMAPS-NEAM project., Istituto Nazionale di Geofisica e Vulcanologia (INGV).
52. Basili R, Brizuela B, Herrero A, et al. (2019) NEAMTHM18 Documentation: the making of the TSUMAPS-NEAM Tsunami Hazard Model 2018, Zenodo.
53. Basili R, Brizuela B, Herrero A, et al. (2021) The making of the NEAM Tsunami Hazard Model 2018 (NEAMTHM18). *Frontiers in Earth Science*.
54. Behrens J, Løvholt F, Jalayer F, et al. (2021) Probabilistic Tsunami Hazard and Risk Analysis – A Review of Research Gaps. *Frontiers in Earth Science*.
55. Leonard G, Power W, Lukovic B, et al. (2008) Interim tsunami evacuation planning zone boundary mapping for the Wellington and Horizons regions defined by a GIS-calculated attenuation rule, Lower Hutt, N.Z., GNS Science.
56. Bernard E, Titov V (2015) Evolution of tsunami warning systems and products. *Philosophical Transactions of the Royal Society A: Mathematical, Physical and Engineering Sciences* 373: 20140371.
57. Chock G, Yu G, Thio HK, et al. (2016) Target Structural Reliability Analysis for Tsunami Hydrodynamic Loads of the ASCE 7 Standard. *Journal of Structural Engineering* 142: 04016092.
58. ASCE (2017) [American Society of Civil Engineers] ASCE 7-16 Tsunami Design Zone Maps For Selected Locations., Reston, VA, American Society of Civil Engineers.
59. NEAMTWS (2007) Tsunami Early Warning and Mitigation System in the North Eastern Atlantic, the Mediterranean and Connected Seas, NEAMTWS, Implementation Plan (Third Session of the Intergovernmental Coordination Group for the Tsunami Early Warning and Mitigation System in the North Eastern Atlantic, the Mediterranean and Connected Seas, NEAMTWS), UNESCO.
60. MCDEM (2008) [New Zealand Ministry of Civil Defence & Emergency Management] Tsunami evacuation zones: director's guideline for Civil Defence Emergency Management Groups., Wellington, N.Z., Ministry of Civil Defence & Emergency Management.
61. MCDEM (2016) [New Zealand Ministry of Civil Defence & Emergency Management] Tsunami evacuation zones: director's guideline for Civil Defence Emergency Management Groups., Wellington, N.Z., Ministry of Civil Defence & Emergency Management.
62. DPC (2018) Dipartimento della Protezione Civile, [Dipartimento della Protezione Civile] Indicazioni alle Componenti ed alle Strutture operative del Servizio nazionale di protezione civile per l'aggiornamento delle pianificazioni di protezione civile per il rischio maremoto - Normativa, 2018. Available from: http://www.protezionecivile.gov.it/amministrazione-trasparente/provvedimenti/dettaglio/-/asset_publisher/default/content/indicazioni-alle-componenti-ed-alle-strutture-operative-del-servizio-nazionale-di-protezione-civile-per-l-aggiornamento-delle-pianificazioni-di-prot-1.
63. Tonini R, Di Manna P, Lorito S, et al. (2021) Testing inundation maps for evacuation planning in Italy. *Frontiers in Earth Science*.
64. Behrens J, Dias F (2015) New computational methods in tsunami science. *Philosophical Transactions of the Royal Society A: Mathematical, Physical and Engineering Sciences* 373: 20140382.
65. Geist E, Lynett P (2014) Source Processes for the Probabilistic Assessment of Tsunami Hazards. *oceanog* 27: 86–93.

66. Molinari I, Tonini R, Lorito S, et al. (2016) Fast evaluation of tsunami scenarios: uncertainty assessment for a Mediterranean Sea database. *Natural Hazards and Earth System Sciences* 16: 2593–2602.
67. Løvholt F, Lorito S, Macias J, et al. (2019) Urgent Tsunami Computing, *2019 IEEE/ACM HPC for Urgent Decision Making (UrgentHPC)*, Denver, CO, USA, IEEE, 45–50.
68. Selva J, Lorito S, Perfetti P, et al. (2019) Probabilistic Tsunami Forecasting (PTF) for Tsunami Early Warning operations, *Geophysical Research Abstracts*, Vienna, EGU2019-17775, 2019.
69. Selva J, Lorito S, Volpe M, et al. (submitted) Probabilistic Tsunami Forecasting (PTF) for Tsunami Early Warning operations.
70. Gibbons SJ, Lorito S, Macias Sanchez J, et al. (2020) Probabilistic Tsunami Hazard Analysis: High Performance Computing for Massive Scale Inundation Simulations. *Frontiers in Earth Science*.
71. Maesano FE, Tiberti MM, Basili R (2017) The Calabrian Arc: three-dimensional modelling of the subduction interface. *Scientific Reports* 7: 8887.
72. Maesano FE, Tiberti MM, Basili R (2020) Deformation and Fault Propagation at the Lateral Termination of a Subduction Zone: The Alfeo Fault System in the Calabrian Arc, Southern Italy. *Front Earth Sci* 8: 107.
73. Harbitz CB, Løvholt F, Bungum H (2014) Submarine landslide tsunamis: how extreme and how likely? *Nat Hazards* 72: 1341–1374.
74. Šepić J, Vilibić I, Monserrat S (2016) Quantifying the probability of meteotsunami occurrence from synoptic atmospheric patterns: Meteotsunami Index. *Geophys Res Lett* 43: 10,377-10,384.
75. Levin BW, Nosov MA (2009) Physics of Tsunamis, Dordrecht, Springer Netherlands.
76. Nosov MA, Kolesov SV (2011) Optimal Initial Conditions for Simulation of Seismotectonic Tsunamis. *Pure Appl Geophys* 168: 1223–1237.
77. Kim J, Løvholt F, Issler D, et al. (2019) Landslide Material Control on Tsunami Genesis—The Storegga Slide and Tsunami (8,100 Years BP). *J Geophys Res Oceans* 124: 3607–3627.
78. Kelfoun K, Druitt TH (2005) Numerical modeling of the emplacement of Socompa rock avalanche, Chile. *J Geophys Res* 110: B12202.
79. Si P, Shi H, Yu X (2018) Development of a mathematical model for submarine granular flows. *Physics of Fluids* 30: 083302.
80. Jop P, Forterre Y, Pouliquen O (2006) A constitutive law for dense granular flows. *Nature* 441: 727–730.
81. Rauter M (in press) The compressible granular collapse in a fluid as a continuum: validity of a Navier-Stokes model with mu(J)-fi(J)-rheology,. *Journal of Fluid Mechanics*.
82. Løvholt F, Bondevik S, Laberg JS, et al. (2017) Some giant submarine landslides do not produce large tsunamis: GIANT LANDSLIDE TSUNAMIS. *Geophys Res Lett* 44: 8463–8472.
83. Watts P (2000) Tsunami Features of Solid Block Underwater Landslides. *J Waterway, Port, Coastal, Ocean Eng* 126: 144–152.
84. Salmanidou DM, Guillas S, Georgiopoulou A, et al. (2017) Statistical emulation of landslide-induced tsunamis at the Rockall Bank, NE Atlantic. *Proc R Soc A* 473: 20170026.
85. Lotto GC, Nava G, Dunham EM (2017) Should tsunami simulations include a nonzero initial horizontal velocity? *Earth Planets Space* 69: 117.
86. Renzi E, Dias F (2014) Hydro-acoustic precursors of gravity waves generated by surface pressure disturbances localised in space and time. *J Fluid Mech* 754: 250–262.
87. Pattiaratchi CB, Wijeratne EMS (2015) Are meteotsunamis an underrated hazard? *Phil Trans R Soc A* 373: 20140377.
88. Williams DA, Horsburgh KJ, Schultz DM, et al. (2020) Proudman resonance with tides, bathymetry and variable atmospheric forcings. *Nat Hazards*.
89. Glimsdal S, Pedersen GK, Atakan K, et al. (2006) Propagation of the Dec. 26, 2004, Indian Ocean Tsunami: Effects of Dispersion and Source Characteristics. *Inter J Fluid Mech Res* 33: 15–43.
90. Qin X, Motley M, LeVeque R, et al. (2018) A comparison of a two-dimensional depth-averaged flow model and a three-dimensional RANS model for predicting tsunami inundation and fluid forces. *Nat Hazards Earth Syst Sci* 18: 2489–2506.

91. Griffin J, Latief H, Kongko W, et al. (2015) An evaluation of onshore digital elevation models for modeling tsunami inundation zones. *Front Earth Sci* 3.
92. Choi BH, Pelinovsky E, Kim KO, et al. (2003) Simulation of the trans-oceanic tsunami propagation due to the 1883 Krakatau volcanic eruption. *Nat Hazards Earth Syst Sci* 3: 321–332.
93. Goda K, Mai PM, Yasuda T, et al. (2014) Sensitivity of tsunami wave profiles and inundation simulations to earthquake slip and fault geometry for the 2011 Tohoku earthquake. *Earth Planet Sp* 66: 105.
94. Davies G, Griffin J, Løvholt F, et al. (2018) A global probabilistic tsunami hazard assessment from earthquake sources. *Geological Society, London, Special Publications* 456: 219–244.
95. González FI, Geist EL, Jaffe B, et al. (2009) Probabilistic tsunami hazard assessment at Seaside, Oregon, for near- and far-field seismic sources. *J Geophys Res* 114: C11023.
96. Sorensen J, Mileti DS (1987) Decision-making Uncertainties in Emergency Warning System Organizations - International Journal of Mass Emergencies and Disasters. 5: 33–61.
97. Woo G, Aspinall W (2005) Need for a risk-informed tsunami alert system. *Nature* 433: 457–457.
98. IOC/UNESCO (2018) [Intergovernmental Oceanographic Commission / UNESCO] IOC/UNESCO Symposium on Advances in Tsunami Warning to Enhance Community Responses, 12–14 February 2018, Paris; Summary Statement.
99. Grezio A, Cinti FR, Costa A, et al. (2020) Multisource Bayesian Probabilistic Tsunami Hazard Analysis for the Gulf of Naples (Italy). *J Geophys Res Oceans* 125.
100. Urgeles R, Camerlenghi A (2013) Submarine landslides of the Mediterranean Sea: Trigger mechanisms, dynamics, and frequency-magnitude distribution: LANDSLIDES IN THE MEDITERRANEAN SEA. *J Geophys Res Earth Surf* 118: 2600–2618.
101. Berndt C, Brune S, Nisbet E, et al. (2009) Tsunami modeling of a submarine landslide in the Fram Strait: TSUNAMI MODELS FOR A LANDSLIDE OFF SVALBARD. *Geochem Geophys Geosyst* 10: n/a-n/a.
102. Harbitz CB, Glimsdal S, Løvholt F, et al. (2014) Rockslide tsunamis in complex fjords: From an unstable rock slope at Åkerneset to tsunami risk in western Norway. *Coastal Engineering* 88: 101–122.
103. Blikra L (2008) The √Öknes rockslide: Monitoring, threshold values and early-warning, In: Chen Z, Zhang J, Li Z, et al. (Eds.), *Landslides and Engineered Slopes. From the Past to the Future*, CRC Press, 1089–1094.
104. Oppikofer T, Jaboyedoff M, Blikra L, et al. (2009) Characterization and monitoring of the Åknes rockslide using terrestrial laser scanning. *Nat Hazards Earth Syst Sci* 9: 1003–1019.
105. Hermanns RL, Oppikofer T, Molina FXY, et al. (2014) Approach for Systematic Rockslide Mapping of Unstable Rock Slopes in Norway, In: Sassa K, Canuti P, Yin Y (Eds.), *Landslide Science for a Safer Geoenvironment*, Cham, Springer International Publishing, 129–134.
106. Hermanns RL, Oppikofer T, Anda E, et al. (2013) HAZARD AND RISK CLASSIFICATION FOR LARGE UNSTABLE ROCK SLOPES IN NORWAY. 245–254.
107. Allen RM, Melgar D (2019) Earthquake Early Warning: Advances, Scientific Challenges, and Societal Needs. *Annu Rev Earth Planet Sci* 47: 361–388.
108. Zollo A, Iannaccone G, Lancieri M, et al. (2009) Earthquake early warning system in southern Italy: Methodologies and performance evaluation. *Geophys Res Lett* 36: L00B07.
109. Allen RM (2003) The Potential for Earthquake Early Warning in Southern California. *Science* 300: 786–789.
110. DPCM (2017) [Direttiva del Presidente del Consiglio dei Ministri] Istituzione del Sistema d'Allertamento nazionale per i Maremoti generati da sisma - SiAM (directive of the President of the Council of Ministers: formation of the SiAM for seismically generated tsunamis). *Gazzetta Ufficiale* 128.
111. Amato A (2020) Some reflections on tsunami Early Warning Systems and their impact, with a look at the NEAMTWS. *BGTA*.
112. Amato A, Avallone A, Basili R, et al. (submitted) From seismic monitoring to tsunami warning in the Mediterranean.

113. Lin I-C, Tung CC (1982) A preliminary investigation of tsunami hazard. *Bulletin of the Seismological Society of America* 72: 2323–2337.
114. Rikitake T, Aida I (1988) Tsunami hazard probability in Japan. *Bulletin of the Seismological Society of America* 78: 1268–1278.
115. Tinti S (1991) Assessment of Tsunami Hazard in the Italian Seas, In: Bernard EN (Ed.), *Tsunami Hazard*, Dordrecht, Springer Netherlands, 267–283.
116. Geist EL, Parsons T (2006) Probabilistic Analysis of Tsunami Hazards*. *Nat Hazards* 37: 277–314.
117. Power W, Downes G, Stirling M (2007) Estimation of Tsunami Hazard in New Zealand due to South American Earthquakes. *Pure appl geophys* 164: 547–564.
118. Annaka T, Satake K, Sakakiyama T, et al. (2007) Logic-tree Approach for Probabilistic Tsunami Hazard Analysis and its Applications to the Japanese Coasts. *Pure appl geophys* 164: 577–592.
119. Thio HK, Somerville P, Ichinose G (2007) PROBABILISTIC ANALYSIS OF STRONG GROUND MOTION AND TSUNAMI HAZARDS IN SOUTHEAST ASIA. *J Earthquake and Tsunami* 01: 119–137.
120. Burbidge D, Cummins PR, Mleczko R, et al. (2008) A Probabilistic Tsunami Hazard Assessment for Western Australia. *Pure appl geophys* 165: 2059–2088.
121. Taubenböck H, Post J, Roth A, et al. (2008) A conceptual vulnerability and risk framework as outline to identify capabilities of remote sensing. *Nat Hazards Earth Syst Sci* 8: 409–420.
122. Heidarzadeh M, Kijko A (2011) A probabilistic tsunami hazard assessment for the Makran subduction zone at the northwestern Indian Ocean. *Nat Hazards* 56: 577–593.
123. Suppasri A, Imamura F, Koshimura S (2012) PROBABILISTIC TSUNAMI HAZARD ANALYSIS AND RISK TO COASTAL POPULATIONS IN THAILAND. *J Earthquake and Tsunami* 06: 1250011.
124. Yadav RBS, Tsapanos TM, Tripathi JN, et al. (2013) An evaluation of tsunami hazard using Bayesian approach in the Indian Ocean. *Tectonophysics* 593: 172–182.
125. Horspool N, Pranantyo I, Griffin J, et al. (2014) A probabilistic tsunami hazard assessment for Indonesia. *Nat Hazards Earth Syst Sci* 14: 3105–3122.
126. Shin JY, Chen S, Kim T-W (2015) Application of Bayesian Markov Chain Monte Carlo method with mixed gumbel distribution to estimate extreme magnitude of tsunamigenic earthquake. *KSCE J Civ Eng* 19: 366–375.
127. Hoechner A, Babeyko AY, Zamora N (2016) Probabilistic tsunami hazard assessment for the Makran region with focus on maximum magnitude assumption. *Nat Hazards Earth Syst Sci* 16: 1339–1350.
128. Griffin JD, Pranantyo IR, Kongko W, et al. (2017) Assessing tsunami hazard using heterogeneous slip models in the Mentawai Islands, Indonesia. *Geological Society, London, Special Publications* 441: 47–70.
129. Davies G, Griffin J (2018) The 2018 Australian probabilistic tsunami hazard assessment: hazard from earthquake generated tsunamis, Geoscience Australia.
130. Sørensen MB, Spada M, Babeyko A, et al. (2012) Probabilistic tsunami hazard in the Mediterranean Sea: TSUNAMI HAZARD IN THE MEDITERRANEAN SEA. *J Geophys Res* 117: n/a-n/a.
131. Cornell CA (1968) Engineering seismic risk analysis. *Bulletin of the Seismological Society of America* 58: 1583–1606.
132. Gerstenberger MC, Marzocchi W, Allen T, et al. (2020) Probabilistic Seismic Hazard Analysis at Regional and National Scales: State of the Art and Future Challenges. *Rev Geophys* 58.
133. NGDC [National Geophysical Data Center] Global Historical Tsunami Database.
134. Lorito S, Selva J, Basili R, et al. (2015) Probabilistic hazard for seismically induced tsunamis: accuracy and feasibility of inundation maps. *Geophys J Int* 200: 574–588.
135. Løvholt F, Glimsdal S, Harbitz CB, et al. (2014) Global tsunami hazard and exposure due to large co-seismic slip. *International Journal of Disaster Risk Reduction* 10: 406–418.
136. Grezio A, Sandri L, Marzocchi W, et al. (2012) Probabilistic tsunami hazard assessment for Messina Strait Area (Sicily, Italy). *Nat Hazards* 64: 329–358.
137. Gutenberg B, Richter C (1954) Seismicity of the Earth and Associated Phenomena, Princeton University Press.
138. Kagan YY (2002) Seismic moment distribution revisited: I. Statistical results: Seismic moment distribution: I. *Geophysical Journal International* 148: 520–541.

139. Douglas J, Edwards B (2016) Recent and future developments in earthquake ground motion estimation. *Earth-Science Reviews* 160: 203–219.
140. Glimsdal S, Løvholt F, Harbitz CB, et al. (2019) A New Approximate Method for Quantifying Tsunami Maximum Inundation Height Probability. *Pure Appl Geophys* 176: 3227–3246.
141. Budnitz R, Apostolakis G, Boore D, et al. (1997) Senior Seismic Hazard Analysis Committee (SSHAC): Recommendations for Probabilistic Seismic Hazard Analysis: Guidance on Uncertainty and Use of Experts: Main Report.
142. Bommer JJ, Scherbaum F (2008) The Use and Misuse of Logic Trees in Probabilistic Seismic Hazard Analysis. *Earthquake Spectra* 24: 997–1009.
143. Marzocchi W, Taroni M, Selva J (2015) Accounting for Epistemic Uncertainty in PSHA: Logic Tree and Ensemble Modeling. *Bulletin of the Seismological Society of America* 105: 2151–2159.
144. Kulkarni R, Youngs R, Coppersmith K (1984) Assessment of confidence intervals for results of seismic hazard analysis, *Proceedings of the Eighth World Conference on Earthquake Engineering*, San Francisco, California, 263–270.
145. Selva J, Sandri L (2013) Probabilistic Seismic Hazard Assessment: Combining Cornell-Like Approaches and Data at Sites through Bayesian Inference. *Bulletin of the Seismological Society of America* 103: 1709–1722.
146. Marzocchi W, Jordan TH (2014) Testing for ontological errors in probabilistic forecasting models of natural systems. *Proceedings of the National Academy of Sciences* 111: 11973–11978.
147. Mulia IE, Satake K (2020) Developments of Tsunami Observing Systems in Japan. *Front Earth Sci* 8.
148. Wang Y, Heidarzadeh M, Satake K, et al. (2020) A Tsunami Warning System Based on Offshore Bottom Pressure Gauges and Data Assimilation for Crete Island in the Eastern Mediterranean Basin. *J Geophys Res Solid Earth* 125.
149. Mulia IE, Gusman AR, Satake K (2017) Optimal Design for Placements of Tsunami Observing Systems to Accurately Characterize the Inducing Earthquake. *Geophys Res Lett* 44.
150. Heidarzadeh M, Wang Y, Satake K, et al. (2019) Potential deployment of offshore bottom pressure gauges and adoption of data assimilation for tsunami warning system in the western Mediterranean Sea. *Geosci Lett* 6: 19.
151. Lacanna E, Ripepe M (2020) Genesis of tsunami waves generated by Pyroclastic flows and the Early-Warning system, *Abstract Volume 4a Conferenza A. Rittmann*, Catania, Italy.
152. Angove M, Arcas D, Bailey R, et al. (2019) Ocean Observations Required to Minimize Uncertainty in Global Tsunami Forecasts, Warnings, and Emergency Response. *Front Mar Sci* 6.
153. Howe BM, Arbic BK, Aucan J, et al. (2019) SMART Cables for Observing the Global Ocean: Science and Implementation. *Front Mar Sci* 6.
154. Blaser L, Ohrnberger M, Riggelsen C, et al. (2011) Bayesian networks for tsunami early warning. *Geophysical Journal International* 185: 1431–1443.
155. Blaser L, Ohrnberger M, Krüger F, et al. (2012) Probabilistic tsunami threat assessment of 10 recent earthquakes offshore Sumatra. *Geophysical Journal International* 188: 1273–1284.
156. Tatsumi D, Calder CA, Tomita T (2014) Bayesian near-field tsunami forecasting with uncertainty estimates. *J Geophys Res Oceans* 119: 2201–2211.
157. Davies G (2019) Tsunami variability from uncalibrated stochastic earthquake models: tests against deep ocean observations 2006–2016. *Geophys J Int* 218: 1939–1960.
158. Jordan TH, Marzocchi W, Michael AJ, et al. (2014) Operational Earthquake Forecasting Can Enhance Earthquake Preparedness. *Seismological Research Letters* 85: 955–959.
159. Field EH, Jordan TH, Jones LM, et al. (2016) The Potential Uses of Operational Earthquake Forecasting: Table 1. *Seismological Research Letters* 87: 313–322.
160. Le Gal M, Violeau D, Benoit M (2017) Influence of timescales on the generation of seismic tsunamis. *European Journal of Mechanics - B/Fluids* 65: 257–273.
161. Okada Y (1985) Surface deformation due to shear and tensile faults in a half-space. *Bulletin of the Seismological Society of America* 75: 1135–1154.
162. Mansinha L, Smylie D (1971) The Displacement Field of Inclined Faults. *Bull Seismol Soc Am* 61.

163. Herrero A, Murphy S (2018) Self-similar slip distributions on irregular shaped faults. *Geophys J Int* 213: 2060–2070.
164. Scala A, Lorito S, Romano F, et al. (2020) Effect of Shallow Slip Amplification Uncertainty on Probabilistic Tsunami Hazard Analysis in Subduction Zones: Use of Long-Term Balanced Stochastic Slip Models. *Pure Appl Geophys* 177: 1497–1520.
165. Sepúlveda I, Liu PL-F, Grigoriu M, et al. (2017) Tsunami hazard assessments with consideration of uncertain earthquake slip distribution and location: TSUNAMI HAZARD AND UNCERTAIN EARTHQUAKES. *J Geophys Res Solid Earth* 122: 7252–7271.
166. LeVeque RJ, Waagan K, González FI, et al. (2016) Generating Random Earthquake Events for Probabilistic Tsunami Hazard Assessment. *Pure Appl Geophys* 173: 3671–3692.
167. Murphy S, Di Toro G, Romano F, et al. (2018) Tsunamigenic earthquake simulations using experimentally derived friction laws. *Earth and Planetary Science Letters* 486: 155–165.
168. Li L, Switzer AD, Chan C-H, et al. (2016) How heterogeneous coseismic slip affects regional probabilistic tsunami hazard assessment: A case study in the South China Sea: The Effect of Rupture Complexity on PTHA. *J Geophys Res Solid Earth* 121: 6250–6272.
169. Romano F, Trasatti E, Lorito S, et al. (2015) Structural control on the Tohoku earthquake rupture process investigated by 3D FEM, tsunami and geodetic data. *Sci Rep* 4: 5631.
170. ChEESE - Centre of Excellence for Exascale Supercomputing in the area of the Solid Earth Available from: https://cheese-coe.eu/.
171. Zengaffinen T, Løvholt F, Pedersen GK, et al. (2020) Effects of rotational submarine slump dynamics on tsunami genesis: new insight from idealized models and the 1929 Grand Banks event. *Geological Society, London, Special Publications* 500: 41–61.
172. Snelling B, Neethling S, Horsburgh K, et al. (2020) Uncertainty Quantification of Landslide Generated Waves Using Gaussian Process Emulation and Variance-Based Sensitivity Analysis. *Water* 12: 416.
173. Løvholt F, Schulten I, Mosher D, et al. (2019) Modelling the 1929 Grand Banks slump and landslide tsunami. *Geological Society, London, Special Publications* 477: 315–331.
174. Trapper PA, Puzrin AM, Germanovich LN (2015) Effects of shear band propagation on early waves generated by initial breakoff of tsunamigenic landslides. *Marine Geology* 370: 99–112.
175. Fritz HM, Hager WH, Minor H-E (2003) Landslide generated impulse waves. 2. Hydrodynamic impact craters. *Experiments in Fluids* 35: 520–532.
176. Heller V, Hager WH (2010) Impulse Product Parameter in Landslide Generated Impulse Waves. *J Waterway, Port, Coastal, Ocean Eng* 136: 145–155.
177. Bullard GK, Mulligan RP, Carreira A, et al. (2019) Experimental analysis of tsunamis generated by the impact of landslides with high mobility. *Coastal Engineering* 152: 103538.
178. Rauter M, Hoße L, Mulligan RP, et al. (2020) Numerical simulation of impulse wave generation by idealized landslides with OpenFOAM. *Coastal Engineering* 103815.
179. Gallotti G, Tinti S (2020) A New Approach for Landslide Modeling: Application to the Scilla 1783 Tsunamigenic Landslide, South Italy. *Pure Appl Geophys* 177: 3563–3576.
180. Latter JH (1981) Tsunamis of volcanic origin: Summary of causes, with particular reference to Krakatoa, 1883. *Bull Volcanol* 44: 467–490.
181. Kienle J, Kowalik Z, Murty TS (1987) Tsunamis Generated by Eruptions from Mount St. Augustine Volcano, Alaska. *Science* 236: 1442–1447.
182. Begét JE (2000) Volcanic Tsunamis, In: Sigurdsson H, Houghton B, Rymer H, et al. (Eds.), *Encyplopedia of volcanoes*, Academic Press, 1005–1013.
183. Day SJ (2015) Volcanic Tsunamis, In: Sigurdsson H, Houghton B, Rymer H, et al. (Eds.), *Encyplopedia of volcanoes*, Academic Press, 993–1009.
184. Le Méhauté B (1971) Theory of Explosion-Generated Water Waves, In: Chow VT (Ed.), *Advances in Hydroscience*, Elsevier, 1–79.
185. Ulvrova M, Paris R, Nomikou P, et al. (2016) Source of the tsunami generated by the 1650 AD eruption of Kolumbo submarine volcano (Aegean Sea, Greece). *Journal of Volcanology and Geothermal Research* 321.

186. Sato H, Taniguchi H (1997) Relationship between crater size and ejecta volume of recent magmatic and phreato-magmatic eruptions: Implications for energy partitioning. *Geophys Res Lett* 24: 205–208.
187. Goto A, Taniguchi H, Yoshida M, et al. (2001) Effects of explosion energy and depth to the formation of blast wave and crater: Field Explosion Experiment for the understanding of volcanic explosion. *Geophys Res Lett* 28: 4287–4290.
188. Monserrat S, Vilibić I, Rabinovich AB (2006) Meteotsunamis: atmospherically induced destructive ocean waves in the tsunami frequency band. *Nat Hazards Earth Syst Sci* 6: 1035–1051.
189. Sibley AM, Cox D, Tappin DR (2020) Convective rear-flank downdraft as driver for meteotsunami along English Channel and North Sea coasts 28–29 May 2017. *Nat Hazards*.
190. Pattiaratchi CB, Wijeratne EMS (2015) Are meteotsunamis an underrated hazard? *Phil Trans R Soc A* 373: 20140377.
191. Pasquet S, Vilibić I, Šepić J (2013) A survey of strong high-frequency sea level oscillations along the US East Coast between 2006 and 2011. *Nat Hazards Earth Syst Sci* 13: 473–482.
192. Pellikka H, Laurila TK, Boman H, et al. (2020) Meteotsunami occurrence in the Gulf of Finland over the past century. *Nat Hazards Earth Syst Sci* 20: 2535–2546.
193. Geist EL, ten Brink US, Gove M (2014) A framework for the probabilistic analysis of meteotsunamis. *Nat Hazards* 74: 123–142.
194. Renault L, Vizoso G, Jansá A, et al. (2011) Toward the predictability of meteotsunamis in the Balearic Sea using regional nested atmosphere and ocean models: TOWARD THE METEOTSUNAMIS PREDICTABILITY. *Geophys Res Lett* 38: n/a-n/a.
195. Artemieva NA, Shuvalov VV (2002) Shock metamorphism on the ocean floor (numerical simulations). *Deep Sea Research Part II: Topical Studies in Oceanography* 49: 959–968.
196. Gault DE, Sonett CP (1982) Laboratory simulation of pelagic asteroidal impact: Atmospheric injection, benthic topography, and the surface wave radiation field, *Geological Society of America Special Papers*, Geological Society of America, 69–92.
197. Matsui T, Imamura F, Tajika E, et al. (2002) Generation and propagation of a tsunami from the Cretaceous-Tertiary impact event, *Catastrophic events and mass extinctions: impacts and beyond*, Geological Society of America.
198. Glimsdal S, Pedersen GK, Langtangen HP, et al. (2007) Tsunami generation and propagation from the Mjølnir asteroid impact. *Meteoritics & Planetary Science* 42: 1473–1493.
199. Wünnemann K, Collins GS, Weiss R (2010) IMPACT OF A COSMIC BODY INTO EARTH'S OCEAN AND THE GENERATION OF LARGE TSUNAMI WAVES: INSIGHT FROM NUMERICAL MODELING. *Rev Geophys* 48: RG4006.
200. Patchett JM, Gisler GR (2017) Deep Water Impact Ensemble Data Set.
201. Kajiura K (1963) The leading wave of a tsunami. *B Earthquake Res Inst* 41: 535–571.
202. Liu C-M (2020) Analytical solutions of tsunamis generated by underwater earthquakes. *Wave Motion* 93: 102489.
203. Satake K (2007) Tsunami, In: Kanamori H, Schubert G (Eds.), *Treatise on geophysics earthquake seismology*, Amsterdam, Elsevier, 483–511.
204. Lotto GC, Jeppson TN, Dunham EM (2019) Fully Coupled Simulations of Megathrust Earthquakes and Tsunamis in the Japan Trench, Nankai Trough, and Cascadia Subduction Zone. *Pure Appl Geophys* 176: 4009–4041.
205. Shuto N, Fujima K (2009) A short history of tsunami research and countermeasures in Japan. *Proc Jpn Acad, Ser B* 85: 267–275.
206. Synolakis CE, Bernard EN (2006) Tsunami science before and beyond Boxing Day 2004. *Phil Trans R Soc A* 364: 2231–2265.
207. Horrillo J, Grilli ST, Nicolsky D, et al. (2015) Performance Benchmarking Tsunami Models for NTHMP's Inundation Mapping Activities. *Pure Appl Geophys* 172: 869–884.
208. Synolakis CE, Bernard EN, Titov VV, et al. (2008) Validation and Verification of Tsunami Numerical Models. *Pure appl geophys* 165: 2197–2228.

209. Abadie S, Morichon D, Grilli S, et al. (2010) Numerical simulation of waves generated by landslides using a multiple-fluid Navier–Stokes model. *Coastal Engineering* 57: 779–794.
210. Dao MH, Tkalich P (2007) Tsunami propagation modelling – a sensitivity study. *Nat Hazards Earth Syst Sci* 7: 741–754.
211. Bonneton P, Barthelemy E, Chazel F, et al. (2011) Recent advances in Serre–Green Naghdi modelling for wave transformation, breaking and runup processes. *European Journal of Mechanics - B/Fluids* 30: 589–597.
212. Fuhrman DR, Madsen PA (2009) Tsunami generation, propagation, and run-up with a high-order Boussinesq model. *Coastal Engineering* 56: 747–758.
213. Kennedy AB, Chen Q, Kirby JT, et al. (2000) Boussinesq Modeling of Wave Transformation, Breaking, and Runup. I: 1D. *Journal of Waterway, Port, Coastal, and Ocean Engineering* 126: 39–47.
214. Kim D-H, Lynett PJ, Socolofsky SA (2009) A depth-integrated model for weakly dispersive, turbulent, and rotational fluid flows. *Ocean Modelling* 27: 198–214.
215. Lynett PJ, Wu T-R, Liu PL-F (2002) Modeling wave runup with depth-integrated equations. *Coastal Engineering* 46: 89–107.
216. Løvholt F, Pedersen G, Gisler G (2008) Oceanic propagation of a potential tsunami from the La Palma Island. *Journal of Geophysical Research: Oceans* 113.
217. Ma G, Shi F, Kirby JT (2012) Shock-capturing non-hydrostatic model for fully dispersive surface wave processes. *Ocean Modelling* 43–44: 22–35.
218. Nwogu O (1993) Alternative Form of Boussinesq Equations for Nearshore Wave Propagation. *J Waterway, Port, Coastal, Ocean Eng* 119: 618–638.
219. Shi F, Kirby JT, Harris JC, et al. (2012) A high-order adaptive time-stepping TVD solver for Boussinesq modeling of breaking waves and coastal inundation. *Ocean Modelling* 43–44: 36–51.
220. Jeschke A, Pedersen GK, Vater S, et al. (2017) Depth-averaged non-hydrostatic extension for shallow water equations with quadratic vertical pressure profile: equivalence to Boussinesq-type equations: Depth-averaged non-hydrostatic extension for shallow water equations with quadratic vertical pressure profile: equivalence to Boussinesq-type equation. *Int J Numer Meth Fluids* 84: 569–583.
221. Satake K, Fujii Y, Harada T, et al. (2013) Time and Space Distribution of Coseismic Slip of the 2011 Tohoku Earthquake as Inferred from Tsunami Waveform Data. *Bulletin of the Seismological Society of America* 103: 1473–1492.
222. Løvholt F, Lynett P, Pedersen G (2013) Simulating run-up on steep slopes with operational Boussinesq models; capabilities, spurious effects and instabilities. *Nonlin Processes Geophys* 20: 379–395.
223. Muhammad A, Goda K, Alexander N (2016) Tsunami Hazard Analysis of Future Megathrust Sumatra Earthquakes in Padang, Indonesia Using Stochastic Tsunami Simulation. *Front Built Environ* 2.
224. Yokoyama I (1987) A scenario of the 1883 Krakatau tsunami. *Journal of Volcanology and Geothermal Research* 34: 123–132.
225. Nomanbhoy N, Satake K (1995) Generation mechanism of tsunamis from the 1883 Krakatau Eruption. *Geophys Res Lett* 22: 509–512.
226. Le Méhauté B, Wang S (1996) Water Waves Generated by Underwater Explosion, WORLD SCIENTIFIC.
227. Watts P, Waythomas CF (2003) Theoretical analysis of tsunami generation by pyroclastic flows. *J Geophys Res* 108: 2563.
228. Okal EA, Synolakis CE (2004) Source discriminants for near-field tsunamis: Near-field tsunamis. *Geophysical Journal International* 158: 899–912.
229. Harbitz C, Løvholt F, Pedersen G, et al. (2006) Mechanisms of tsunami generation by submarine landslides: A short review. *Norsk Geologisk Tidsskrift* 86: 255–264.
230. Bellotti G, Cecioni C, De Girolamo P (2008) Simulation of small-amplitude frequency-dispersive transient waves by means of the mild-slope equation. *Coastal Engineering* 55: 447–458.
231. Maeno F, Imamura F (2011) Tsunami generation by a rapid entrance of pyroclastic flow into the sea during the 1883 Krakatau eruption, Indonesia. *J Geophys Res* 116: B09205.

232. Glimsdal S, Pedersen GK, Harbitz CB, et al. (2013) Dispersion of tsunamis: does it really matter? *Natural Hazards and Earth System Sciences* 13: 1507–1526.
233. Selva J, Bonadonna C, Branca S, et al. (2020) Multiple hazards and paths to eruptions: A review of the volcanic system of Vulcano (Aeolian Islands, Italy). *Earth-Science Reviews* 207: 103186.
234. Selva J, Acocella V, Bisson M, et al. (2019) Multiple natural hazards at volcanic islands: a review for the Ischia volcano (Italy). *J Appl Volcanol* 8: 5.
235. Lavelle JW, Thacker WC (2008) A pretty good sponge: Dealing with open boundaries in limited-area ocean models. *Ocean Modelling* 20: 270–292.
236. Maeda T, Tsushima H, Furumura T (2016) An effective absorbing boundary condition for linear long-wave and linear dispersive-wave tsunami simulations. *Earth Planet Sp* 68: 63.
237. Harig S, Chaeroni, Pranowo WS, et al. (2008) Tsunami simulations on several scales: Comparison of approaches with unstructured meshes and nested grids. *Ocean Dynamics* 58: 429–440.
238. Synolakis CE (1987) The runup of solitary waves. *J Fluid Mech* 185: 523–545.
239. Synolakis CE (1991) Tsunami runup on steep slopes: How good linear theory really is. *Nat Hazards* 4: 221–234.
240. Tadepalli S, Synolakis CE (1994) The run-up of N-waves on sloping beaches. *Proceedings of the Royal Society of London Series A: Mathematical and Physical Sciences* 445: 99–112.
241. Madsen PA, Schäffer HA (2010) Analytical solutions for tsunami runup on a plane beach: single waves, *N* -waves and transient waves. *J Fluid Mech* 645: 27–57.
242. Pelinovsky EN, Mazova RKh (1992) Exact analytical solutions of nonlinear problems of tsunami wave run-up on slopes with different profiles. *Nat Hazards* 6: 227–249.
243. Løvholt F, Glimsdal S, Harbitz CB, et al. (2012) Tsunami hazard and exposure on the global scale. *Earth-Science Reviews* 110: 58–73.
244. van Hinsbergen DJJ, Torsvik TH, Schmid SM, et al. (2020) Orogenic architecture of the Mediterranean region and kinematic reconstruction of its tectonic evolution since the Triassic. *Gondwana Research* 81: 79–229.
245. Wdowinski S, Ben-Avraham Z, Arvidsson R, et al. (2006) Seismotectonics of the Cyprian Arc. *Geophysical Journal International* 164: 176–181.
246. Devoti R, Riguzzi F, Cuffaro M, et al. (2008) New GPS constraints on the kinematics of the Apennines subduction. *Earth and Planetary Science Letters* 273: 163–174.
247. Nocquet J-M (2012) Present-day kinematics of the Mediterranean: A comprehensive overview of GPS results. *Tectonophysics* 579: 220–242.
248. Carafa MMC, Kastelic V, Bird P, et al. (2018) A “Geodetic Gap” in the Calabrian Arc: Evidence for a Locked Subduction Megathrust? *Geophys Res Lett* 45: 1794–1804.
249. Reilinger R, McClusky S, Vernant P, et al. (2006) GPS constraints on continental deformation in the Africa-Arabia-Eurasia continental collision zone and implications for the dynamics of plate interactions: EASTERN MEDITERRANEAN ACTIVE TECTONICS. *J Geophys Res* 111: n/a-n/a.
250. Hollenstein Ch, Müller MD, Geiger A, et al. (2008) Crustal motion and deformation in Greece from a decade of GPS measurements, 1993–2003. *Tectonophysics* 449: 17–40.
251. Howell A, Jackson J, Copley A, et al. (2017) Subduction and vertical coastal motions in the eastern Mediterranean. *Geophysical Journal International* 211: 593–620.
252. Stiros SC (2010) The 8.5+ magnitude, AD365 earthquake in Crete: Coastal uplift, topography changes, archaeological and historical signature. *Quaternary International* 216: 54–63.
253. Shaw B, Ambraseys NN, England PC, et al. (2008) Eastern Mediterranean tectonics and tsunami hazard inferred from the AD 365 earthquake. *Nature Geosci* 1: 268–276.
254. Platania G (1909) Il maremoto dello stretto di Messina del 28 dicembre 1908. *Boll Soc Sismol Ital* 13: 369–458.
255. Pino NA, Piatanesi A, Valensise G, et al. (2009) The 28 December 1908 Messina Straits Earthquake (MW 7.1): A Great Earthquake throughout a Century of Seismology. *Seismological Research Letters* 80: 243–259.
256. Galanopoulos AG (1960) Tsunamis Observed on the Coasts of Greece from Antiquity to Present Time. *Annals of Geophysics* 13: 369–386.

257. Galanopoulos AG (1957) The seismic sea wave of 9 July 1956. *Prakt Akad Athens* 32: 90–101.
258. Schambach L, Grilli ST, Tappin DR, et al. (2020) New simulations and understanding of the 1908 Messina tsunami for a dual seismic and deep submarine mass failure source. *Marine Geology* 421: 106093.
259. Ambraseys NN (1960) The seismic sea wave of July 9, 1956, in the Greek archipelago. *J Geophys Res* 65: 1257–1265.
260. Stucchi M, Rovida A, Gomez Capera AA, et al. (2013) The SHARE European Earthquake Catalogue (SHEEC) 1000–1899. *J Seismol* 17: 523–544.
261. Grünthal G, Wahlström R (2012) The European-Mediterranean Earthquake Catalogue (EMEC) for the last millennium. *J Seismol* 16: 535–570.
262. Albini P, Musson RMW, Rovida A, et al. (2014) The Global Earthquake History. *Earthquake Spectra* 30: 607–624.
263. Guidoboni E, Comastri A, Traina G, et al. (Eds.) (1994) Catalogue of ancient earthquakes in the Mediterranean area up to the 10th century, Rome, Istituto nazionale di geofisica.
264. Field EH, Arrowsmith RJ, Biasi GP, et al. (2014) Uniform California Earthquake Rupture Forecast, Version 3 (UCERF3)--The Time-Independent Model. *Bulletin of the Seismological Society of America* 104: 1122–1180.
265. Field EH, Jordan TH, Page MT, et al. (2017) A Synoptic View of the Third Uniform California Earthquake Rupture Forecast (UCERF3). *Seismological Research Letters* 88: 1259–1267.
266. Woessner J, Laurentiu D, Giardini D, et al. (2015) The 2013 European Seismic Hazard Model: key components and results. *Bull Earthquake Eng* 13: 3553–3596.
267. Taroni M, Selva J (2020) GR_EST: An OCTAVE/MATLAB Toolbox to Estimate Gutenberg–Richter Law Parameters and Their Uncertainties. *Seismological Research Letters*.
268. Tonini R, Basili R, Maesano FE, et al. (2020) Importance of earthquake rupture geometry on tsunami modelling: the Calabrian Arc subduction interface (Italy) case study. *Geophysical Journal International* 223: 1805–1819.
269. de la Asunción M, Castro MJ, Fernández-Nieto ED, et al. (2013) Efficient GPU implementation of a two waves TVD-WAF method for the two-dimensional one layer shallow water system on structured meshes. *Computers & Fluids* 80: 441–452.
270. Lomax A, Michelini A (2009) Mwpd: A duration–amplitude procedure for rapid determination of earthquake magnitude and tsunamigenic potential from P waveforms. *Geophys J Int* 176: 200–214.
271. Lomax A, Michelini A (2009) Tsunami early warning using earthquake rupture duration. *Geophys Res Lett* 36: L09306.
272. Lomax A, Michelini A (2011) Tsunami early warning using earthquake rupture duration and P-wave dominant period: the importance of length and depth of faulting: Tsunami early warning using P-wave measures. *Geophysical Journal International* 185: 283–291.
273. Lomax A, Michelini A (2013) Tsunami Early Warning Within Five Minutes. *Pure Appl Geophys* 170: 1385–1395.
274. Bernardi F, Lomax A, Michelini A, et al. (2015) Appraising the Early-est earthquake monitoring system for tsunami alerting at the Italian Candidate Tsunami Service Provider. *Natural Hazards and Earth System Sciences* 15: 2019–2036.
275. Annunziato A, Galliano D, Bonaita M (2016) IDSL sea level measurement devices., European Commission. Joint Research Centre.
276. Fraser S, Power WL (2013) Validation of a GIS-based attenuation rule for indicative tsunami evacuation zone mapping.
277. Basili R, Carafa MMC, Kastelic V, et al. (2018) Project SERA - Deliverable 25.2. Updated databases of seismicity, faults, and strain rates for ESHM20.
278. IOC/UNESCO (2017) [Intergovernmental Oceanographic Commission / UNESCO] NEAMWave17 – A Tsunami Warning and Communication Exercise for the North-eastern Atlantic, the Mediterranean, and Connected Seas Region, 31 October – 3 November 2017: Exercise Instructions, Intergovernmental Oceanographic Commission of UNESCO.

279. Tinti S, Graziani L, Brizuela B, et al. (2012) Applicability of the Decision Matrix of North Eastern Atlantic, Mediterranean and connected seas Tsunami Warning System to the Italian tsunamis. *Nat Hazards Earth Syst Sci* 12: 843–857.
280. Alasset P-J, Hébert H, Maouche S, et al. (2006) The tsunami induced by the 2003 Zemmouri earthquake (MW= 6.9, Algeria): modelling and results. *Geophys J Int* 166: 213–226.
281. Newman AV, Okal EA (1998) Teleseismic estimates of radiated seismic energy: The E/M 0 discriminant for tsunami earthquakes. *Journal of Geophysical Research: Solid Earth* 103: 26885–26898.
282. Blewitt G, Kreemer C, Hammond WC, et al. (2006) Rapid determination of earthquake magnitude using GPS for tsunami warning systems. *Geophysical Research Letters* 33.
283. Duputel Z, Rivera L, Kanamori H, et al. (2012) W phase source inversion for moderate to large earthquakes (1990–2010). *Geophysical Journal International* 189: 1125–1147.
284. Hirshorn B, Weinstein S, Tsuboi S (2013) On the Application of Mwp in the Near Field and the March 11, 2011 Tohoku Earthquake. *Pure Appl Geophys* 170: 975–991.
285. Melgar D, Allen RM, Riquelme S, et al. (2016) Local tsunami warnings: Perspectives from recent large events. *Geophysical Research Letters* 43: 1109–1117.
286. Sahakian VJ, Melgar D, Muzli M (2019) Weak Near-Field Behavior of a Tsunami Earthquake: Toward Real-Time Identification for Local Warning. *Geophysical Research Letters* 46: 9519–9528.
287. Lay T, Liu C, Kanamori H (2019) Enhancing Tsunami Warning Using P Wave Coda. *Journal of Geophysical Research: Solid Earth* 124: 10583–10609.
288. Di Bucci D, Savadori L (2018) Defining the acceptable level of risk for civil protection purposes: a behavioral perspective on the decision process. *Nat Hazards* 90: 293–324.
289. Chiocci FL, Romagnoli C, Tommasi P, et al. (2008) The Stromboli 2002 tsunamigenic submarine slide: Characteristics and possible failure mechanisms. *J Geophys Res* 113: B10102.
290. Fornaciai A, Favalli M, Nannipieri L (2019) Numerical simulation of the tsunamis generated by the Sciara del Fuoco landslides (Stromboli Island, Italy). *Scientific Reports* 9: 18542.
291. Marchetti E, Genco R, Ripepe M (2009) Ground deformation and seismicity related to the propagation and drainage of the dyke feeding system during the 2007 effusive eruption at Stromboli volcano (Italy). *Journal of Volcanology and Geothermal Research* 182: 155–161.
292. Di Traglia F, Nolesini T, Intrieri E, et al. (2014) Review of ten years of volcano deformations recorded by the ground-based InSAR monitoring system at Stromboli volcano: a tool to mitigate volcano flank dynamics and intense volcanic activity. *Earth-Science Reviews* 139: 317–335.
293. Valade S, Lacanna G, Coppola D, et al. (2016) Tracking dynamics of magma migration in open-conduit systems. *Bull Volcanol* 78: 78.
294. Giudicepietro F, López C, Macedonio G, et al. (2020) Geophysical precursors of the July-August 2019 paroxysmal eruptive phase and their implications for Stromboli volcano (Italy) monitoring. *Sci Rep* 10: 10296.
295. Macias J, De'Michieli Vitturi M, Esposti Ongaro T, et al. (2018) Modelling and numerical simulations of tsunami waves generated by landslides at Stromboli volcano (Aeolian islands, Italy). *AGU Fall Meeting Abstracts* 41.
296. Esposti Ongaro T, De'Michieli Vitturi M, Fornaciai A, et al. (submitted) Modelling and simulations of tsunami waves generated by landslides and pyroclastic avalanches at Stromboli volcano (Aeolianislands, Italy): a numerical benchmark study.
297. Macías J, Vázquez JT, Fernández-Salas LM, et al. (2015) The Al-Borani submarine landslide and associated tsunami. A modelling approach. *Marine Geology* 361: 79–95.
298. Fernández-Nieto ED, Bouchut F, Bresch D, et al. (2008) A new Savage–Hutter type model for submarine avalanches and generated tsunami. *Journal of Computational Physics* 227: 7720–7754.
299. Fernández-Nieto ED, Parisot M, Penel Y, et al. (2018) A hierarchy of dispersive layer-averaged approximations of Euler equations for free surface flows. *Communications in Mathematical Sciences* 16: 1169–1202.
300. Savage SB, Hutter K (1989) The motion of a finite mass of granular material down a rough incline. *J Fluid Mech* 199: 177–215.

301. Pouliquen O, Forterre Y (2002) Friction law for dense granular flows: application to the motion of a mass down a rough inclined plane. *J Fluid Mech* 453: 133–151.
302. Macias J, de la Asuncion M (2019) Faster and faster tsunami simulations with ChEESE. *AGU Fall Meeting Abstracts* 33.
303. DPC, RS (2015) [Dipartimento della Protezione Civile and Regione Sicilia] Isola di Stromboli - Piano nazionale di emergenza a fronte di eventi vulcanici di rilevanza nazionale.
304. Ripepe M, Delle Donne D, Lacanna G, et al. (2009) The onset of the 2007 Stromboli effusive eruption recorded by an integrated geophysical network. *Journal of Volcanology and Geothermal Research* 182: 131–136.
305. Ripepe M, Donne DD, Genco R, et al. (2015) Volcano seismicity and ground deformation unveil the gravity-driven magma discharge dynamics of a volcanic eruption. *Nat Commun* 6: 6998.
306. Bertolaso G, De Bernardinis B, Bosi V, et al. (2009) Civil protection preparedness and response to the 2007 eruptive crisis of Stromboli volcano, Italy. *Journal of Volcanology and Geothermal Research* 182: 269–277.
307. Lacanna E, Ripepe M (in prep) Tsunami wave generated by Pyroclastic flows recorded in the near field.
308. Ripepe M, Lacanna G, Pistolesi M, et al. (in press) Ground deformation reveals the scale-invariant conduit dynamics driving explosive basaltic eruptions. *Nature Communications*.
309. Graziani L, Maramai A, Tinti S (2006) A revision of the 1783–1784 Calabrian (southern Italy) tsunamis. *Natural Hazards and Earth System Sciences* 6: 1053–1060.
310. Wang Y, Maeda T, Satake K, et al. (2019) Tsunami Data Assimilation Without a Dense Observation Network. *Geophysical Research Letters* 46: 2045–2053.
311. Migeon S, Cattaneo A, Hassoun V, et al. (2009) Submarine instabilities along the Ligurian Margin (NW Mediterranean): types, distribution, and causes. *Rendiconti Online Societa Geologica Italiana* 7.
312. Migeon S, Mascle J, Coste M, et al. (2012) Mediterranean submarine canyons and channels: Morphological and geological backgrounds.
313. Petit C, Migeon S, Coste M (2015) Numerical models of continental and submarine erosion: application to the northern Ligurian Margin (Southern Alps, France/Italy). *Earth Surface Processes and Landforms* 40: 681–695.
314. Assier-Rzadkieaicz S, Heinrich P, Sabatier PC, et al. (2000) Numerical Modelling of a Landslide-generated Tsunami: The 1979 Nice Event. *Pure appl geophys* 157: 1707–1727.
315. Ioualalen M, Migeon S, Sardoux O (2010) Landslide tsunami vulnerability in the Ligurian Sea: case study of the 1979 October 16 Nice international airport submarine landslide and of identified geological mass failures. *Geophysical Journal International*.
316. Orsi G, Gallo G, Zanchi A (1991) Simple-shearing block resurgence in caldera depressions. A model from Pantelleria and Ischia. *Journal of Volcanology and Geothermal Research* 47: 1–11.
317. de Vita S, Sansivero F, Orsi G, et al. (2006) Cyclical slope instability and volcanism related to volcano-tectonism in resurgent calderas: The Ischia island (Italy) case study. *Engineering Geology* 86: 148–165.
318. de Alteriis G, Insinga DD, Morabito S, et al. (2010) Age of submarine debris avalanches and tephrostratigraphy offshore Ischia Island, Tyrrhenian Sea, Italy. *Marine Geology* 278: 1–18.
319. de Alteriis G, Violante C (2009) Catastrophic landslides off Ischia volcanic island (Italy) during prehistory. *Geological Society, London, Special Publications* 322: 73–104.
320. Della Seta M, Marotta E, Orsi G, et al. (2011) Slope instability induced by volcano-tectonics as an additional source of hazard in active volcanic areas: The case of Ischia island (Italy). *Bulletin of Volcanology* 74: 79–106.
321. Paparo MA, Tinti S (2017) Analysis of Seismic-Driven Instability of Mt. Nuovo in the Ischia Island, Italy. *Bulletin of the Seismological Society of America* 107: 750–759.
322. Tinti S, Zaniboni F, Armigliato A, et al. (2010) Tsunami hazard and risk evaluation in the Gulf of Naples: state of the art and perspectives, In: Mazzolani FM (Ed.), *Urban Habitat Constructions under Catastrophic Events (Final Report)*, London.

323. Selva J, Orsi G, Di Vito MA, et al. (2012) Probability hazard map for future vent opening at the Campi Flegrei caldera, Italy. *Bull Volcanol* 74: 497–510.
324. Bevilacqua A, Isaia R, Neri A, et al. (2015) Quantifying volcanic hazard at Campi Flegrei caldera (Italy) with uncertainty assessment: 1. Vent opening maps. *Journal of Geophysical Research: Solid Earth* 120: 2309–2329.
325. Neri A, Bevilacqua A, Ongaro TE, et al. (2015) Quantifying volcanic hazard at Campi Flegrei caldera (Italy) with uncertainty assessment: 2. Pyroclastic density current invasion maps. *Journal of Geophysical Research: Solid Earth* 120: 2330–2349.
326. Robin C, Colantoni P, Gennesseaux M, et al. (1987) Vavilov seamount: A mildly alkaline Quaternary volcano in the Tyrrhenian Basin. *Marine Geology* 78: 125–136.
327. Marani M, Gamberi F (2004) Distribution and nature of submarine volcanic landforms in the Tyrrhenian Sea: the arc vs the backarc. *Memoir Carta Geologica D'Italia* 64: 109–126.
328. Arcangeli D (2019) Scenarios of lateral collapses of the Vavilov seamount in the central Tyrrhenian sea.
329. Caratori Tontini F, Cocchi L, Muccini F, et al. (2010) Potential-field modeling of collapse-prone submarine volcanoes in the southern Tyrrhenian Sea (Italy). *Geophysical Research Letters* 37: L03305.
330. Ventura G, Milano G, Passaro S, et al. (2013) The Marsili Ridge (Southern Tyrrhenian Sea, Italy): An island-arc volcanic complex emplaced on a 'relict' back-arc basin. *Earth-Science Reviews* 116: 85–94.
331. Gallotti G, Tinti S, Zaniboni F, et al. (2019) Scenarios of Tsunamis Induced by Submarine Landslides on the Eastern Flank of Marsili Seamount (Southern Tyrrhenian Sea, Italy), Montréal, Canada, JP05p-049.
332. Cocchi L, Passaro S, Tontini FC, et al. (2017) Volcanism in slab tear faults is larger than in island-arcs and back-arcs. *Nature Communications* 8: 1451.
333. Passaro S, Milano G, D'Isanto C, et al. (2010) DTM-based morphometry of the Palinuro seamount (Eastern Tyrrhenian Sea): Geomorphological and volcanological implications. *Geomorphology* 115: 129–140.
334. Chiocci FL, De Rosa R, Iannaccone G, et al. (2018) Vulcani sottomarini: finalizzazione e sintesi delle conoscenze dello stato attuale dei vulcani sottomarini e delle porzioni sommerse di vulcani insulari e costieri e dei possibili scenari di pericolosità.
335. Achilli V, Baldi P, Baratin L, et al. (1998) Digital photogrammetric survey on the Island of Vulcano. *Acta Vulcanol* 10: 1–5.
336. Maramai A, Graziani L, Tinti S (2005) Tsunamis in the Aeolian Islands (southern Italy): a review. *Marine Geology* 215: 11–21.
337. Rasà R, Villari L (1991) Geomorphological and morpho-structural investigations on the Fossa cone (Vulcano, Aeolian Islands): a first outline. *Acta Vulcanologica* 1: 127–133.
338. Marsella M, Salino A, Scifoni S, et al. (2013) Stability Conditions and Evaluation of the Runout of a Potential Landslide at the Northern Flank of La Fossa Active Volcano, Italy, In: Margottini C, Canuti P, Sassa K (Eds.), *Landslide Science and Practice*, Berlin, Heidelberg, Springer Berlin Heidelberg, 309–314.
339. Bozzano F, Lenti L, Martino S, et al. (2011) Earthquake triggering of landslides in highly jointed rock masses: Reconstruction of the 1783 Scilla rock avalanche (Italy). *Geomorphology* 129: 294–308.
340. Mazzanti P, Bozzano F (2011) Revisiting the February 6th 1783 Scilla (Calabria, Italy) landslide and tsunami by numerical simulation. *Mar Geophys Res* 32: 273–286.
341. Zaniboni F, Armigliato A, Tinti S (2016) A numerical investigation of the 1783 landslide-induced catastrophic tsunami in Scilla, Italy. *Nat Hazards* 84: 455–470.
342. Zaniboni F, Pagnoni G, Gallotti G, et al. (2019) Assessment of the 1783 Scilla landslide–tsunami's effects on the Calabrian and Sicilian coasts through numerical modeling. *Nat Hazards Earth Syst Sci* 19: 1585–1600.
343. Piatanesi A, Tinti S (2002) Numerical modelling of the September 8, 1905 Calabrian (southern Italy) tsunami. *Geophysical Journal International* 150: 271–284.

344. Casalbore D, Bosman A, Ridente D, et al. (2014) Coastal and Submarine Landslides in the Tectonically-Active Tyrrhenian Calabrian Margin (Southern Italy): Examples and Geohazard Implications, In: Krastel S, Behrmann J-H, Völker D, et al. (Eds.), *Submarine Mass Movements and Their Consequences: 6th International Symposium*, Cham, Springer International Publishing, 261–269.
345. Colantoni P, Gennesseaux M, Venney JR, et al. (1992) Processi dinamici del canyon sottomarino di Gioia Tauro (Mare Tirreno). *Giornale di Geologia* 54: 199–213.
346. Zaniboni F, Armigliato A, Pagnoni G, et al. (2014) Continental margins as a source of tsunami hazard: The 1977 Gioia Tauro (Italy) landslide–tsunami investigated through numerical modeling. *Marine Geology* 357: 210–217.
347. Ceramicola S, Caburlotto A, Coste M, et al. (2010) Seabed features in relation to geohazards on the Ionian Calabrian margin: results from the MAGIC Project, Venice, Italy.
348. Ceramicola S, Tinti S, Zaniboni F, et al. (2014) Reconstruction and Tsunami Modeling of a Submarine Landslide on the Ionian Margin of Calabria (Mediterranean Sea), In: Sassa K, Canuti P, Yin Y (Eds.), *Landslide Science for a Safer Geoenvironment*, Cham, Springer International Publishing, 557–562.
349. Zecchin M, Accaino F, Ceramicola S, et al. (2018) The Crotone Megalandslide, southern Italy: Architecture, timing and tectonic control. *Sci Rep* 8: 7778.
350. Antoncecchi I, Ciccone F, Dialuce G, et al. (2020) Progetto SPOT - Sismicità Potenzialmente Innescabile Offshore e Tsunami: Report integrato di fine progetto, Zenodo.
351. Ridente D, Martorelli E, Bosman A, et al. (2014) High-resolution morpho-bathymetric imaging of the Messina Strait (Southern Italy). New insights on the 1908 earthquake and tsunami. *Geomorphology* 208: 149–159.
352. Bonini L, Bucci DD, Toscani G, et al. (2011) Reconciling deep seismogenic and shallow active faults through analogue modelling: the case of the Messina Straits (southern Italy). *Journal of the Geological Society* 168: 191–199.
353. Chiocci FL, Coltelli M, Bosman A, et al. (2011) Continental margin large-scale instability controlling the flank sliding of Etna volcano. *Earth and Planetary Science Letters* 305: 57–64.
354. Argnani A, Mazzarini F, Bonazzi C, et al. (2013) The deformation offshore of Mount Etna as imaged by multichannel seismic reflection profiles. *Journal of Volcanology and Geothermal Research* 251: 50–64.
355. Gross F, Krastel S, Chiocci FL, et al. (2014) Evidence for Submarine Landslides Offshore Mt. Etna, Italy, In: Krastel S, Behrmann J-H, Völker D, et al. (Eds.), *Submarine Mass Movements and Their Consequences*, Cham, Springer International Publishing, 307–316.
356. Gross F, Krastel S, Geersen J, et al. (2016) The limits of seaward spreading and slope instability at the continental margin offshore Mt Etna, imaged by high-resolution 2D seismic data. *Tectonophysics* 667: 63–76.
357. De Novellis V, Atzori S, De Luca C, et al. (2019) DInSAR Analysis and Analytical Modeling of Mount Etna Displacements: The December 2018 Volcano-Tectonic Crisis. *Geophys Res Lett* 46: 5817–5827.
358. Pareschi MT, Boschi E, Mazzarini F, et al. (2006) Large submarine landslides offshore Mt. Etna. *Geophys Res Lett* 33: L13302.
359. Argnani A, Armigliato A, Pagnoni G, et al. (2012) Active tectonics along the submarine slope of south-eastern Sicily: The January 11, 1693 earthquake and tsunami. *Natural Hazards and Earth System Sciences* 12: 1311–1319.
360. Tonini R, Armigliato A, Pagnoni G, et al. (2011) Tsunami hazard for the city of Catania, eastern Sicily, Italy, assessed by means of Worst-case Credible Tsunami Scenario Analysis (WCTSA). *Nat Hazards Earth Syst Sci* 11: 1217–1232.
361. Gerardi F, Barbano M, De Martini PM, et al. (2008) Discrimination of Tsunami Sources (Earthquake versus Landslide) on the Basis of Historical Data in Eastern Sicily and Southern Calabria. *Bulletin of the Seismological Society of America* 98: 2795–2805.
362. Paparo MA, Armigliato A, Pagnoni G, et al. (2017) Earthquake-triggered landslides along the Hyblean-Malta Escarpment (off Augusta, eastern Sicily, Italy) – assessment of the related tsunamigenic potential. *Adv Geosci* 44: 1–8.

363. Minisini D, Trincardi F, Asioli A, et al. (2007) Morphologic variability of exposed mass-transport deposits on the eastern slope of Gela Basin (Sicily channel). *Basin Research* 19: 217–240.
364. Trincardi F, Argnani A (1990) Gela submarine slide: A major basin-wide event in the plio-quaternary foredeep of Sicily. *Geo-Marine Letters* 10: 13–21.
365. Mueller C, Micallef A, Spatola D, et al. (2020) The Tsunami Inundation Hazard of the Maltese Islands (Central Mediterranean Sea): A Submarine Landslide and Earthquake Tsunami Scenario Study. *Pure Appl Geophys* 177: 1617–1638.
366. Minisini D, Trincardi F (2009) Frequent failure of the continental slope: The Gela Basin (Sicily Channel). *J Geophys Res* 114: F03014.
367. Kuhlmann J, Asioli A, Trincardi F, et al. (2017) Landslide Frequency and Failure Mechanisms at NE Gela Basin (Strait of Sicily): Landsliding at Gela Basin. *J Geophys Res Earth Surf* 122: 2223–2243.
368. Zaniboni F, Pagnoni G, Paparo MA, et al. (2021) Tsunamis From Submarine Collapses Along the Eastern Slope of the Gela Basin (Strait of Sicily). *Front Earth Sci* 8: 602171.
369. Cavallaro D, Coltelli M (2019) The Graham Volcanic Field Offshore Southwestern Sicily (Italy) Revealed by High-Resolution Seafloor Mapping and ROV Images. *Front Earth Sci* 7: 311.
370. Lodolo E, Zampa L, Civile D (2019) The Graham and Terrible volcanic province (NW Sicilian Channel): gravimetric constraints for the magmatic manifestations. *Bull Volcanol* 81: 17.
371. Innangi S, Tonielli R, Romagnoli C, et al. (2019) Seabed mapping in the Pelagie Islands marine protected area (Sicily Channel, southern Mediterranean) using Remote Sensing Object Based Image Analysis (RSOBIA). *Mar Geophys Res* 40: 333–355.
372. Tonielli R, Innangi S, Di Martino G, et al. (2019) New bathymetry of the Linosa volcanic complex from multibeam systems (Sicily Channel, Mediterranean Sea). *Journal of Maps* 15: 611–618.
373. Minisini D, Trincardi F, Asioli A (2006) Evidence of slope instability in the Southwestern Adriatic Margin. *Natural Hazards and Earth System Sciences* 6: 1–20.
374. Ridente D, Fracassi U, Di Bucci D, et al. (2008) Middle Pleistocene to Holocene activity of the Gondola Fault Zone (Southern Adriatic Foreland): Deformation of a regional shear zone and seismotectonic implications. *Tectonophysics* 453: 110–121.
375. Trincardi F, Foglini F, Verdicchio G, et al. (2007) The impact of cascading currents on the Bari Canyon System, SW-Adriatic Margin (Central Mediterranean). *Marine Geology* 246: 208–230.
376. Dalla Valle G, Campiani E, Foglini F, et al. (2014) Mass Transport Complexes from Contourite and Shelf-Edge Deposits Along the South-Western Adriatic Margin (Italy), In: Krastel S, Behrmann J-H, Völker D, et al. (Eds.), *Submarine Mass Movements and Their Consequences: 6th International Symposium*, Cham, Springer International Publishing, 447–457.
377. Dalla Valle G, Gamberi F, Foglini F, et al. (2015) The Gondola Slide: A mass transport complex controlled by margin topography (South-Western Adriatic Margin, Mediterranean Sea). *Marine Geology* 366: 97–113.
378. Di Bucci D, Burrato P, Vannoli P, et al. (2010) Tectonic evidence for the ongoing Africa-Eurasia convergence in central Mediterranean foreland areas: A journey among long-lived shear zones, large earthquakes, and elusive fault motions. *J Geophys Res* 115: B12404.
379. Šepić J, Vilibić I, Rabinovich A, et al. (2018) Meteotsunami ("Marrobbio") of 25–26 June 2014 on the Southwestern Coast of Sicily, Italy. *Pure Appl Geophys* 175: 1573–1593.
380. Šepić J, Vilibić I, Rabinovich AB, et al. (2015) Widespread tsunami-like waves of 23-27 June in the Mediterranean and Black Seas generated by high-altitude atmospheric forcing. *Sci Rep* 5: 11682.
381. Bazzurro P, Cornell CA (1999) Disaggregation of seismic hazard. *Bulletin of the Seismological Society of America* 89: 501–520.
382. Kanazawa T (2013) Japan Trench earthquake and tsunami monitoring network of cable-linked 150 ocean bottom observatories and its impact to earth disaster science, *2013 IEEE International Underwater Technology Symposium (UT)*, Tokyo, IEEE, 1–5.
383. Crowell BW, Schmidt DA, Bodin P, et al. (2018) G-FAST Earthquake Early Warning Potential for Great Earthquakes in Chile. *Seismological Research Letters* 89: 542–556.
384. Marzocchi W, Taroni M, Falcone G (2017) Earthquake forecasting during the complex Amatrice-Norcia seismic sequence. *Sci Adv* 3: e1701239.

385. Behrens J, Androsov A, Babeyko AY, et al. (2010) A new multi-sensor approach to simulation assisted tsunami early warning. *Natural Hazards and Earth System Sciences* 10: 1085–1100.
386. Maeda T, Obara K, Shinohara M, et al. (2015) Successive estimation of a tsunami wavefield without earthquake source data: A data assimilation approach toward real-time tsunami forecasting. *Geophys Res Lett* 42: 7923–7932.
387. Tanioka Y, Gusman AR (2018) Near-field tsunami inundation forecast method assimilating ocean bottom pressure data: A synthetic test for the 2011 Tohoku-oki tsunami. *Physics of the Earth and Planetary Interiors* 283: 82–91.
388. Mulia IE, Gusman AR, Satake K (2018) Alternative to non-linear model for simulating tsunami inundation in real-time. *Geophysical Journal International* 214: 2002–2013.
389. Pondrelli S, Salimbeni S, Morelli A, et al. (2011) European–Mediterranean Regional Centroid Moment Tensor catalog: Solutions for 2005–2008. *Physics of the Earth and Planetary Interiors* 185: 74–81.
390. Zoback ML (1992) First- and second-order patterns of stress in the lithosphere: The World Stress Map Project. *J Geophys Res* 97: 11703.
391. Asch K (2005) The 1:5 Million International Geological Map of Europe and Adjacent Areas, *BGR - Geology 1:5,000,000*, Hannover.
392. Siebert L, Simkin T (2013) Volcanoes of the World: an Illustrated Catalog of Holocene Volcanoes and their Eruptions.
393. Amante C, Eakins BW (2009) ETOPO1 1 Arc-Minute Global Relief Model: Procedures, Data Sources and Analysis.

Figures

Figure 1: *Seismotectonic map of the Mediterranean region. Regional centroid moment tensors (RCMT;* [389]*) with mechanisms classified based on the Zoback* [390] *rules (TF: thrust faulting, TS: Thrust strike, SS: Strike-slip, NF: Normal faulting, NS: Normal strike, UN: Undetermined). Tectonic structures were modified and simplified from* [391] *and various other regional geologic maps. Volcanoes from* [392]*. Topo-bathymetry from* [393].

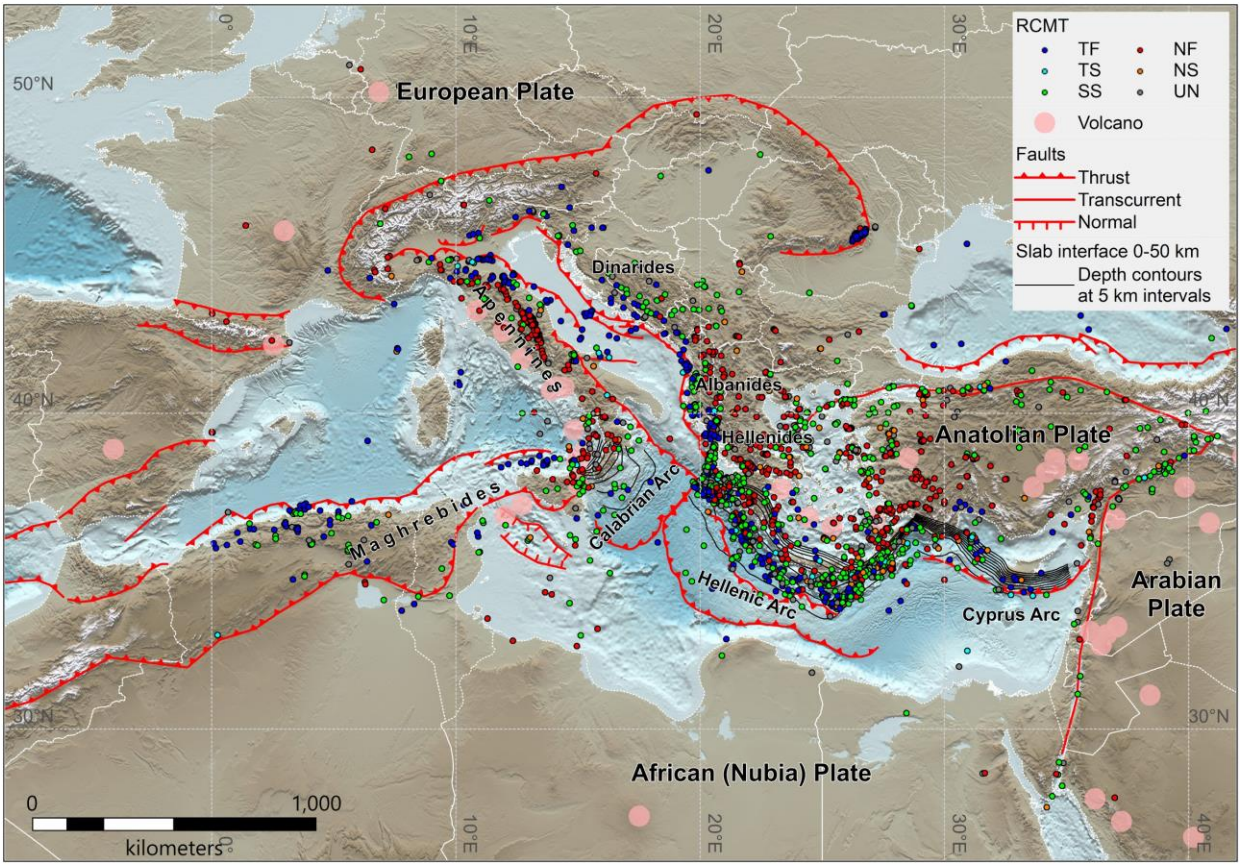

Figure 2: *a) NEAMTHM18 results, publicly accessible through the project website (http://www.tsumaps-neam.eu/). b) NEAMTHM18 hazard curves and reference intensity extraction.*

a

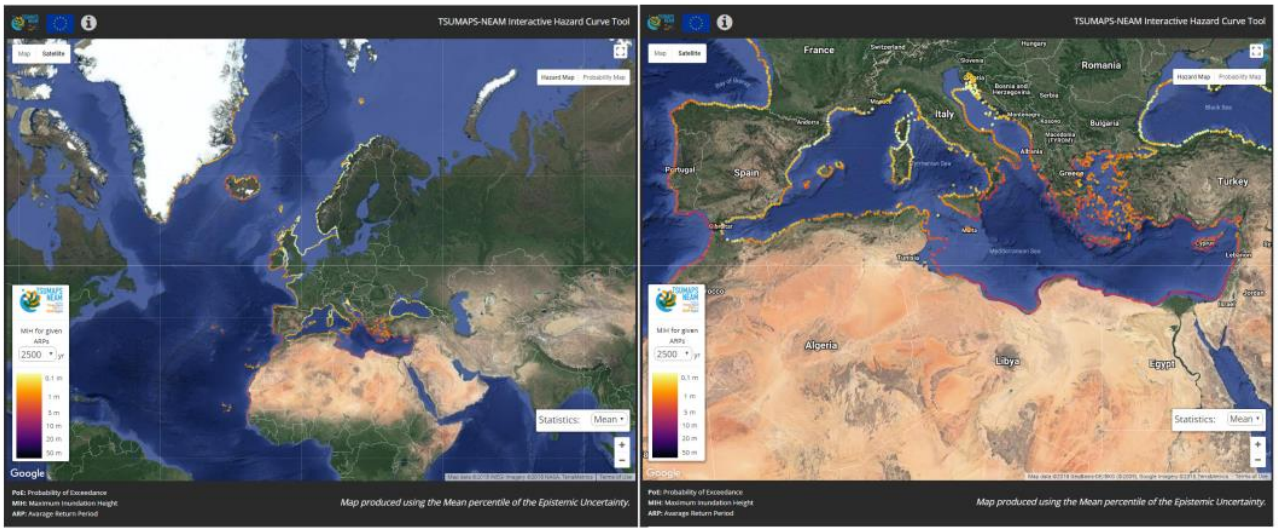

b

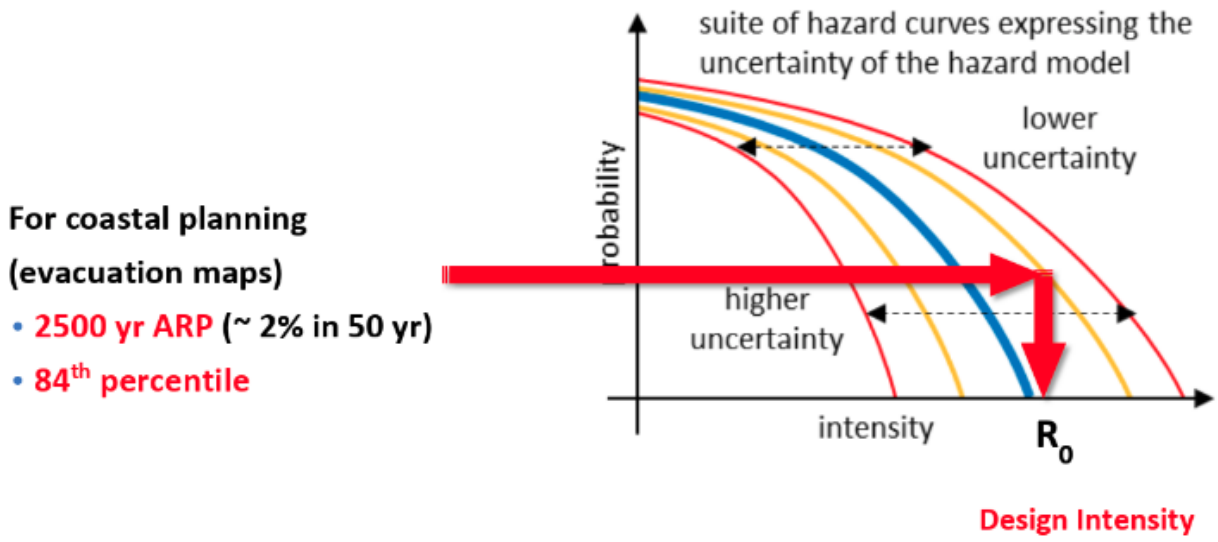

Figure 3: *a) CAT-INGV Monitoring area and seismic sources that caused the generation of alert messages until 2020 (from http://www.ingv.it/cat/it/): circles indicate epicentral position and the red/orange/green colour indicates the maximum alert level delivered (watch/advisory/information). b) Application of the CAT-INGV DM for the M6.8 2003 Zemmouri-Boumerdes earthquake: red/orange/green triangles indicated watch/advisory/information alert levels; the dotted circles indicated local/regional/basin spatial domain, as defined by the decision matrix (Table 1); ; the red star indicates the epicentral location. c) As b, for the M6.8 2017 Kos-Bodrum earthquake.*

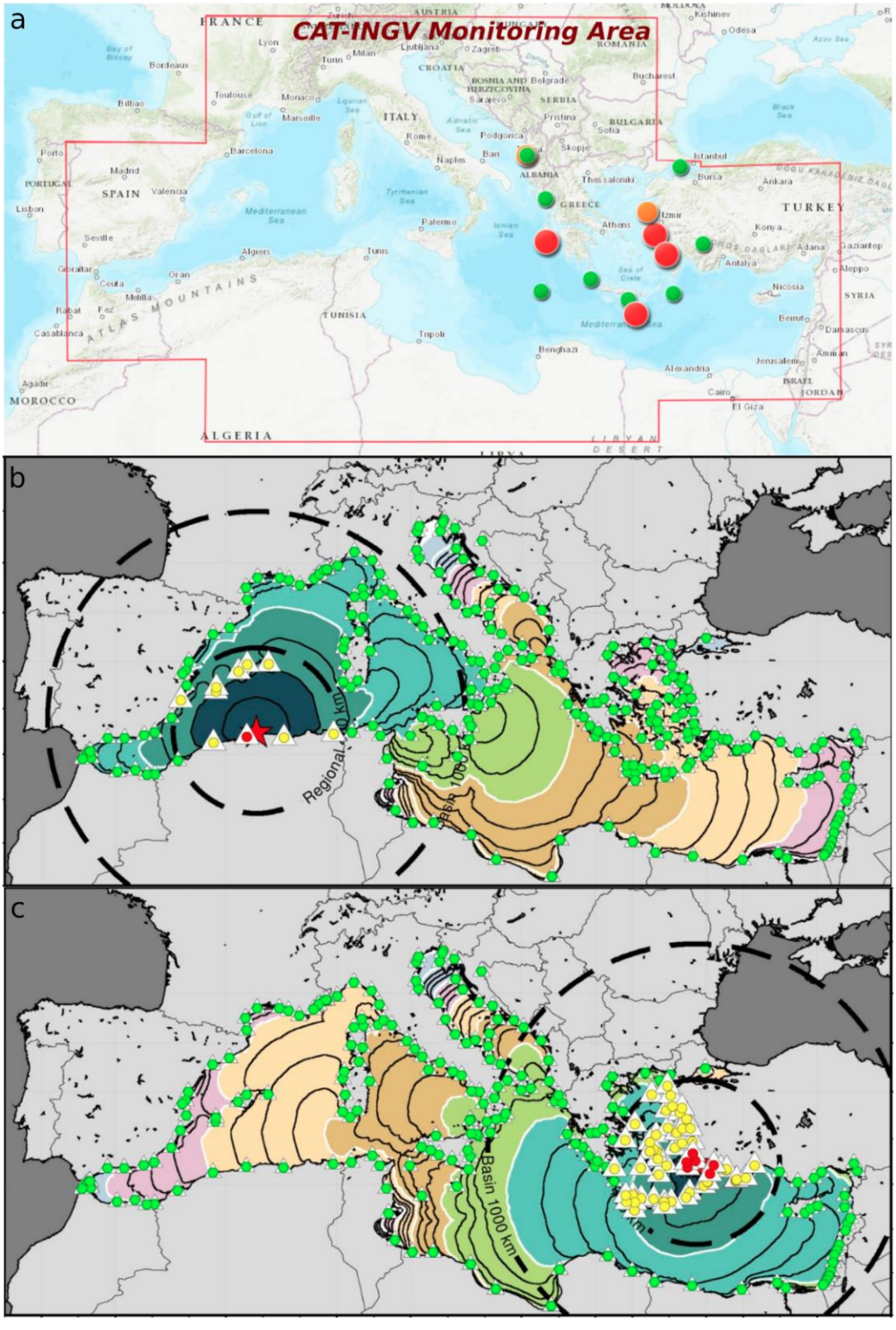

Figure 4: *Definition of the inundation zones (modified from* [63]*). The inundation distance (D_d^*) is calculated differently if the horizontal projection of the maximum wave height at the coast (R_d^*) crosses the topography before the projected ray on the sea level (top panel) or vice versa (bottom panel).*

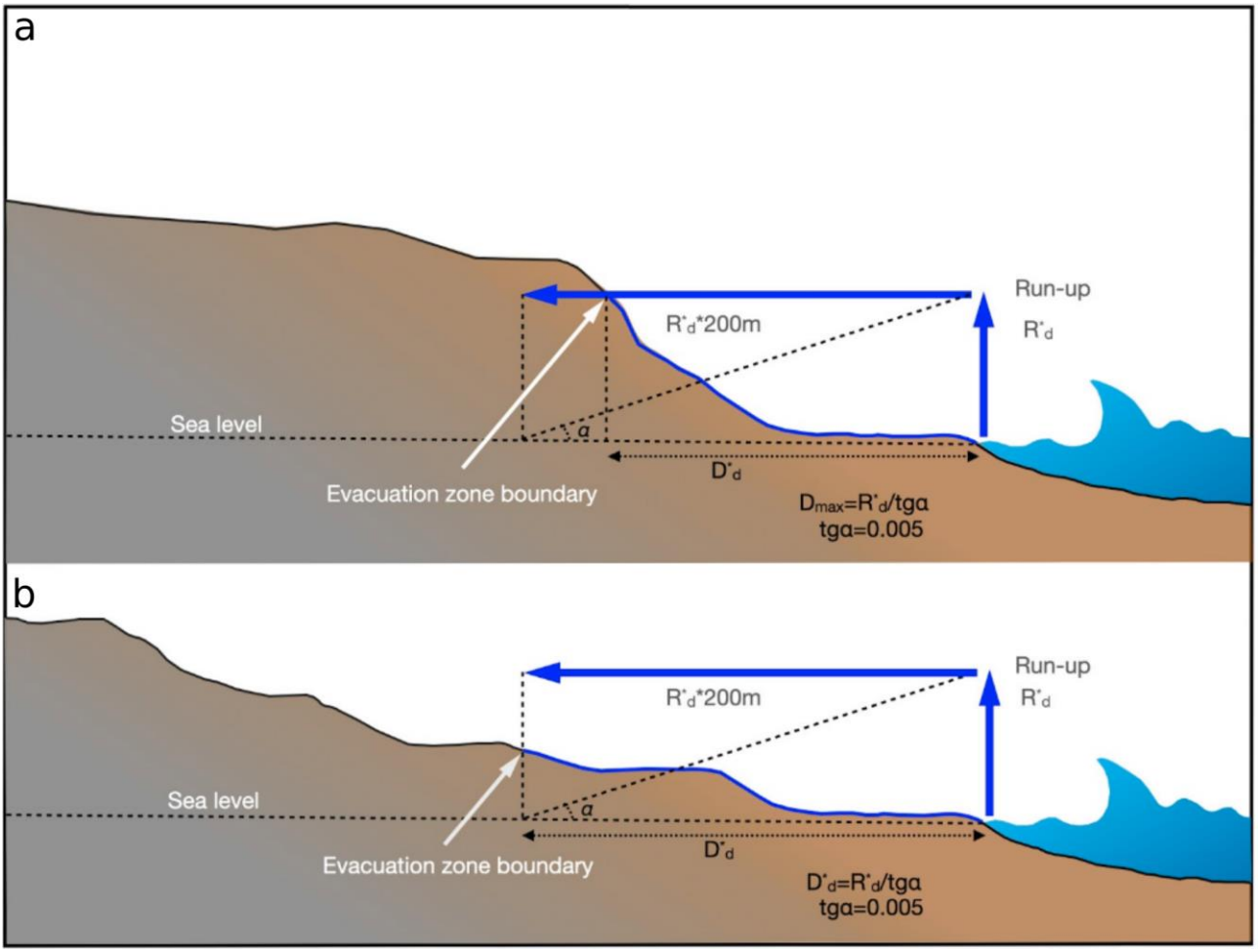

Figure 5: *Application of the DM to the Norcia 2016 (Mw=6.7) events and to the Peloponnese (Mw 8.5) scenario adopted in the NEAMWave17 exercise. As in Figure 3, red/orange/green triangles indicate watch/advisory/information alert levels; the dotted circles indicate local/regional/basin spatial domain, as defined by the decision matrix (Table 1); the red star indicates the epicentral location.*

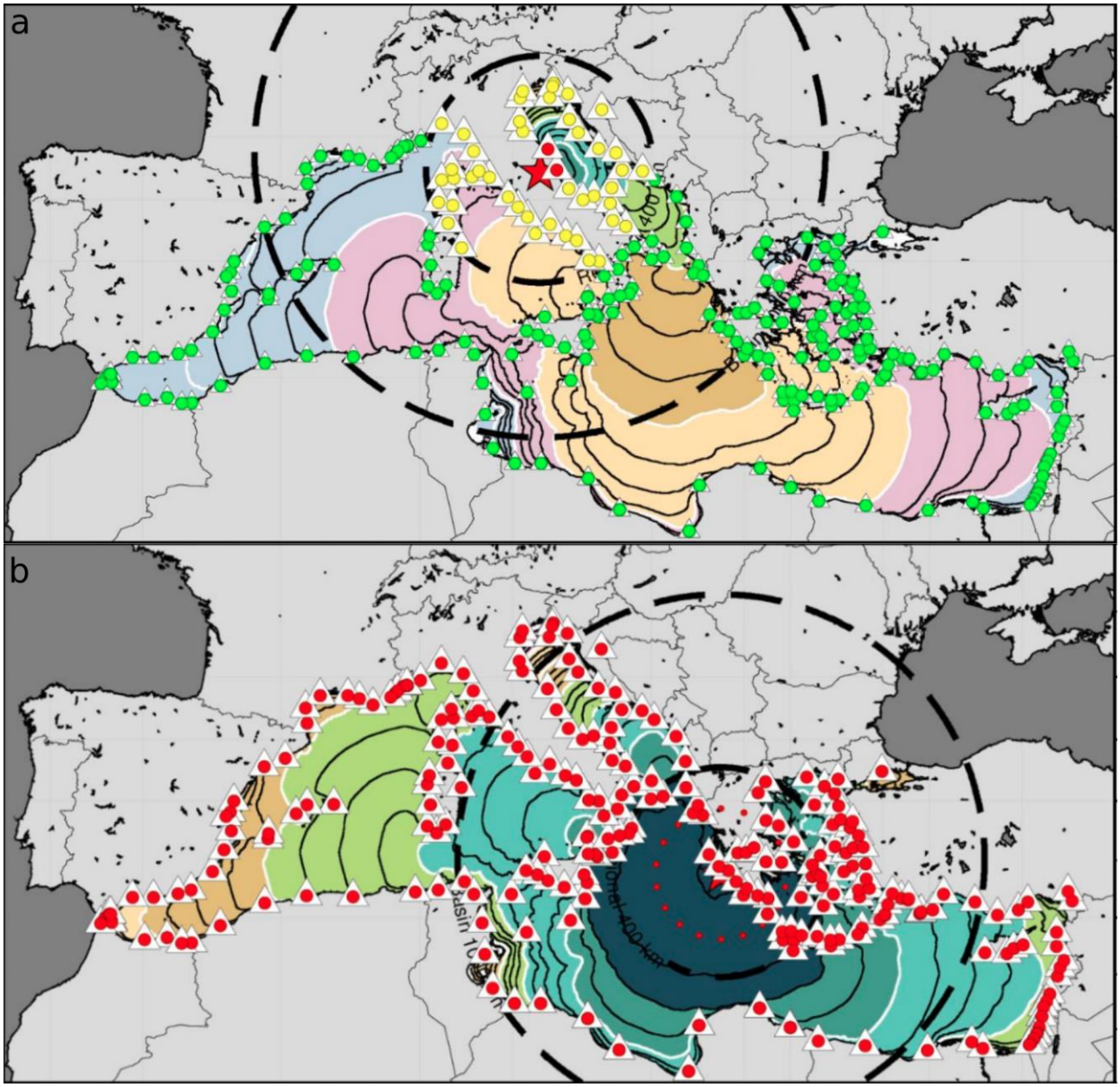

Figure 6: *a) Example of PTF results for the Zemmouri-Boumerdes M6.8 earthquake and tsunami, reporting the map of the probability of exceeding 1 m at all target points in the Mediterranean. b) The passage between PTF results and alert levels can be automated by mapping PTF statistics (e.g., the mean) into the intensity intervals of reference for each alert level. Here, the three alert levels defined within the NEAMTWS are considered.*

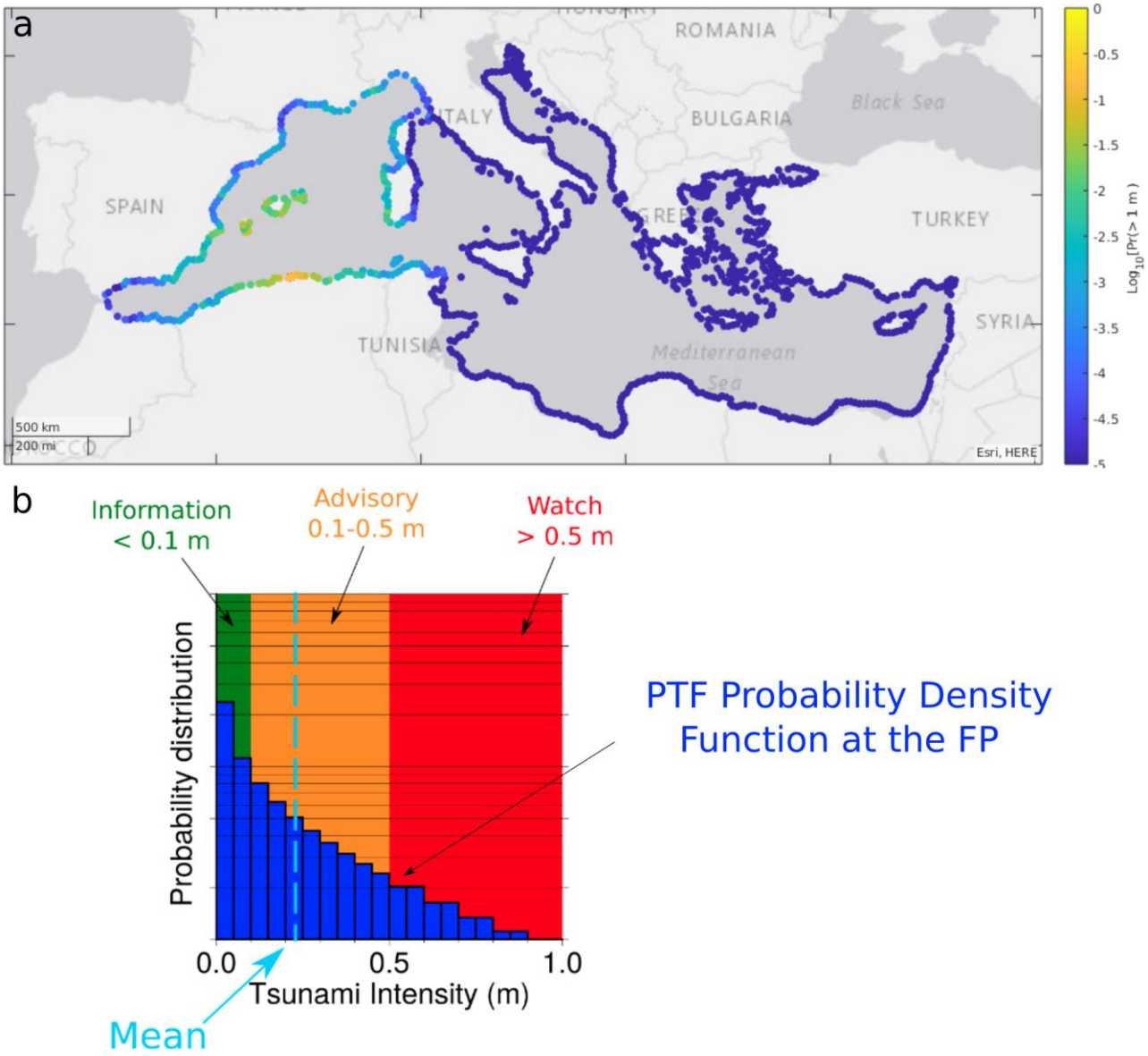

***Figure 7**: a) DEM of Stromboli Island with main geographic features, from Bertolaso et al.* [306]*. The white star indicates the location of the Civil Protection Advanced Operational Centre (COA). b) Synthetic waveforms obtained with a rigid landslide source of 6 millions of m^3 and different wave models. Synthetic waveforms obtained from numerical models have been used to calibrate the tsunami alert system. c-d) Example of numerical simulation of the proximal wave field for a tsunami generated by a landslide of 5 Mm^3 along the SdF (Sciara del Fuoco, Stromboli reporting the wave height (m) and travel time (s)).*

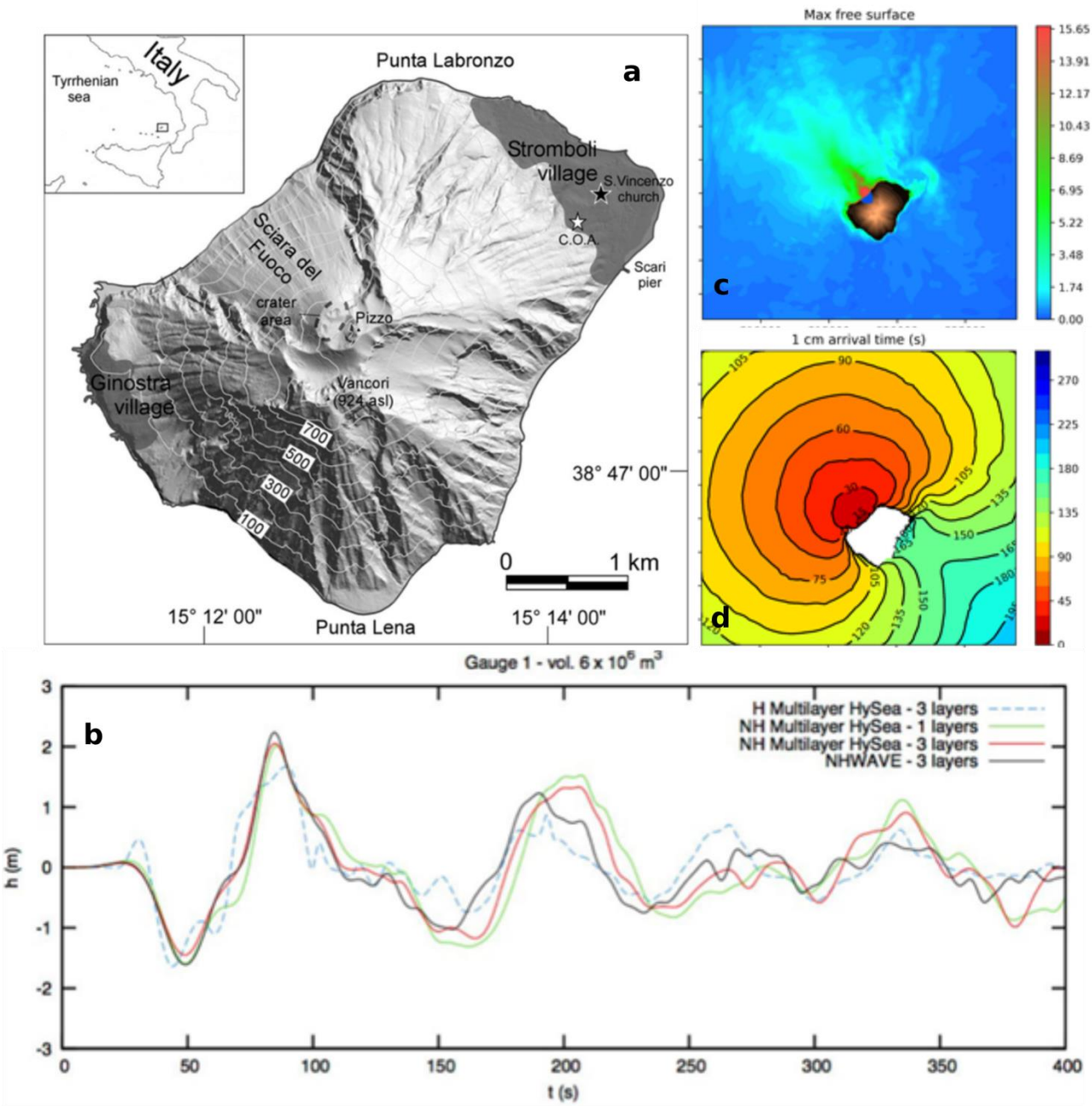

Figure 8: *Elastic beacons and communication schemes. a) Position and anchorage of the elastic beacons (MEDA). b) The elastic beacons – MEDA event just after the 03/07/2019 pyroclastic flow (photos courtesy of the Italian Coast Guard; modified from http://lgs.geo.unifi.it/index.php/blog/tsunami-registrato-stromboli-3-luglio-2019). c-d-e) location of the MEDA and the three networks that send data to the Advanced Operational Centre (COA).*

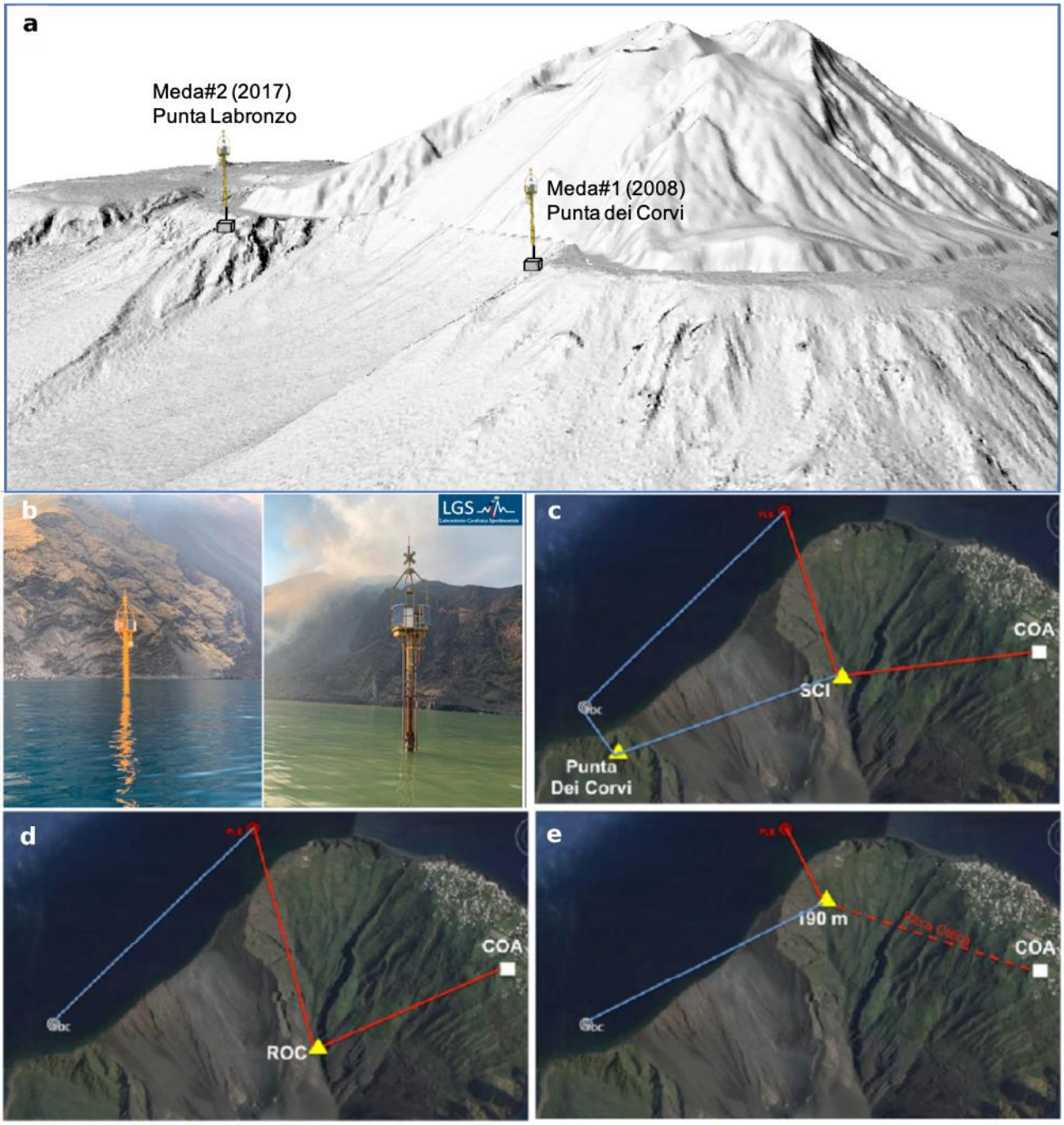

Figure 9: *a) Acoustic warning system and main connections; b) Connection between the MEDAs record of a tsunami and the acoustic warning system.*

a

b

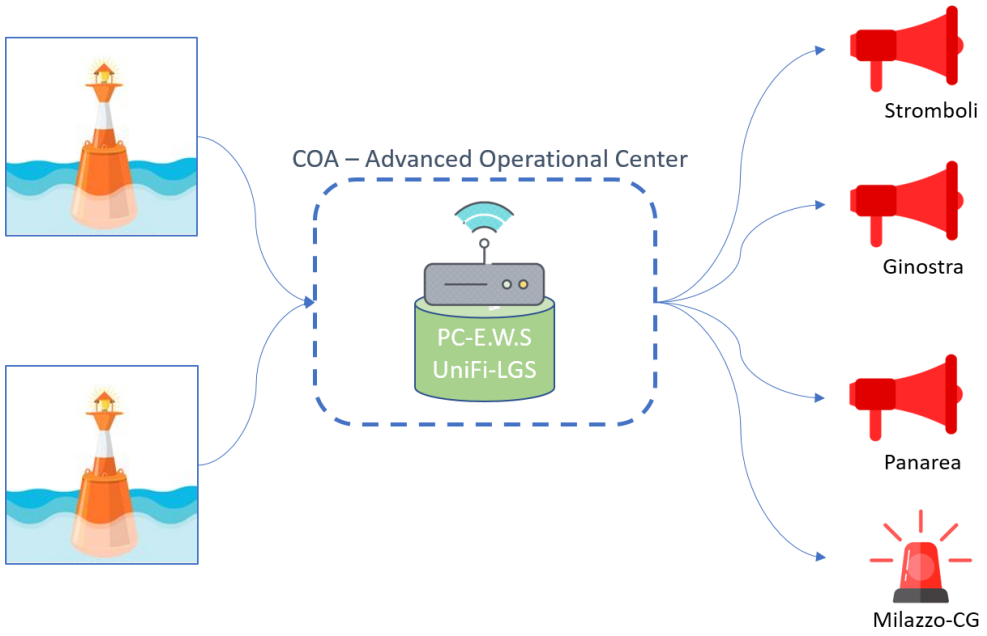

Figure 10: *Tsunami signals and triggering for the 2019 tsunamis at Stromboli* [307]. *a) Recorded tsunami at the MEDA of Punta Labronzo during the 3 July 2019; the arrow indicates the time at which the pyroclastic flow entered the sea. b) Same as a), for the 28 August 2019 tsunami. c) Automated triggering for the 28 August 2019 event occurred 24" after the tsunami generation (approximately 15" after the tsunami onset and 1' and 15" after the volcanic explosion).*

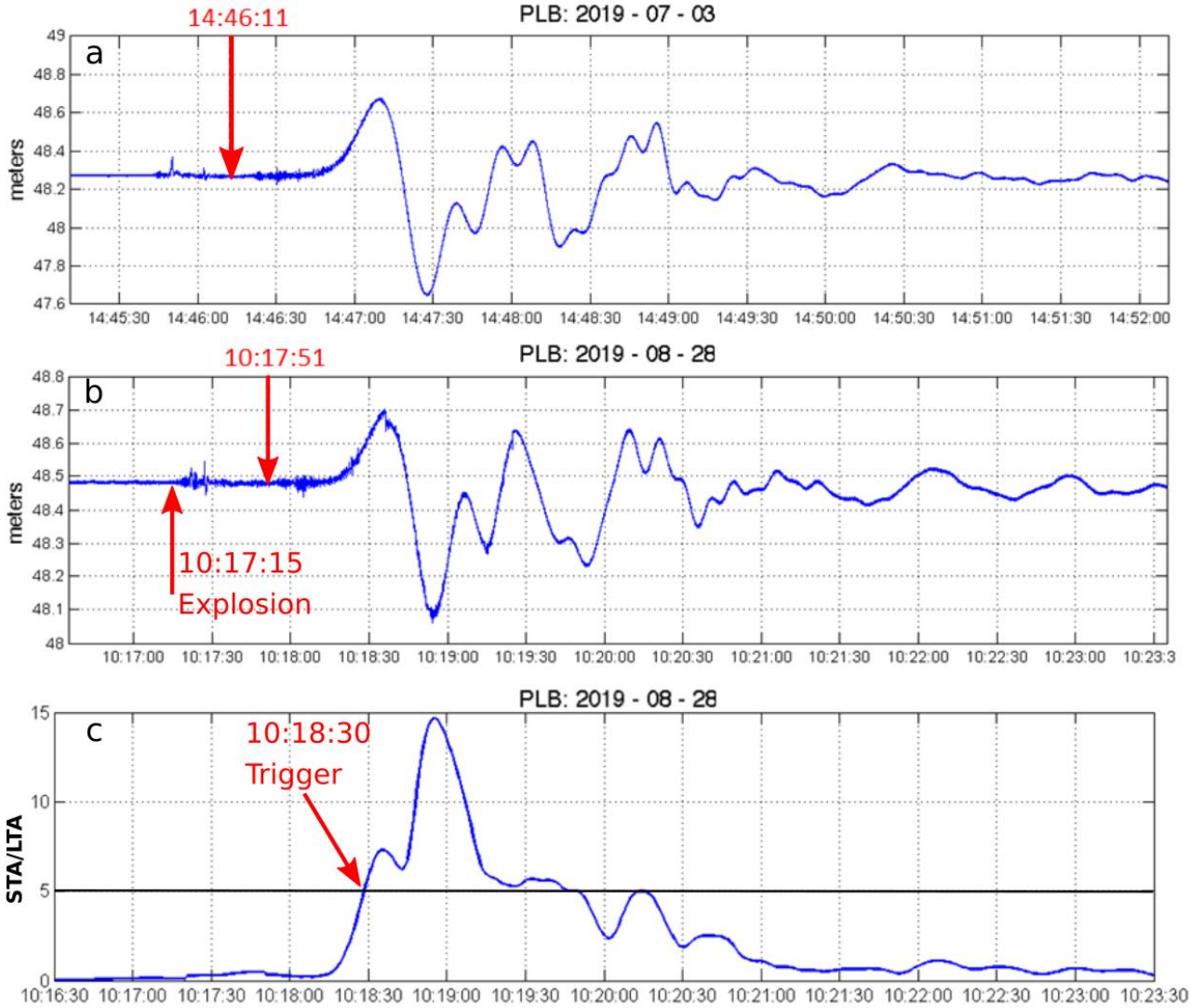

***Figure 11**. a) Portion of the Euro-Mediterranean Tsunami Catalogue* [36]*(Maramai et al., 2014) involving historical events generated by offshore or coastal/inland earthquakes. The tsunami intensity is expressed in the Sieberg-Ambraseys scale. b) Portion of the Euro-Mediterranean Tsunami Catalogue* [36] *involving historical events generated by non-seismic sources. The tsunami intensity is expressed in the Sieberg-Ambraseys scale.*

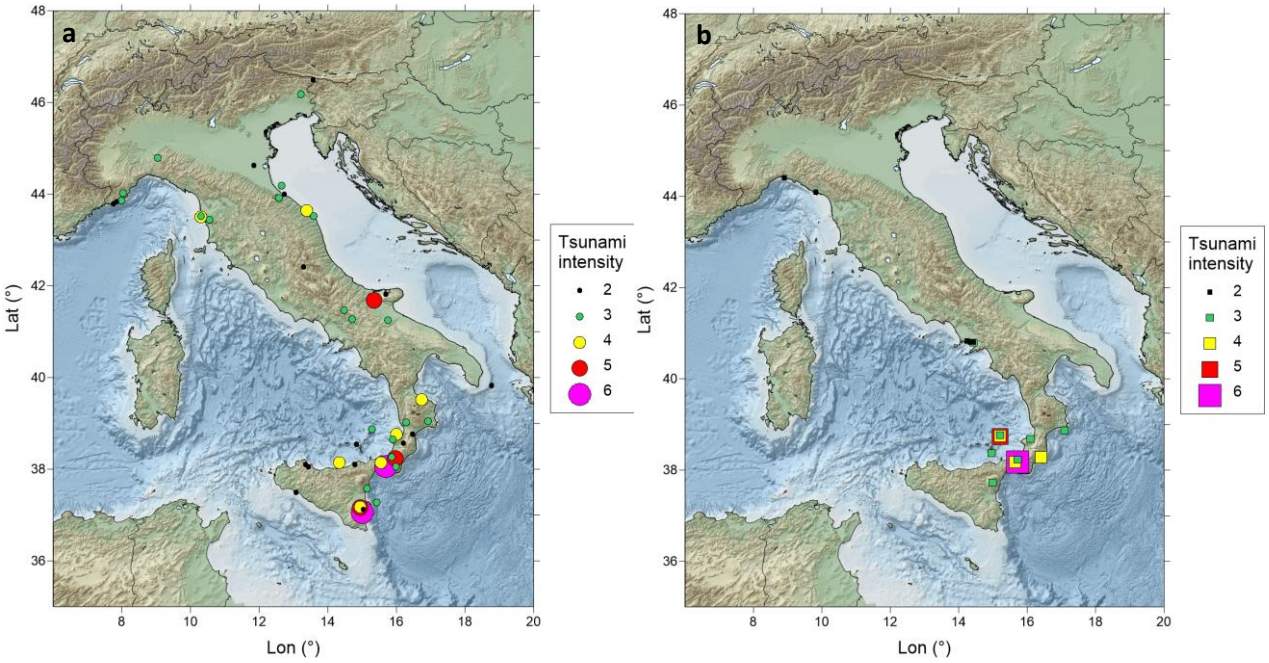

***Figure 12**. Main geographical domains with known historical, pre-historical, or future potential non-seismic tsunami sources. LS – Ligurian Sea; IGN – Ischia and Gulf of Naples; STSM – Southern Tyrrhenian SeaMounts; AA – Aeolian Archipelago; WCM – Western Calabria Margin; ECM – Eastern Calabria Margin; ES – Eastern Sicily; GM – Gela Margin; SC - Sicily Channel; SAM – Southern Adriatic Margin.*

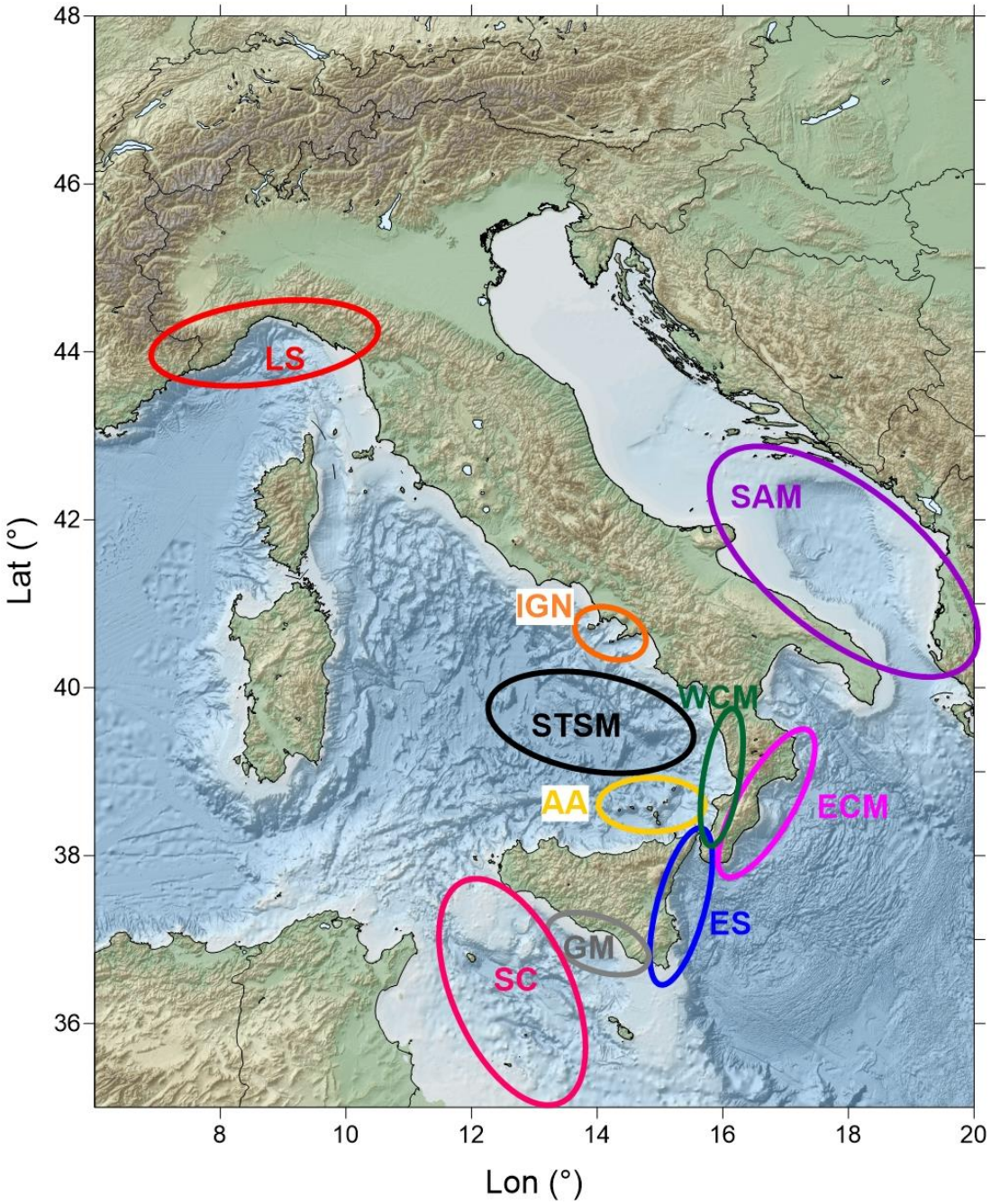

Figure 13. *a) Locations of meteotsunami events (red sparkles) observed in the Mediterranean and Black Seas during late June 2014 superimposed on meteotsunami-favourable coastal areas for which 0.9 < Fr < 1.1, where Fr is the Froude number (from Šepić et al.,*[380]*). Stars indicate air pressure observations, circles indicate sea-level stations, and black dotted lines indicate onset times of high-frequency sea level oscillations* [380]*. b) tide-gauge signals of a meteotsunami recorded in the central Adriatic Sea in August 2019.*

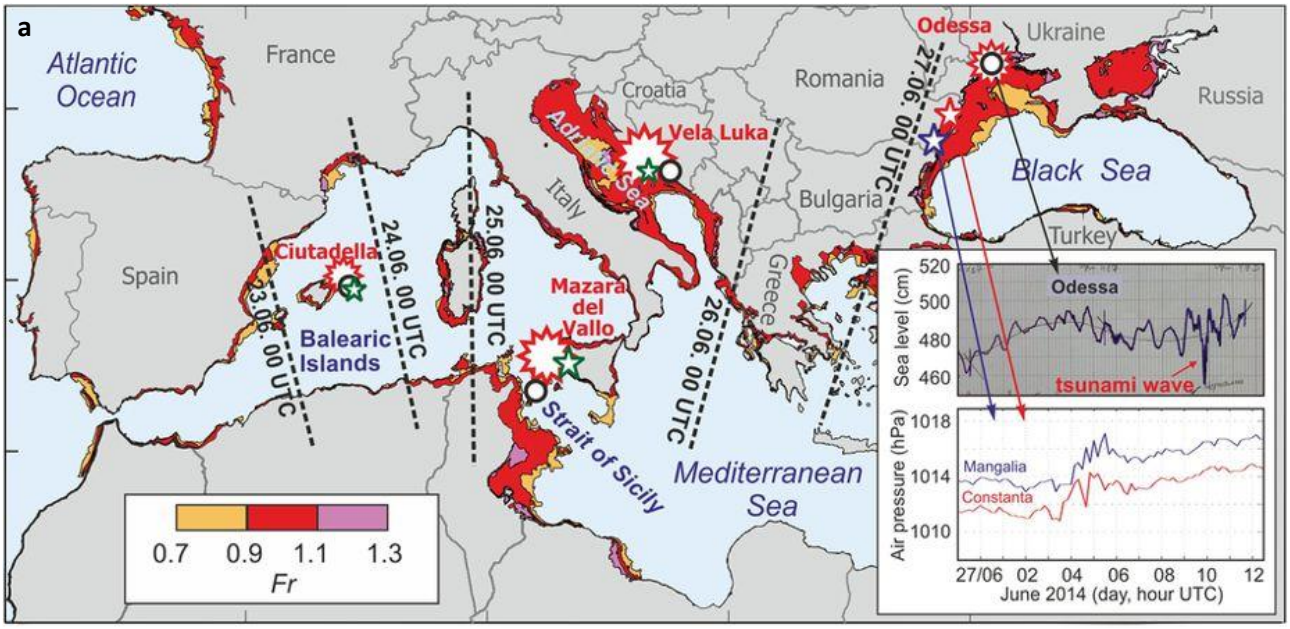

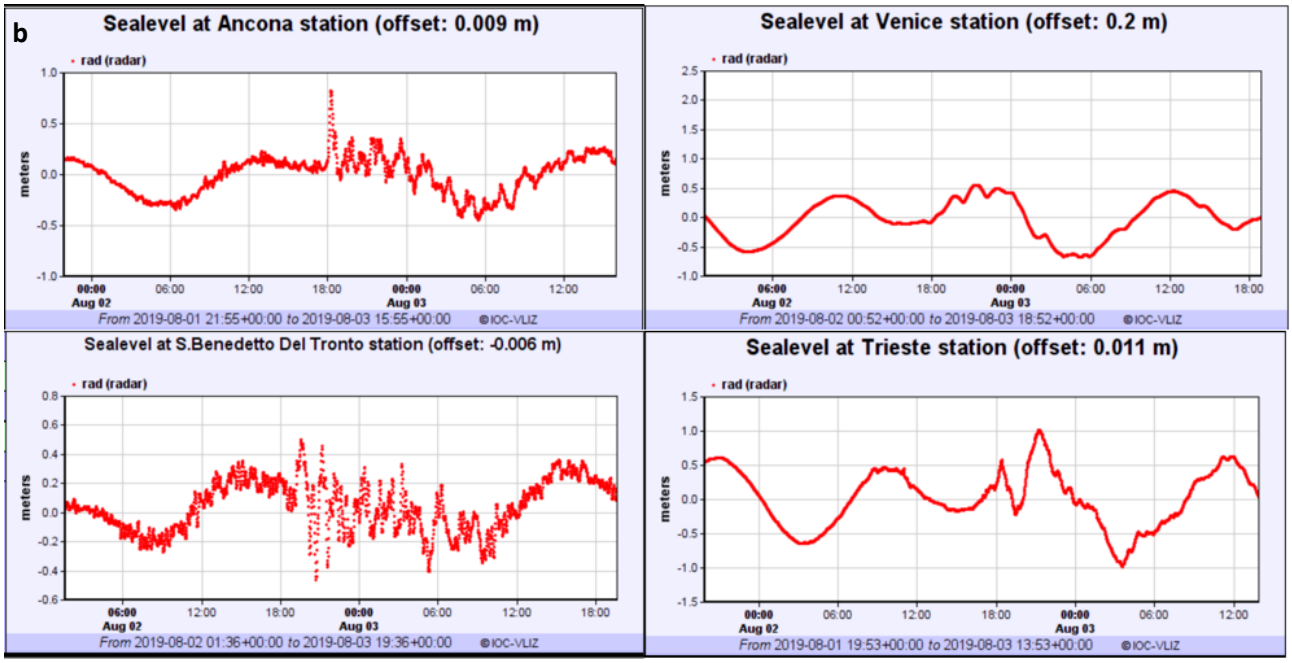

Tables

***Table 1**: CAT-INGV NEAMTWS DM for the Mediterranean Sea* [111,112].

Depth	Epicentre Location	M	Tsunami Potential	Type of Bulletin		
<100km	Offshore or close the coast (≦ 40 km inland)	5.5≦ M≦ 6.0	Nil	**Information Bulletin**	**Information Bulletin**	**Information Bulletin**
		6.0<M≦ 6.5	Weak potential of local tsunami	**Local Tsunami Advisory**	**Information Bulletin**	**Information Bulletin**
	Inland (>40km and ≦ 100km	5.5≦ M≦ 6.5	Nil	**Information Bulletin**	**Information Bulletin**	**Information Bulletin**
	Offshore or close the coast (≦ 100 km inland)	6.5<M≦ 7.0	Potential of destructive local tsunami <100km	**Local Tsunami Watch**	**Regional Tsunami Advisory**	**Information Bulletin**
		7.0<M≦ 7.5	Potential of destructive regional tsunami <400km	**Local Tsunami Watch**	**Regional Tsunami Watch**	**Basin-wide Tsunami Advisory**
		M>7.5	Potential of destructive tsunami in the whole basin >400km	**Local Tsunami Watch**	**Regional Tsunami Watch**	**Basin-wide Tsunami Watch**
≧ 100km	Offshore or close to the coast (≦ 100 km inland)	M≧ 5.5	Nil	**Information Bulletin**	**Information Bulletin**	**Information Bulletin**
				Local≦ 100 km	100≦ Regional <400	Basin−wide ≧ 400